A REAL-TIME CONTROL SYSTEM FOR A FREQUENCY RESPONSE-BASED PERMITTIVITY SENSOR

by

NING TANG

B.S., China Agricultural University, China, 2004
M.S., China Agricultural University, China, 2006

A THESIS

submitted in partial fulfillment of the requirements for the degree

MASTER OF SCIENCE

Department of Biological and Agricultural Engineering
College of Engineering

KANSAS STATE UNIVERSITY
Manhattan, Kansas

2009

Approved by:

Major Professor
Naiqian Zhang

Abstract

Permittivity is an important property of dielectric materials. By measuring the permittivity of a material, it is possible to obtain information about the material's physical and chemical properties, which are of great importance to many applications. In this study, a real-time control system for a frequency-response (FR) permittivity sensor was developed. The core of the hardware was a kitCON167 microcontroller (PHYTEC America, LLC), which controlled and communicated with peripheral devices. The system consisted of circuits for waveform generation, signal conditioning, signal processing, data acquisition, data display, data storage, and temperature measurement. A C program was developed in the TASKING Embedded Development Environment (EDE) to control the system.

The control system designed in this study embodied improvements over a previously designed version in the following aspects: 1) it used a printed circuit board (PCB); 2) the measurement frequency range was extended from 120 MHz to 400 MHz; 3) the resolution of measured FR data was improved by using programmable gain amplifiers; 4) a data storage module and a real-time temperature measurement module were added to the system; 5) an LCD display and a keypad were added to the system to display the FR data with corresponding frequencies and to allow users to enter commands.

Impedance transformation models for the sensor probe, the coaxial cable that connects the control system with the sensor probe, and the signal processing circuit were studied in order

to acquire information on the permittivity of measured materials from measured FR data. Coaxial cables of the same length terminated with different loads, including an open circuit, a short circuit, a 50Ω resistor, and a 50Ω resistor paralleled by a capacitor, were tested. The results indicated that the models were capable of predicting the impedances of these specific loads using the FR data. Sensor probes with different sizes and coaxial cables with two different lengths terminated with the same sensor probe were also tested. The results were discussed.

Additional tests for the gain and phase detector were conducted to compare FR data measured by the gain and phase detector with those observed on an oscilloscope. The results were discussed.

Table of Contents

List of Figures

List of Tables

Acknowledgements

I would like to express my deep gratitude to my major professor, Dr. Naiqian Zhang, for his guidance and encouragement continually during the period of my master program study. He has been a mentor, a father and a friend in my mind. His rigorous scholarship, meticulous research spirit influenced me deeply and will play an important role for my future life and career. I am also grateful for the opportunities he supplied to me so that I have this chance to study in the US.

I would like to extend my sincere gratitude to my supervisory committee members, Dr. William B. Kuhn, Dr. Mitchell L. Neilsen. Thanks to Dr. Kuhn for his patience and kindness, for spending his precious time on answering my questions on the transmission problems, for giving me many suggestions and guidance. Thanks to Dr. Neilsen for his suggestions and help on part of the software design.

I would like to thank many experts who helped me overcome the obstacles during my master program. I thank Dr. Donald Lenhert for his suggestions on solving the hardware problem of the microcontroller. I thank Dr. Philip L. Barnes for guiding me to know the concentration of the harmful impurities in water. I thank Dr. Stoyan Ganchev at Agilent Technologies for helping me setting up the impedance analyzer and giving me many suggestions on how to calibrate. I thank many technical supports at Analog Devices, Inc. for answering me many questions on the

DDS evaluation board and guiding me how to modify it so that it can be well used for my research.

My gratitude also goes to Mr. Darrell Oard for his valuable suggestions and assistance in constructing the sensor probe and guiding me how to use the mechanical machines in the workshop. Many thanks to Mrs. Barb Moore and Mr. Randy Erickson for helping me in all related to my study and research in the department.

Profound thanks and appreciation also go to Dr. Gary A. Clark, the former department head, Dr. Joe P. Harner, the current department head, Dr. James M. Steichen, Dr. Donghai Wang, Dr. Wenqiao Yuan, and all other faculty members and staff in the department.

I also would like to extend my gratitude to all the fellow students in the Instrumentation and Control Lab: Ms. Yali Zhang, Mr. Wei Han, Mr. Peng Li, Ms. Ling Xue, Dr. Jizhong Deng, Ms. Sarah Shultz and Mr. Alan Bauerly for their help on my research and profound friendship among us.

Finally, my deep appreciation is given to my family for their patience, continuous support and encouragement, which have made me finish my study smoothly. Special thanks are given to my husband, Peng Li, who is also a student in the Instrumentation and Control Lab, for his academic suggestions and help on my research, for his support and encouragement when I met difficulties, for his patience and unconditional love during the life, which have helped me complete my master program study.

CHAPTER 1 - Introduction

Permittivity is a physical quantity that describes the dielectric and conductive properties of dielectric materials. It is determined by the ability of a material to polarize in response to an electric field, and thereby reduce the total electric field inside the material. When an external electric field is applied to a dielectric material, dipole molecules in the material tend to align up in the opposite directions. This process of alignment, called polarization, hinders current flow. The response of a material to an external alternating electric field typically depends on the frequency of the electric field. Therefore, permittivity of dielectric materials is frequency-dependent.

Permittivity is an important characteristic of a material. By knowing the dielectric property of a material, it is possible to obtain information about its physical and chemical properties, which are of great importance to many applications in industry, agriculture, production of food, and biological materials, and medicine. For example, dielectric property was used to study the moisture content in grain and other materials, and to measure fruit maturity (Nelson 1991; Nelson et al., 1995). During microwave heating, reflection, transmission, and absorption of microwave energy are controlled by the dielectric properties of the materials. Therefore, dielectric property plays an important role in studying the absorption of electromagnetic energy (Tanaka et al., 2002). Moreover, dielectric properties of materials are important in the design of electrical and electronic equipment where they are used as insulating components, in studying biological substances, as well as thin plates of semiconductor and magnetic materials (Nelson 2003; Stuchly et al., 1974). Because of the wide application areas of

dielectric properties, there is an increasing demand for various dielectric materials. As a result, more and more researchers have proposed many different methods for measuring the permittivity of dielectric materials.

Since the permittivity of a dielectric material is a function of frequency, study of permittivity should be conducted in a wide range of frequencies. However, the frequency range of dielectric spectroscopy covers nearly 21 orders of magnitude from 10^{-6} to 10^{15} Hz; no single method of permittivity measurement is able to cover this range. Therefore, different measurement techniques are adopted for different applications, depending on the frequency of interest, the nature of the dielectric material to be measured, and the degree of accuracy required. Normally, at the low frequency range of 10^{-6}~10^{3} Hz, time domain measurement is frequently used. Frequency domain measurement is adequate for the frequency range of 10^{-5}~10^{6} Hz. Reflective coaxial methods and transmission coaxial methods are frequently used for the frequency ranges of 10^{6}~10^{10} Hz and 10^{8}~10^{11} Hz, respectively. Fourier-transform methods are working in the frequency range of 10^{11}~10^{15} Hz (Chen et al., 2004).

Some measurement techniques can cover a relatively wide frequency range. For example, conventional bridges are used over a frequency range of approximately 50Hz to 25MHz. A Q-meter is suitable for a rather higher band of frequencies, from 100 kHz to 100 MHz. The principle of the bridge and Q-meter is to measure the capacitance and conductance of a material, because a material can be modeled electrically as a series or parallel equivalent circuit at any given radio frequency. If the circuit parameter, such as impedance or admittance, can be measured appropriately, the dielectric properties of the material can be determined at that

particular frequency (Nelson 1999).

Many researchers have been conducting research on the development of dielectric property measurement instruments based on different measurement principles. Stoakes and Brock (1973) designed a permittivity sensor using a capacitor method to determine the permittivity of oil and its lubricating ability. This oil permittivity sensor obtained a United States Patent. A dielectric sensor using the principle of resonant cavity was developed by Fort Motor Co in early 1990s to measure alcohol concentration in methanol or ethanol-gasoline blends (Meitzler and Saloka, 1992). Hewlett Packard (HP) developed impedance, spectrum or network analyzers with high accuracy to measure permittivity. However, these analyzers are very expensive and need complicated calibrations.

A permittivity sensor using a frequency-response (FR) method for simultaneous measurement of multiple properties of dielectric materials in real time has been developed by researchers in the Instrumentation and Control Laboratory of the Biological and Agricultural Engineering Department at Kansas State University since 2000. The sensor was originally developed to measure soil properties (Fan, 2002; Zhang et al., 2004; Lee, 2005; Lee et al., 2007a; Lee and Zhang, 2007b). Since 2005, the sensor has been modified to measure other dielectric materials – water, biofuel, and air (Zhang et al., 2006; Zhang et al., 2007). In 2005, a control box was developed to control the modified sensor. In this study, a new control box was developed to improve the performance of the sensor. This thesis describes the hardware and software of the new control box. Studies on impedance transformation models for the sensor probe and the control box are also reported in this thesis.

CHAPTER 2 - Objectives

The overall objective of this research is to develop a real-time control system with improvements over a previously developed version for a FR permittivity sensor.

Specific objectives are as follows:

1. Develop an integrated, microcontroller-based system, including circuits for waveform generation, signal conditioning, signal processing, data collection, data display, data storage, and temperature measurement.

2. Develop a C program to control the system.

3. Investigate impedance transformation models for the sensor probe, the coaxial cable that connects the control system with the sensor probe, and the signal processing circuit with a goal of obtaining information on the permittivity of measured materials from measured FR data.

CHAPTER 3 - Literature Review

3.1 Theory of permittivity

The term "permittivity" used in this thesis implies the relative complex permittivity, which is the permittivity of a material relative to that of free space (Equation 3.1).

$$\varepsilon = \varepsilon_r \varepsilon_0 \tag{3.1}$$

$$\varepsilon_r = \varepsilon'_r - j\varepsilon''_r \tag{3.2}$$

where ε is permittivity,

ε_r is relative permittivity,

ε_0 = 8.85 $\times 10^{-12}$ F m^{-1} (permittivity of free space),

ε'_r is dielectric constant, and

ε''_r is dielectric loss factor.

The real part of the relative permittivity is dielectric constant, which describes energy storage in the material. The imaginary part is loss factor, which describes the rate of energy dissipation in the material (Nelson, 2003). Dielectric constant and dielectric loss factor can be expressed by the following equations:

$$\varepsilon''_r = \varepsilon''_d + \sigma / \omega\varepsilon_0 \quad (3.3)$$

$$\varepsilon'_r = \varepsilon''_r / \tan\delta \quad (3.4)$$

where ε''_d is dielectric loss,

σ is electrical conductivity,

ω is angular frequency,

$\sigma / \omega\varepsilon_0$ is conductive loss, and

δ is loss angle.

Permittivity is a good indicator of multiple material properties and is frequency-dependent. Both the real and imaginary parts of relative permittivity are dependent on frequency. At low frequencies, the energy dissipation process $\sigma / \omega\varepsilon_0$ caused by ionic conduction is inversely proportional to frequency and becomes critical for energy loss. The polarity of the electric field changes slowly enough at such frequencies to allow dipole molecules in the material to reach equilibrium before the electric field has changed. For frequencies at which dipole orientation can not follow the applied electric field due to the binding force between atoms, absorption of the field's energy leads to energy dissipation, in the form of dielectric relaxation (Robinson et al., 2003; Topp et al., 2000). Therefore, dipolar energy dissipation is the predominant loss at high frequencies. The combination of polarization, relaxation, and ionic conduction makes the interpretation of dielectric properties of materials complex. Changes of

any of these three properties caused by changes in material composition can be detected by complete measurement of permittivity (Lee, 2005).

3.2 Permittivity measurement techniques

Many papers reporting diverse methods for permittivity measurement can be found in the literature. Many researchers all over the world also studied on different methods for permittivity measurement. Many types of permittivity sensors and instruments have been developed as modern electronics fast evolving. Choices of measurement methods for particular applications depend upon the physical and electrical properties of the material under test, the frequency range of interest, and the operative constraints. The most commonly used techniques - time domain reflectometry (TDR), capacitance probe, transmission line, resonator, open-ended coaxial probe, and free-space method, are reviewed in this section.

3.2.1 TDR

The TDR method was developed in the 1980s and has become a major technique for permittivity measurement since then (Afsar et al., 1986). This method covers a wide frequency range from radio frequency to microwave (Nozaki and Bose, 1990). The basic principle of TDR measurement is to measure the time difference between the reflected and the incident pulse, which was produced by a step voltage pulse generator, through a coaxial line. The recorded time difference can be related to the dielectric properties of materials.

Topp and Davis (1985) used the TDR method to measure volumetric water content of unsaturated soils. A strong relationship between the volumetric water content and dielectric constant for a wide range of soils was reported. Sri Ranjan and Domytrak (1997) measured

effective volume of soils using different TDR miniprobes with three and five rods, respectively. The result showed that the three-rod miniprobes were easier to install. However, orientation of the three-rod miniprobes easily influenced the effective volume measured in saturated soils. Robinson et al. (1999) adopted the TDR method in measuring relative permittivity of sandy soils. Payero et al. (2006) used TDR to continuously monitor the nitrate-nitrogen in soil and water. Good correlation, between the bulk electrical conductivity measurements by TDR in water and nitrate-nitrogen concentrations, was achieved.

3.2.2 Capacitance probe

Robinson et al. (1999) adopted a surface capacitance insertion probe (SCIP) to measure relative permittivity of sandy soils. The SCIP consists of two parallel stainless steel electrodes which define a capacitor. The capacitance is a function of the relative permittivity of the material where the probe is embedded and the geometric configuration of the probe:

$$C = \varepsilon_r g \varepsilon_0 \qquad (3.5)$$

where C is the capacitance,

ε_r is relative permittivity, and

g is a geometric constant.

The capacitor formed by the probe and an inductor form an oscillator circuit. The frequency of oscillation is a function of both the inductance and capacitance in the circuit (Equation 3.6) (Dean et al., 1987). Therefore, permittivity of the material embedding the probe can be derived by measuring the oscillation frequency.

$$F = \frac{1}{2\pi\sqrt{LC}} \tag{3.6}$$

where L is the circuit inductance, and

C is the capacitance of the probe embedded in the material to be measured.

Lee (2005) developed a frequency-response permittivity sensor, with a four-electrode probe arranged in a Wenner-array structure, for simultaneously measuring multiple soil properties. The sensor probe consisted of four rectangular metal plates. In order to increase the capacitance effect, a relatively large plate area and a relatively small separation between the plates were chosen. Impedance of the probe inserted in the materials to be tested can be related to the relative permittivity of the material to be tested:

$$\varepsilon_r^{'} = \frac{C}{\varepsilon_0} g \tag{3.7}$$

$$\varepsilon_r^{''} = \frac{G}{2\pi f \varepsilon_0} g \tag{3.8}$$

where C is the capacitance between the plates,

G is the conductance between the plates, and

g is the geometric factor of the sensor.

The geometric factor was determined from the conductivity σ of the medium surrounding the sensor probe (material to be tested) and the load resistance R measured between sensor electrodes.

$$R = \rho g = \frac{1}{\sigma} g \qquad (3.9)$$

$$g = R\sigma \qquad (3.10)$$

where ρ is the resistance of the material, and

σ is the conductivity of the material.

3.2.3 Resonator

Depending on the type of transmission line used, microwave resonators have different names such as coaxial, microstrip, slotline, and cavity resonator (Nyfors, 2000). In general, a microwave resonant cavity is a box fabricated from high-conductivity metal. The shape of the cavity is always rectangular or cylindrical so that the distribution of electric and magnetic inside is easily calculated. The size of the cavity is inversely proportional to the desired frequency. That is, for higher frequencies, the cavity should be smaller.

The basic principle of the resonant method is that the resonant frequency shifts and the energy absorption characteristics change when a resonator is filled with a sample. Changes in the resonant frequency provide information that can be used to calculate the real part of material permittivity - dielectric constant. Changes in the energy absorption, which can be expressed as

Q-factor (ratio of energy stored to energy dissipated), are used to estimate the imaginary part of the material permittivity - dielectric loss (Venkatesh and Raghavan, 2005).

As early as 1960s, the resonant cavity technique was frequently used for studying the dielectric properties of materials at microwave frequencies. This technique still has a unique place now, owing to its high sensitivity and relative simplicity. Especially when data are required at only one microwave frequency, the resonant cavity method is probably the most logical choice (Bussey, 1967). Yu et al. (2000) proposed an approach using a cylindrical cavity resonator to measure the complex permittivity of lossy liquids.

Matytsin et al. (1996) proposed a method of dielectric permittivity measurement based on a slotted coaxial resonator with decimeter wavelengths, which can be applied in industry for non-destructive testing of sheet materials. Raveendranath et al. (1996) used an open-ended coaxial resonator to measure the complex permittivity of water within the frequency range from 0.6 GHz to 14 GHz. Dudorov et al. (2005) developed a method using a spherical open resonator at millimeter wavelengths for dielectric constant measurement of thin films on optically dense substrates.

Many researchers developed sensors based on the resonant technique. Dionigi et al. (2004) designed a resonant sensor for dielectric permittivity measurements of powdered, granular and liquid materials. The results on measuring silica sand are of good accuracy. Fratticcioli et al. (2004) developed a microstrip resonant sensor, its equivalent circuit, and the driving electronic circuitry for the measurement of material permittivity.

3.2.4 Open-ended coaxial probe

The coaxial probe method is a modification base on the transmission line method. It measures the reflected signal from a material through a coaxial line ending with a tip, which is in contact with the material being tested. The tip is located at the center of a probe. For measuring solid materials, the probe needs to touch a flat surface of the material. For liquid, on the other hand, the probe needs to be immersed in the liquid during measurement. The measured reflection coefficient is related to the sample permittivity (Sheen and Woodhead, 1999). The coaxial probe method is easy to use because it does not require a particular sample shape or special containers. Moreover, it is possible to measure the dielectric properties over a wide range of frequencies, from 500 MHz to 110 GHz. However, this method requires elaborate calibration procedures. It is also of limited accuracy with the materials with low relative permittivity values (Venkatesh and Raghavan, 2005).

3.2.5 Transmission line

Transmission line techniques based on one-port measurements or two-port measurements have been broadly used over the past 50 years (Catala-Civera et al., 2003). Transmission lines have many different forms: coaxial cable, waveguide, and microstrip lines. The principle of the transmission line technique is that when an incident signal in an electromagnetic field transmits through a sample, which is precisely fully filled in an enclosed transmission line, the related measured S-parameters for the reflection and transmission can provide the information on the permittivity of the materials (Baker-Jarvis et al., 1990).

Abdulnour et al. (1995) proposed to use discontinuity in a rectangular waveguide to measure the permittivity of dielectric materials. Bois et al. (1999) reported a permittivity

measurement technique that uses dielectric plug-loaded, two-port transmission line to measure the dielectric property of granular and liquid materials, such as cement powder, corn oil, antifreeze solution, and tap water. Ocera et al. (2006) reported a technique for measuring complex permittivity based on a four-port device using microstrip.

The transmission line method is of good accuracy and sensitive, but it is difficult to use and time consuming. It covers a narrower range of frequencies, compared to the coaxial probe method. Moreover, the thickness of the sample for the transmission line method should be one-quarter of the wavelength of the signal source that penetrated the sample. Therefore, at lower frequencies, the sample size has to be quite large.

3.2.6 Free-space method

The free-space method is also based on transmission line techniques. It is a non-destructive and contact-less measuring method. This method uses two antennas, one transmitting and the other receiving. The principle is to measure the attenuation and phase shift of a microwave signal, which transmits through the material under test along the path from the transmitting antenna to the receiving antenna. The measured attenuation and phase shift can be used to compute the permittivity of the material. Ghodgaonkar et al. (1990) used the free-space method to measure the complex permittivity of various materials, such as teflon, sodium borosilicate glass, and microwave-absorbing materials. Trabelsi and Nelson (2003) also used the free-space transmission method to measure the dielectric properties of cereal grain and oilseed.

CHAPTER 4 - Design of a Real-time Control System for the Permittivity Sensor

A real-time control system for the FR permittivity sensor was developed in this study. This control system was developed based upon a previous version (Zhang et al., 2006). In this thesis, the previously developed control system will be referred to as the "old control box", whereas the control system developed in this study will be referred to as the "new control box" hereafter.

A functional block diagram of the old control box is shown in Figure 4.1. It consisted of a microcontroller, a signal generator, and a gain and phase detector. The signal generator generated sinusoidal waves with frequencies up to 120 MHz. The signal from the signal generator was sent to channel A of the gain and phase detector. The signal from the output of a voltage divider that consisted of a constant resistance R_{ref} and impedance Zin was sent to channel B. Thus, the gain and phase detector measured FR of the following transfer function:

$$\frac{V_A}{V_B} = \frac{R_{ref} + Z_{in}}{Z_{in}} \qquad (4.1)$$

The output signals for gain (V_{MAG}) and phase (V_{PHS}) from the gain and phase detector were sent to the microcontroller for processing. Because Z_{in} can be related the sensor probe impedance Z_{load} through impedance transformation, Z_{load} at given frequencies can be derived

from the measured gains and phases at these frequencies. The old control box is shown in Figure 4.2.

Figure 4.1 Block diagram of the old control box

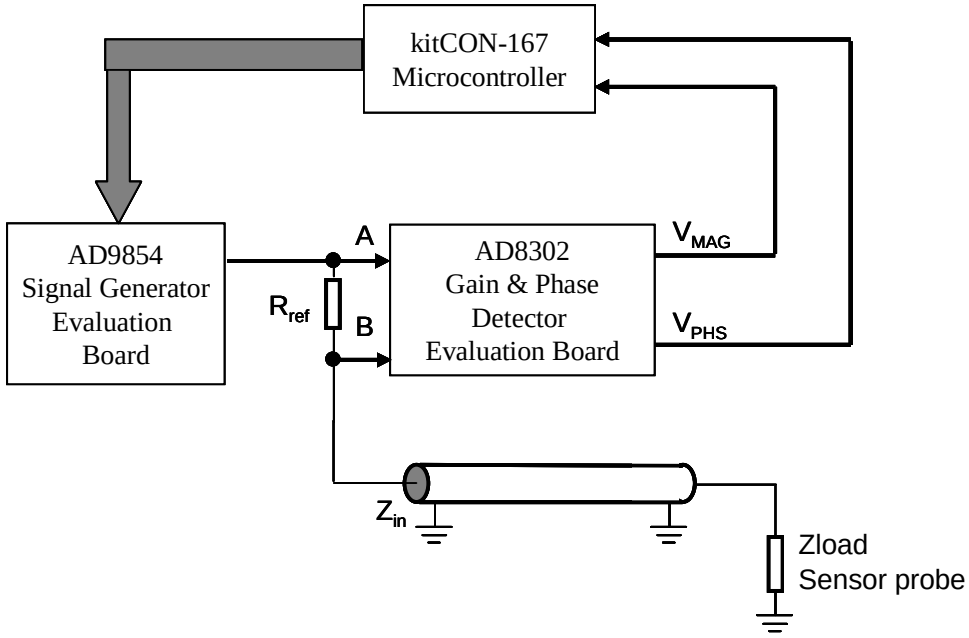

Figure 4.2 Old control box (Zhang et al., 2006)

The new control box embodied improvements over the old box in many aspects. Detail descriptions of hardware and software improvements are reported in the following sections.

4.1 System Hardware Design

Figure 4.3 gives an inside view of the new control box. The core of the hardware was a kitCON167 microcontroller (PHYTEC America, LLC). Four peripheral modules - analog module (A/D), digital I/O module (DI/O), serial communication module (RS232), and synchronous serial interface module (SPI) - were used to control and communicate with peripheral devices. Two direct digital synthesizers (DDS) with analog outputs (AD9858 evaluation board and AD9833, Analog Devices, Inc.) were used for waveform generation; A multiplexer (AD8186, Analog Devices, Inc.) was used for signal conditioning; A gain and phase detector (AD8302, Analog Devices, Inc.), two programmable gain amplifiers (MCP6S21, Microchip Technology Inc.) and a buffer amplifier (TS925, STMicroelectronics) were used for signal processing; A LCDKBD1 (Micro/Sys Inc.) interface, a keypad (Keypad16, Micro/Sys Inc.), and a 2-line, 40-character LCD display (LC0240, Micro/Sys Inc.) were used for data display; A serial EEPROM (25AA1024, Microchip Technology Inc.) was used for data storage; A thermistor and a type-T thermocouple were used for temperature measurement. The functional diagram of the system is shown in Figure 4.4.

Figure 4.3 The new control box

Figure 4.4 Functional diagram of the control system

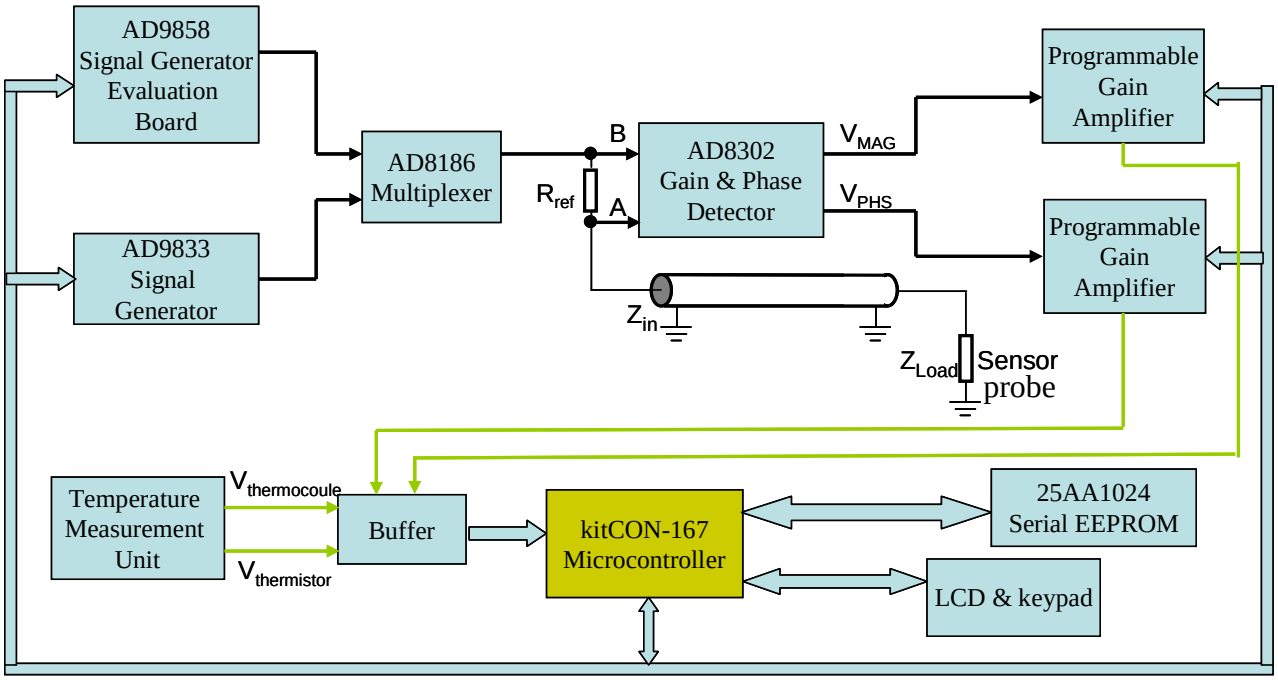

4.1.1 Microcontroller

A kitCON-167 microcontroller (PHYTEC America, LLC, 1999) was the core of the hardware, which controlled and communicated with peripheral devices. The connections between I/O ports of the microcontroller and peripheral devices are shown in Figure 4.5.

Figure 4.5 Connections between the I/O ports of microcontroller and peripheral devices

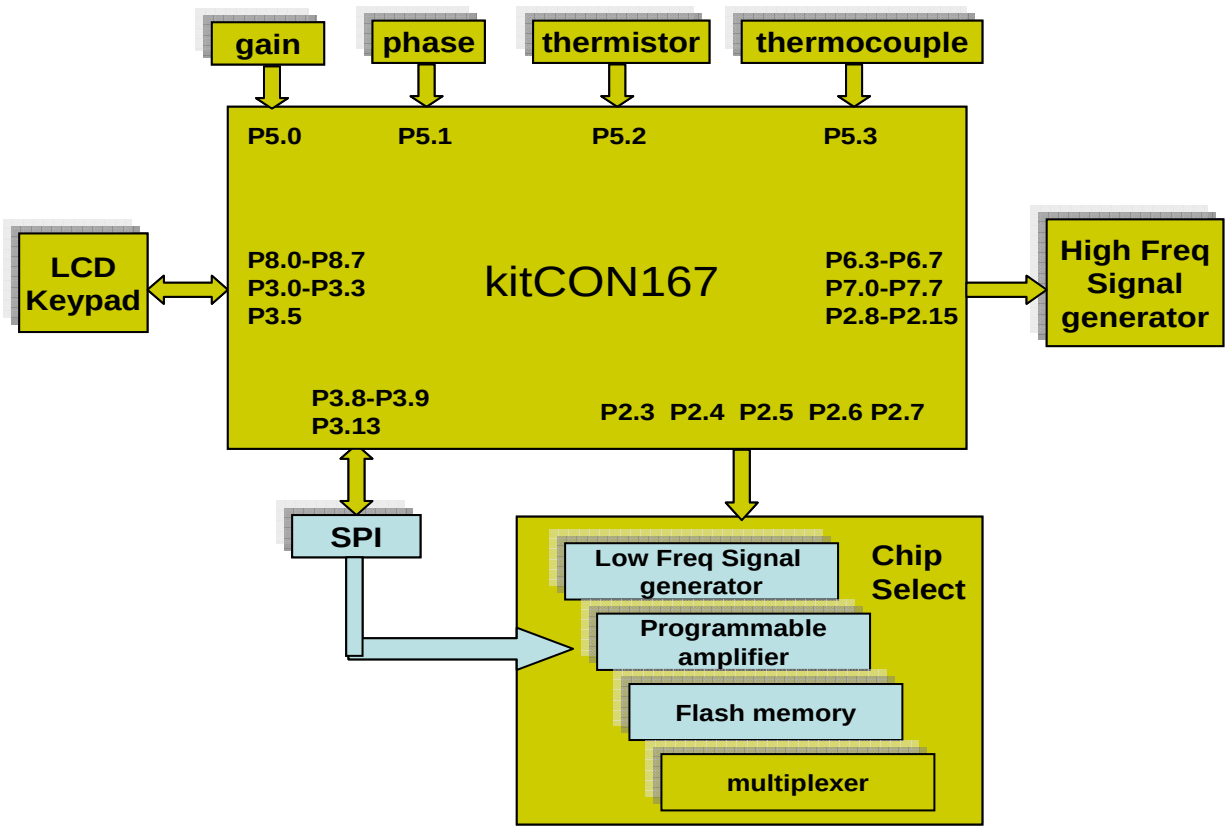

The kitCON-167 was an evaluation board for an Infineon C167CR microcontroller, which was one of the C16x-microcontroller family members in a MQFP-144 package (Infineon Technologies, 2001). C167CR was a high performance 16-bit CPU that combined many on-chip peripheral modules, including a 16-channel, 10-bit A/D converter with programmable conversion

time of 7.8us, two 16-channel capture and compare units, 4-channel PWM units, two serial channels, and a CAN interface with 15 message objects. C167CR can achieve 80/60 ns instruction cycle time at 25/33 MHz CPU clock. The memory space of the C167CR was configured in a Von Neumann architecture so that code memory, data memory, registers, and I/O ports were organized within the same 16 MByte linear address space. C167CR has a 16-priority-level interrupt system and up to 111 general purpose I/O lines, of which 47 I/O ports were used in this study.

The kitCON-167 featured 256 kByte flash, 64 kByte SRAM and 512 Byte serial EEPROM on the evaluation board. It allowed on-chip bootstrap loader, which was controlled by a bit of an 8-bit DIP-switch. The DIP-switch on the evaluation board allowed executions of different functions. In this study, switches 1, 2, and 3 were used. Switch 1 (Table 4.1) was used to control program online debugging or program offline executing. When switch 1 was on, the kitCON-167 was in program online debugging or downloading mode, otherwise, it was in the program execution mode.

Table 4.1 Boot-switch S3 (switch 1)

Boot-jumper	S3 switch 1
Bootstrap mode	On*
Normal program execution	Off

The C167CR provided up to five chip-select signals at Port P6 for easy selection of external peripherals or memory bank. For example, /CS0 (P6.0) was used to control the Flash devices on U8 and U9, whereas /CS1 (P6.1) was used to control the RAM on U10 and U11. By

default, P6.0-P6.4 can not be used for general purpose. However, in this study, P6.3 and P6.4 were used as a part of control ports for AD9858, which was used for waveform generation. Thereby, switches 2 and 3 (Table 4.2) had to be adjusted to the “on” state so that P6.3 and P6.4 can be used for general purpose.

Table 4.2 Chip-select signals S3 (switch 2 and 3)

Chip-Select Signals	S3 switch 2	S3 switch 3
Five (/CS0-/CS4)	OFF*	OFF*
Three (/CS0-/CS2)	ON	ON
Two (/CS0-/CS1)	OFF	ON
none	ON	OFF

All the I/O ports, as well as the data and address lines, extended from the microcontroller to the pins located at the center of the kitCON-167 evaluation board for convenient use. Each I/O port consisted of a data register, a direction control register and an open drain control register. The direction register was used to configure the port as input or output. The open drain control register was used to set the output driver in the push/pull or open drain mode. For the push/pull mode (Figure 4.6 (a)), a port output driver had an upper and a lower field-effect transistor; thus, it can actively drive the line either to a high or a low level. For the open drain mode (Figure 4.6 (b)), a port output can be connected with an external voltage through a pull-up resistor so that the high level can be controller by the external voltage. In this study, some of the kitCON-167 I/O ports were used to control AD9858 through a parallel interface. The kitCON-167 adopted 0-5V CMOS logic while the AD9858 used 0-3.3V with a maximum input current of 12uA. Therefore, the open-drain mode with an external voltage of 3.3V was used.

Figure 4.6 Output Drivers in Push/Pull and Open Drain Modes

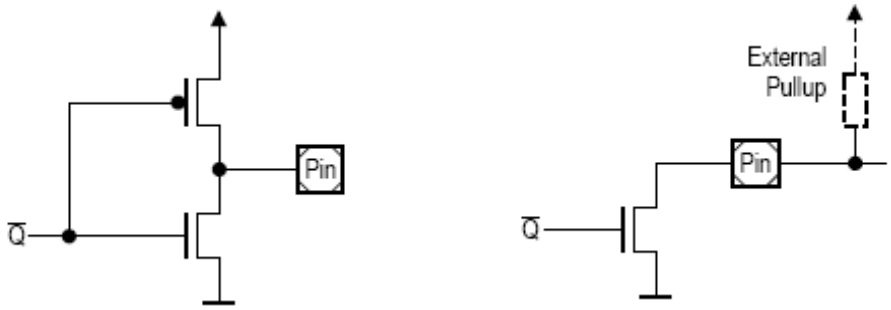

(a) Push/pull mode (b) Open drain mode

4.1.2 Signal generator

Two digital direct synthesizers were used for waveform generation. In order to increase the frequency range, an AD9858 (Analog Devices, Inc., 2003a) evaluation board, which can generate up to 400 MHz sinusoidal signals was adopted in this study. The output signal of the AD9858 was found noisy at frequencies below 1 MHz. To solve this problem, another digital direct synthesizer - AD9833 (Analog Devices, Inc., 2003b) - was used to generate sinusoidal signals with frequencies below 1MHz.

4.1.2.1 Low frequency signal generator

An AD9833 was adopted for generating sine wave signals with frequencies below 1 MHz. The output frequency was software programmable. The frequency registers was 28 bits and the frequency resolution was 0.1Hz. AD9833 needed a 25 MHz clock supplied to pin 5 - MCLK (Figure 4.7).

Figure 4.7 Connection diagram of AD9833

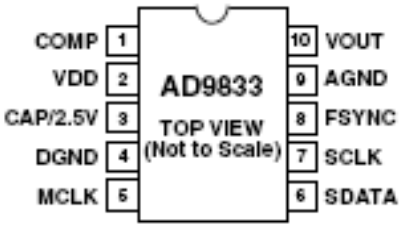

Commands for AD9833 were written via a standard 3-wire serial interface compatible with the SPI. The connection between AD9833 and kitCON-167 microcontroller is shown in Figure 4.8. P3.9 and P3.13 on port P3 of the kitCON-167 were operated in alternate functions so that port P3.9, which was Synchronous Serial Channel (SSC) with master transmit/slave receive (MTSR), drove the serial data line SDATA. Port P3.13 (SCLK) was a clock signal, which was set through the SSC Baud Rate register - SSCBR. The FSYNC pin was controlled by P2.6. When data was ready to be transmitted to AD9833, P2.6 was set to low; otherwise, P2.6 was always high.

Figure 4.8 Connections between kitCON-167 and AD9833

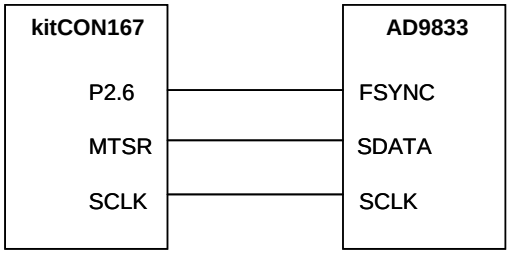

The desired frequency of the analog output signal from AD9833 is determined by:

$$f_{DESIRED} = f_{MCLK} / 2^{28} \times FREQTREG \qquad (4.2)$$

where f_{MCLK} =25 MHz, and

FREQTREG is the value loaded into the selected frequency register.

Thus, the value loaded into the selected frequency register can be derived from the following equation:

$$FREQTREG = f_{DESIRED} \times 2^{28} / f_{MCLK} \quad (4.3)$$

4.1.2.2 High frequency signal generator

An AD9858 DAC-output evaluation board was used for generating sine wave signals with frequencies higher than 1 MHz. The AD9858 evaluation board had three functions: direct digital synthesizer (DDS), analog mixer, and phase-locked loop (PLL). The latter two functions were not used in this study. The AD9858 board can generate analog sine waves of up to 400MHz when referenced to an external 1GHz clock input. The AD9858 also featured a divide-by-2 on the clock input, allowing the external clock to be as high as 2GHz. In this study, a 1GHz oscillator (Crystek Crystals Corporation, 2005) was used as an external reference clock. The minimum output power of the oscillator was 10dBm. For the reference clock, the input sensitivity was from -20dBm to +5dBm. Therefore, a 10dBm attenuator was connected to the output of the 1GHz reference clock oscillator.

AD9858 featured a 32-bit frequency tuning word, allowing a fine tuning resolution. The frequency tuning and control words can be loaded into the AD9858 via parallel (8-bit) or serial communication format. In this study, parallel communication format was selected. The interface consisted of 21 pins featuring an 8-bit data bus (D0-D7), a 6-bit address bus (A0-A5), RD, WR,

SPMODE, RESET, PS0, PS1 and FUD. The I/O port configuration of the kitCON167 for the AD9858 is shown in Table 4.3.

Table 4.3 I/O port configuration of kitCON167 for AD9858

kitCON-167 I/O port	Direction	Pins on interface	Function
P7.0-P7.7	Output	D0-D7	Data bus
P2.8-P2.13	Output	A0-A5	Address Bus
P2.14	Output	WR	Write bit
P2.15	Output	RD	Read Bit
P6.3	Output	PS0	Profile select
P6.4	Output	PS1	Profile select
P6.5	Output	RESET	Reset
P6.6	Output	FUD	Frequency update
P6.7	Output	SPMODE	Serial/Parallel communication

AD9858 had four user profiles (0-3), each of which can be selected by PS0 and PS1. The user can load different frequency tuning words into different profiles. Each profile may have its own frequency tuning word, which made it possible to change the frequency of the output signal at a high speed. In this study, only one user profile was used. Thus, a new frequency needed to be repeatedly written into the frequency tuning word register. The sine wave signal with the new frequency was then produced by strobing the frequency update pin (FUD).

AD9858 had an integrated 10-bit current output DAC. The full-scale current I_{OUT} was determined by an external resistor (R_{SET}) connected between the DACISET pin and the analog ground. The relationship between the R_{SET} and I_{OUT} is:

$$R_{SET} = 39.19 / I_{OUT} \qquad (4.4)$$

In order to provide the best spurious-free dynamic range performance, the AD9858 evaluation board limited the output to 20mA so that the value of R_{SET} was 1.98K. By observing output signals of AD9858, it was found that the amplitude of the output sinusoidal signal can reach 1V at some frequencies. However, the gain and phase detector following the signal generator allowed an input voltage range from -73dBV to -13dBV, which can be converted to 0.3 mV~ 320 mV. Therefore, the output amplitude of the AD9858 had to be attenuated to satisfy the input range requirement of the next stage. In this study, the 1.98K resistor on the AD9858 evaluation board was replaced by a 6K resistor so that I_{OUT} was reduced. The amplitude of the output signal, which was controlled by $I_{OUT,}$ was then decreased to satisfy the input requirement of the gain and phase detector.

4.1.3 Multiplexer

AD8186 (Analog Devices, Inc., 2003c) is a high speed, single-supply and triple 2-to-1 multiplexer (Figure 4.9). An AD8186 was used in this circuit to select from the two signal generators, AD9833 and AD9858.

Figure 4.9 Pin Diagram of AD8186

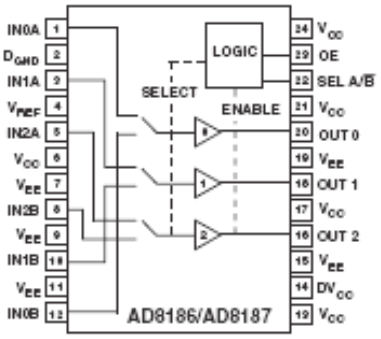

In this circuit, only one of the three 2-to-1 channel was used. The output-enable control pin (OE) was connected to a high level. An input was selected via the logic pin (SEL $A/\overline{B}$). The input signal for IN0A or IN0B was selected when SEL $A/\overline{B}$ was set to high or low, respectively.

Both input and output of the AD8186 can swing to within ~1.3V of either rail. This allowed the user 2.4V of dynamic range (1.3V~ 3.7V) for both input and output signals. For the output signals from both signal generators, the amplitude was lower than 1.3V. Therefore, an external reference voltage of 2.5V was applied to the V_{REF} pin of AD8186. This reference voltage raised the level of the input signal to satisfy the input requirement of AD8186. The 2.5V reference voltage was provided by a micropower voltage reference diode LM185-2.5 (National Semiconductor, 2008). Figure 4.10 is the schematic for the AD8186 multiplexer circuit.

Figure 4.10 Schematic for the AD8186 multiplexer circuit

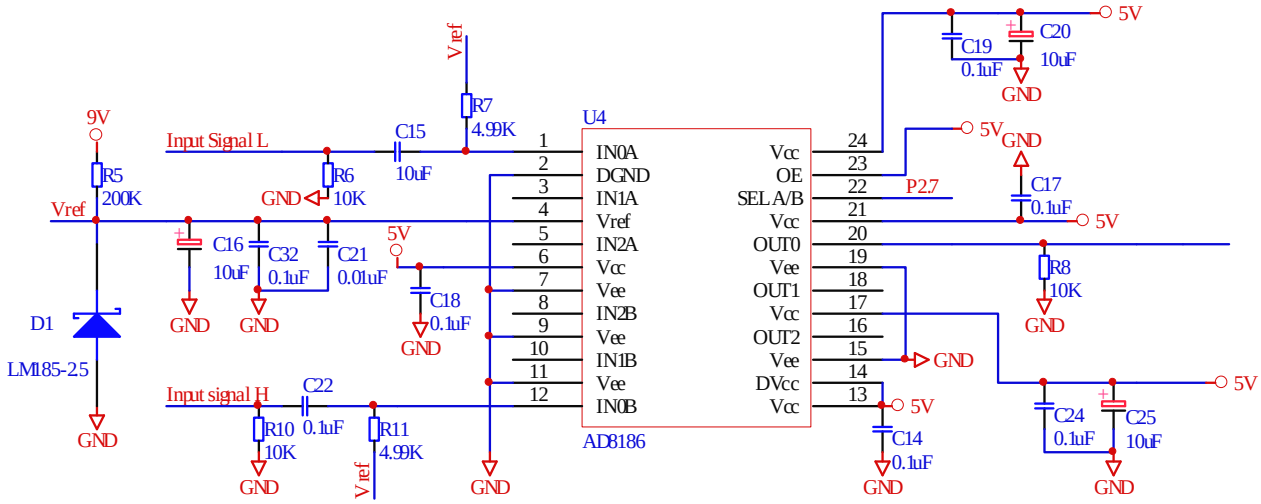

4.1.4 Gain and phase detector

AD8302 (Analog Devices, Inc., 2002) is a gain and phase detector, which was used to measure the magnitude ratio and phase difference between two input signals in channel A and channel B (Figure 4.11). The signal in channel B was from the signal generator selected by the multiplexer. The signal in channel A was the output of a voltage divider that consisted of a constant resistance R_{ref} and impedance Zin (Figure 4.11). It should be pointed out that this connection was reversed from that used in the old control box (Figure 4.1). Thus, in the new control box, the gain and phase detector measured FR of the following transfer function, which was different from that shown in Equation 4.1.

$$\frac{V_A}{V_B} = \frac{Z_{in}}{R_{ref} + Z_{in}} \tag{4.5}$$

Figure 4.11 Two input signals for the gain and phase detector

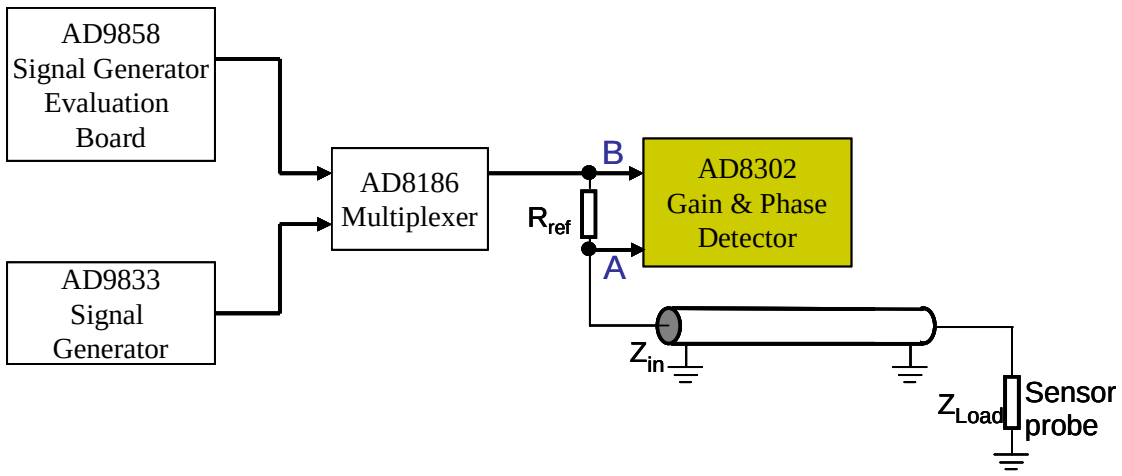

The ac-coupled input signal of AD8302 can range from -60dBm to 0dBm in a 50 Ω system, from low frequencies up to 2.7GHz. The output provided an accurate measurement of gain over a ±30 dB range scaled to 30mV/dB, and the phase over a 0°-180° range scaled to 10mV/degree. The gain and phase output voltages were simultaneously available at ground referenced outputs over the standard output range of 0 V to 1.8 V. The gain and phase output voltages V_{MAG} and V_{PHS} can be calculated by:

$$V_{MAG} = R_F I_{SLP} \log(V_{INA} / V_{INB}) + V_{CP} \quad (4.6)$$

$$V_{PHS} = -R_F I_{\Phi}(\left|\Phi(V_{INA}) - \Phi(V_{INB})\right| - 90^{\circ}) + V_{CP} \quad (4.7)$$

where $R_F I_{SLP}$ is 600mV/decade or 30mV/dB,

V_{CP} is 900mV, and

$R_F I_{\Phi}$ is 10mV/degree.

For the gain function (Equation 4.6), a range of -30dB to +30dB covered the full-scale swing from 0V to 1.8V, with a center point of 900mV for 0dB gain. For the phase function (Equation 4.7), with a center point of 900mV for 90°, a range of 0° to 180° covers the full-scale swing from 1.8 V to 0 V. The range of 0° to –180° covers the same full-scale swing but with the opposite slope (Figure 4.12).

Figure 4.12 Idealized transfer characteristics for the gain and phase measurement mode (Analog Devices, Inc., 2002)

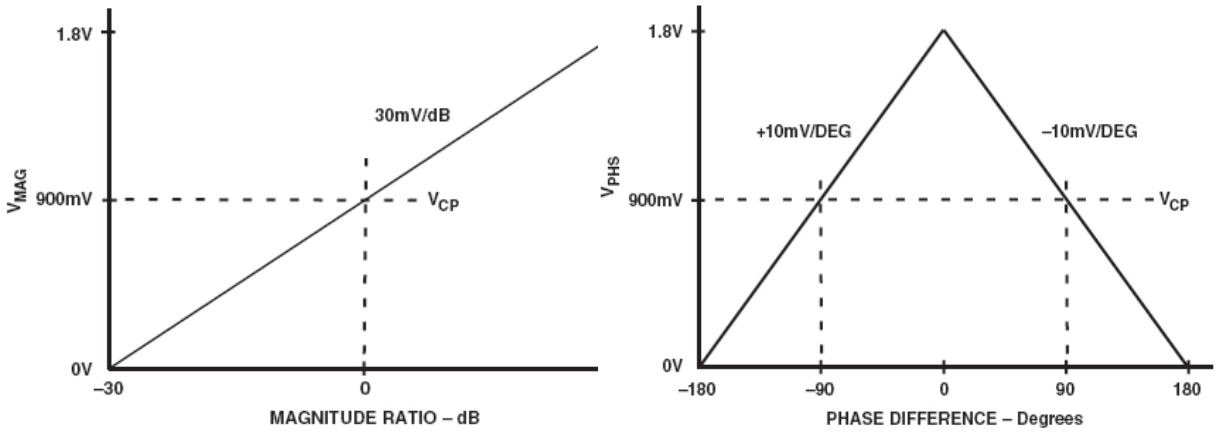

The gain function (Equation 4.7) indicated that V_{MAG} was determined by V_{INA}/V_{INB}. From Figure 4.11, it can be seen that the amplitude of the signal sent to channel A was always lower than that to channel B. Thus, the measured V_{INA}/V_{INB} would always be less than 1. As a result, the measured magnitude ratio would be in the range of -30 dB to 0dB and V_{MAG} would be in the range of 0V to 900mV.

Configurations of the two single-ended inputs of AD8302 are identical. Each consists of a driving pin (INPA or INPB), and an ac grounding pin (OFSA or OFSB) (Figure 4.13). For the grounding pins, the coupling capacitor (C_4 or C_6) has two functions: it provides ac grounding and sets the high-pass corner frequency for an internal offset compensation loop. An internal 10pF capacitor sets the maximum corner frequency to approximately 200MHz. The corner can be adjusted according the equation below:

$$f_{HP}\,(\text{MHz}) = 2/C_C\,(\text{nF}) \qquad (4.8)$$

where C_C is the total capacitance from OFSA or OFSB to ground , including the internal 10pF capacitor which is parallel with the capacitor connected between OFSA or OFSB to ground, and

f_{HP} is the corner frequency of the high pass filter (MHz).

In this study, 22uF capacitors were used for C_4 and $C_{6,}$ which lowered the corner frequency to 98Hz. To avoid measurement errors caused by mismatching external capacitances to the two signal inputs, 22uF capacitors were also used for C_1 and C_5 (Lee, 2005).

Figure 4.13 Basic connections in measurement mode with 30mV/dB and 10mV/degree scaling (Analog Devices, Inc., 2002)

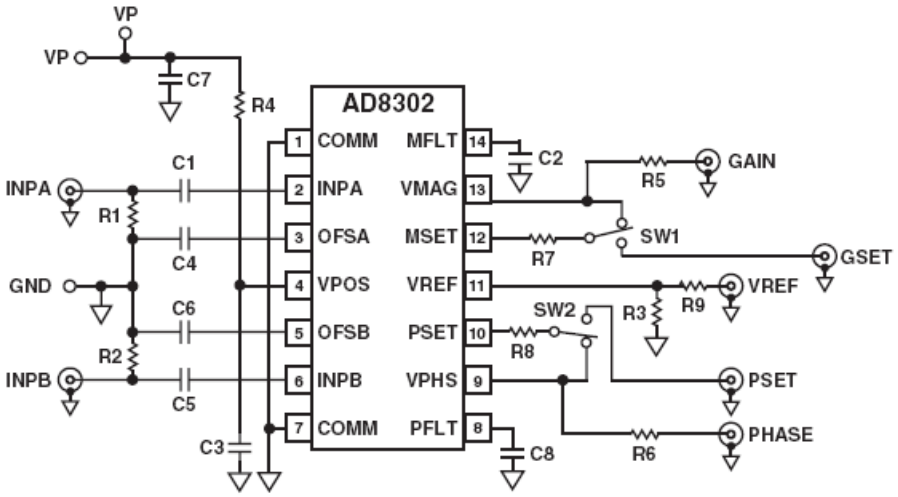

4.1.5 Programmable gain amplifier

In this study, to improve the resolution of the measured FR data, two single-ended, rail-to-rail input and output, and low gain analog programmable gain amplifiers MCP6S21

(Microchip Technology Inc., 2003) (Figure 4.14) were used to amplify the magnitude ratio and phase difference signals V_{MAG} and V_{PHS}, respectively. Reversing the input signals to the gain and phase detector in the design of the new control box (Figure 4.11) from that of the old control box (Figure 4.1) reduced the range of V_{MAG} to 0-900mV, thus allowing the V_{MAG} signal to be amplified to achieve a higher resolution.

Figure 4.14 Pin connection diagram of MCP6S21 (Microchip Technology Inc., 2003)

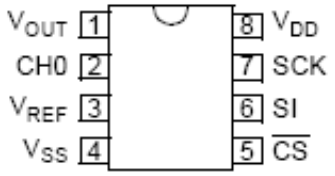

In this study, MCP6S21 PGA used a standard SPI-compatible serial interface to receive instructions from the kitCON-167 microcontroller (Figure 4.15). P3.9 and P3.13 on Port P3 of the kitCON-167 microcontroller were operated in alternate functions so that port P3.9 (MTSR), which was SSC with master transmit/slave receive, drove the serial data line SI. Port P3.13 (SCLK) was a clock signal, which was set through the register SSCBR. Ports P2.3 and P2.4 were used for chip select.

Figure 4.15 Interface connections between kitCON-167 and MCP6S21

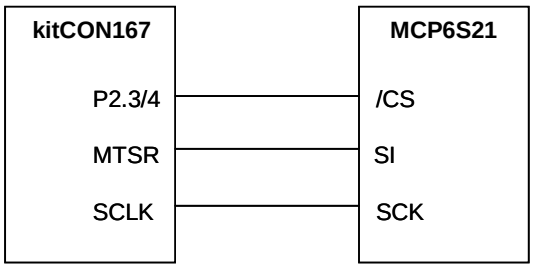

4.1.6 LCD and keypad

A keypad (Keypad16, Micro/Sys Inc., 2001) and a 2-line, 40-character LCD display (LC0240, Micro/Sys Inc., 2001) were added to the system to allow users to enter commands and to display the frequency response data with corresponding frequencies (Figure 4.16).

Figure 4.16 LCD and keypad

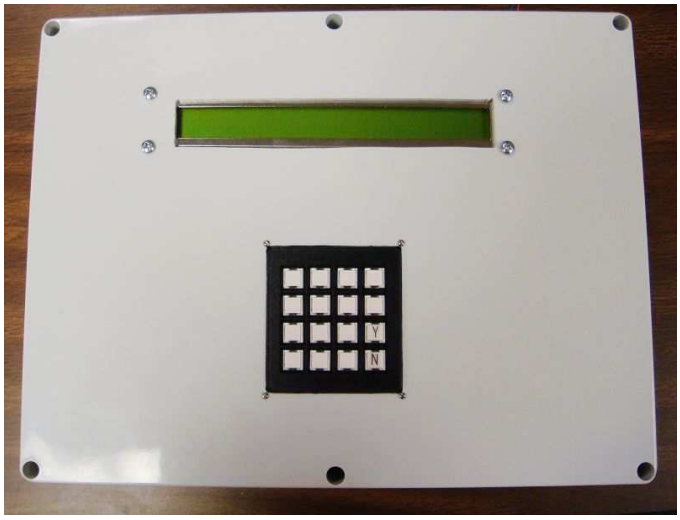

The LCD display and keypad were connected to an interface board (LCDKBD1, Micro/Sys Inc.), which was powered by +5V. Both the LCD and keypad were controlled by 26 digital I/O lines from the kitCON-167 microcontroller through a ribbon cable. Of the 26 lines, eight were used for a bi-directional data bus and five for additional control lines (Table 4.4). All keys on the keypad are de-bounced (Wang 2002).

Table 4.4 I/O function of kitCON-167 for the LCDKBD1

kitCON-167 I/O port	Function
P8.0-P8.7	Data & Address bus
P3.0	Write
P3.1	Strobe
P3.2	ACK
P3.3	ADDR
P3.5	BUSY

The instruction register and data register of the LCD display could be directly accessed by the digital I/O port of the microcontroller. The control signals were used to cause the LCDKBD1 to latch the data lines into various registers, to determine the direction of data transfer and to select operations as indicated in Table 4.5.

Table 4.5 LCDKBD1 address bus latch

Address Bus Latch Contents	Operation
0000	Read LCD status
0001	Read LCD data
0010	Write LCD command
0011	Write LCD data
0110	Read keypad data
0111	Write acknowledgement to keypad
1000	Write LCD data latch
1111	Idle/standby pattern

4.1.7 Temperature measurement

The real-time temperature measurement module consisted of a thermistor, a type-T thermocouple, and an amplifier. The thermistor was calibrated using a voltage divider formed by the thermistor and a 10k resistor. The Steinhart-Hart equation (Equation 4.9) was used to obtain the temperature from measured thermistor resistance. In order to determine the three coefficients constant A, B and C, the thermistor was measured at three temperatures: icepoint (0°C), room temperature (26°C), and boiling point (100°C).

$$\frac{1}{T} = A + B\ln R + C(\ln R)^3 \qquad (4.9)$$

where R is the resistance of thermistor (Ω),

T is the temperature to be measured (K), and

A, B and C are the coefficients.

The type-T thermocouples used in this study were inexpensive, rugged and reliable. They can be used over a wide temperature range from −200 to 350 °C. The temperature-emf relationship of a thermocouple was not linear. For the type-T thermocouple, a 7^{th} order polynomial provided a good fit for this relationship (Equation 4.10).

$$T = a_0 + a_1 x + a_2 x^2 + \ldots + a_7 x^7 \qquad (4.10)$$

where x is measured emf (V),

T is the measured temperature (°C), and

a_0=0.100860910, a_1=25727.94369, a_2=-767345.8295, a_3=78025595.81

a_4=-9247486589, a_5=6.97688E+11, a_6=-2.66192E+13, a_7=3.94078E+14

The sensitivity of a type-T thermocouple was about 43μV/°C. In this study, the emf signal from the thermocouple was to be sent to a 10-bit ADC module of the kitCON-167 microcontroller. With a 5V measurement range for single-ended analog signals, the resolution of the ADC was 4.9mv, which did not fit the small signals from the type-T thermocouple. Therefore, an amplifier AD623 (Analog Devices, Inc., 1999) was used to amplify the thermocouple signal.

AD623 is an integrated instrumentation amplifier that delivers rail-to-rail output swing (Figure 4.17). The $+V_s$ and $-V_s$ terminals were connected to +5V and 0V, respectively. The input signal, which can be either single-ended (tie –IN or +IN to ground) or differential, was amplified with a programmed gain. The amplified signal was the voltage difference between the OUTPUT pin and the externally applied reference voltage on the REF input.

Figure 4.17 Pin connection diagram of AD623 (Analog Devices, Inc.)

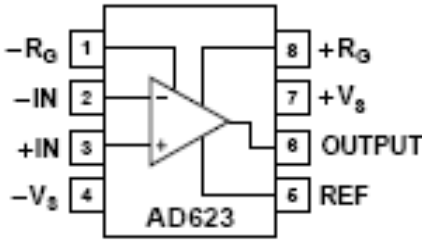

In this study, single +5V power was supplied. According to Table 4.6, the REF pin should be 2.5V. The 2.5V reference voltage was supplied by a micropower voltage reference diode LM185-2.5 (National Semiconductor, 2008). The gain of the amplifier was set by a resistor $R_{G,}$ which was connected between Pins 1 and 8 (Figure 4.17). For a gain below 118, R_G can be calculated using the following equation:

$$R_G = 100k\Omega/(G-1) \qquad (4.11)$$

In this study, R_G was chosen as 1 k so that the gain was 101.

Table 4.6 Maximum attainable gain and resulting output swing for different input conditions (Analog Devices, Inc., 1999)

V_{CM}	V_{DIFF}	REF Pin	Supply Voltages	Max Gain	Closest 1% Gain Resistor, Ω	Resulting Gain	Output Swing
0 V	±10 mV	2.5 V	+5 V	118	866	116	±1.2 V
0 V	±100 mV	2.5 V	+5 V	11.8	9.31 k	11.7	±1.1 V
0 V	±10 mV	0 V	±5 V	490	205	488	±4.8 V
0 V	±100 mV	0 V	±5 V	49	2.1 k	48.61	±4.8 V
0 V	±1 V	0 V	±5 V	4.9	26.1 k	4.83	±4.8 V
2.5 V	±10 mV	2.5 V	+5 V	242	422	238	±2.3 V
2.5 V	±100 mV	2.5 V	+5 V	24.2	4.32 k	24.1	±2.4 V
2.5 V	±1 V	2.5 V	+5 V	2.42	71.5 k	2.4	±2.4 V
1.5 V	±10 mV	1.5 V	+3 V	142	715	141	±1.4 V
1.5 V	±100 mV	1.5 V	+3 V	14.2	7.68 k	14	±1.4 V
0 V	±10 mV	1.5 V	+3 V	118	866	116	±1.1 V
0 V	±100 mV	1.5 V	+3 V	11.8	9.31 k	11.74	±1.1 V

4.1.8 Buffer amplifier

In this study, four voltage signals, including the gain and phase detector outputs, and signals from the thermistor and the thermocouple, needed to be delivered to the ADC of the kitCON-167 microcontroller. During circuit testing, it was found that the voltage signals delivered at the ADC ports were always lower than those observed at the previous stage in the signal conditioning circuit. For example, when the measured thermocouple signal at the output of the amplifier AD623 was 2.510V, the voltage measured at port P5.3 of the ADC was 2.497V. Similar reduction could be observed on other three voltage signals. This was probably caused by the fact that the output impedances of the amplifiers were not sufficiently low and the input impedance of the ADC module of kitCON167 was not sufficiently high. To solve this problem, a voltage buffer TS925 (STMicroelectronics, 1999) was added on each ADC channel. TS925 is a

rail-to-rail, quad BiCMOS operational amplifier (Figure 4.18). It featured high output current which allowed driving load with input impedance of as low as 32Ω.

Figure 4.18 Pin connection diagram of TS925 (STMicroelectronics, 1999)

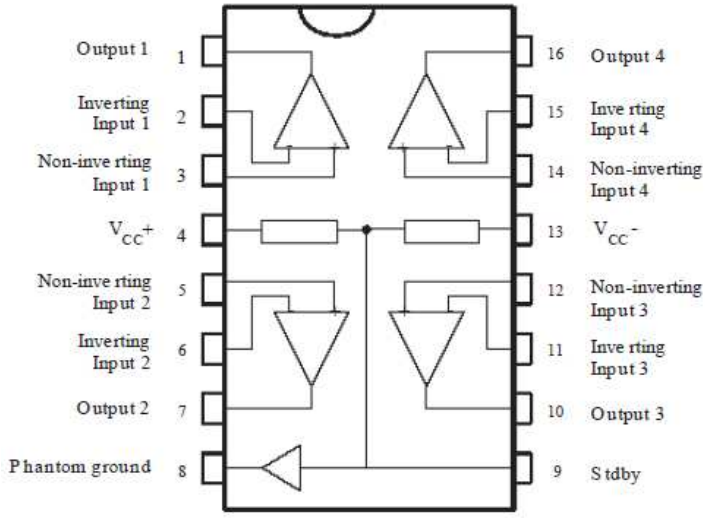

4.1.9 Serial EEPROM

A 512 Byte serial EEPROM on the kitCON-167 microcontroller evaluation board was too small to store the frequency response data. Therefore, a serial EEPROM 25AA1024 (Microchip Technology Inc., 2006) with 1Mbit was added to the system. The 25AA1024 serial EEPROM allowed 20MHz maximum clock speed and adopts the low-power CMOS technology. The memory was accessed via a SPI compatible serial bus which can be controlled by the kitCON-167 microcontroller. The SPI signal consisted of a clock input (SCK) and separate data-in (SI) and data-out (SO) lines. Access to the device was controlled by a chip select (CS) input. The connection between kitCON-167 and serial EEPROM is shown in Figure 4.19. P3.8, P3.9 and P3.13 on Port P3 of the kitCON-167 microcontroller were operated in alternate functions so that port P3.9 (MTSR), which was SSC with master transmit/slave receive, drove the serial data line SI. Port P3.8, which was SSC with master receive/slave transmit (MRST), was driven by the

serial data line SO. Port P3.13 (SCLK) was a clock signal, which was set through the register SSCBR.

Figure 4.19 Connections between kitCON-167 and 25AA1024

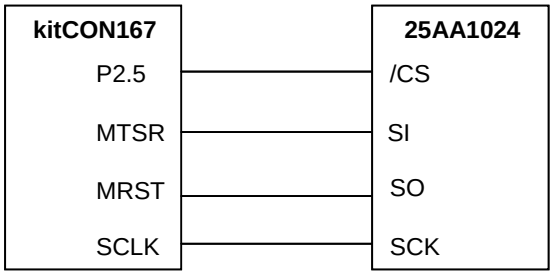

4.2 System Software Design

A C program was written for the kitCON-167 microcontroller to control the system. The program was complied, debugged and downloaded in the Tasking EDE.

4.2.1 Low frequency signal generator

An AD9833 was used to generate sinusoidal signals with user selected frequencies below 1MHz. The frequency of signal was determined by a 28-bit frequency tuning word and a system clock. The frequency tuning word is related to the frequency by:

$$F_o = \frac{FTW \times SYSCLK}{2^N} \qquad (4.12)$$

where F_0 = selected frequency,

FTW = frequency tuning word,

SYSCLK= system clock (25MHz), and

N= 28.

AD9833 contains a 16-bit control register and two 28-bit frequency registers. Table 4.7 describes functions of the control bits. Table 4.8 is a description of the frequency register.

Table 4.7 Function of Control Bits of the control register in AD9833

(Analog Devices, Inc., 2003b)

Bit	Name	Function
D15	0	To inform the AD9833 that the contents of the control register will be altered, D15 and D14 must be set to 0.
D14	0	
D13	B28	B28=1 allows a complete word to be loaded into a frequency register in two consecutive writes. The first write contains the 14 LSBs of the frequency word, and the next the 14 MSBs. B28=0, the 28-bit frequency register operates as two 14-bit registers, one containing the 14 MSBs and the other 14 LSBs. The 14 MSBs of the frequency word can be altered independent of the 14 LSBs, and vice versa.
D12	HLB	This control bit allows the user to continuously load the MSBs or LSBs of a frequency register while ignoring the remaining 14 bits. D13 (B28) must be set to 0 to be able to change the MSBs and LSBs separately. When D13 (B28) =1, this control bit is ignored. HLB=1 allows a wirte to the 14 MSBs of the addressed frequency register HLB=0 allows a wirte to the 14 LSBs of the addressed frequency register
D11	FSELECT	The bit defines whether the FREQ0 register or the FREQ1 register is used in the phase accumulator.
D10	PSELECT	The bit defines whether the PHASE0 register or the PHASE1 register data is added to the output of the phase accumulator.
D9	Reserved	This bit should be set to 0
D8	RESET	RESET = 1 resets internal registers to 0, which corresponds to an analog output of midscale. RESET =0 disables RESET.
D7	SLEEP1	SLEEP1 =1, the internal MCLK clock is disabled, the DAC output will remain at its present value as the NCO is no longer accumulating. SLEEP1 =0, MCLK is enabled.
D6	SLEEP12	SLEEP12 = 1 powers down the on-chip DAC. SLEEP12 = 0 implies that the DAC is active.
D5	OPBITEN	This bit, in association with D1 (MODE), is to control what is output at the VOUT pin. When OPBITEN=1, the output of the DAC is no long available at the VOUT pin. Instead, the MSB (or MSB/2) of the DAC data is connected to the VOUT pin. When OPBITEN=0, the DAC is connected to VOUT. The MODE bit determines whether it is a sinusoidal or a ramp output.
D4	Reserved	This bit must be set to 0.
D3	DIV2	DIV2 is used in association with D5 (OPBITEN) When DIV2=1, the MSB of the DAC data is passed directly to the VOUT pin When DIV2=0, the MSB/2 of the DAC data is output at the VOUT pin.
D2	Reserved	This bit must be set to 0.
D1	MODE	This bit is used in association with D5 (OPBITEN). When MODE=1, the output from the DAC is a triangle signal. When MODE=0, the output is a sinusoidal signal.
D0	Reserved	This bit must be set to 0.

Table 4.8 Frequency Register Bits in AD9833 (Analog Devices, Inc., 2003b)

D15	D14	D13		D0
0	1	MSB	14 FREQ0 REG Bits	LSB
1	0	MSB	14 FREQ1 REG Bits	LSB

AD9833 allowed two write operations to load a complete 16-bit word into either of the frequency registers selected by bit DB13. When bit DB13 was set to 1, it allowed a complete word to be loaded into a frequency register in two consecutive writes. The first write contained the 14 LSBs of the frequency word, and the next write the 14MSBs. The first two bits D15 and D14 of each 16-bit word (Table 4.8) decide to which frequency register the word was loaded and, therefore, they should be the same for both of the consecutive writes. When bit DB13 was set to 0, it indicated the 28-bit frequency register can be operated as two 14-bit registers, one containing the 14 MSBs and the other one containing the 14 LSBs. Thus, the 14 MSBs of the frequency word can be altered independently from the 14 LSBs, and vice versa. In this study, the two consecutive writes mode was selected. Therefore, DB13 was set to 1. The control bit DB12 allowed users to continuously load the MSBs or LSBs of a frequency register while ignoring the remaining 14 bits. It is only useful when DB13 is set to 0. Therefore, DB12 was ignored in this study. The control bit DB11, which is named FSELECT, defines whether the FREQ0 register or the FREQ1 register is used. In this study, it was set to 0 to select the frequency register 0. Bits DB10, DB7, DB6, DB5, DB3 and DB1 were set to 0 in this study.

Both the control and frequency register bits were accessed via a standard 3-wire serial interface compatible with SPI. Port P3.9 and P3.13 of kitCON-167 were set to the alternate functions, which provided flexible, high-speed serial communication with SPI-compatible

devices. The operation mode of the serial channel was controlled by its bit-addressable control register SSCCON (Table 4.9).

Table 4.9 SSCCON register for the synchronous serial interface of C167CR (Infineon technologies, 2000)

Bit	Name	Function (Programming mode, SSCEN = '0')
0-3	SSCBM	SSC data width selection
4	SSCHB	SSC heading control bit
5	SSCPH	SSC clock phase control bit
6	SSCPO	SSC clock polarity control bit
7	-	
8	SSCTEN	SSC transmit error enable bit
9	SSCREN	SSC receive error enable bit
10	SSCPEN	SSC phase error enable bit
11	SSCBEN	SSC baudrate error enable bit
12	SSCAREN	SSC automatic reset enable bit
13	-	
14	SSCMS	SSC master select bit
15	SSCEN	SSC enable bit

The serial channel was disabled by setting SSCEN to 0, which provided access to a set of control bits for programming. In this study, when initializing serial communication, the register SSCCON was set to 0x407F, which selected the following settings: 16 bit transfer data width (bit 0,1,2 and 3), transmit/receive MSB first (bit 4), latch receive data on leading clock edge, shift on trailing edge (bit 5); idle clock line is high, leading clock edge is high-to-low transition (bit 6); ignore transmit errors, receive errors, phase errors and baud rate errors (bit 8,9,10 and 11); master mode, which generated shift clock and output it via SCLK (bit 14). After setting the control register, the SSCEN bit was set to 1 to enable serial communication.

In this study, 25 frequencies were selected within the range of 200 Hz to 1 MHz: five frequencies in a linear scale from 200 Hz to 1 kHz at 200Hz intervals, twenty frequencies in a base-10 log scale from 1 kHz to 1 MHz. After the sine wave signal was generated at each frequency, a wait command with a waiting period 100msec was issued to allow the generated signals to be stabilized. The flow chart for AD9833 control is shown in Figure 4.20.

Figure 4.20 Flow chart for the AD9833 signal generator

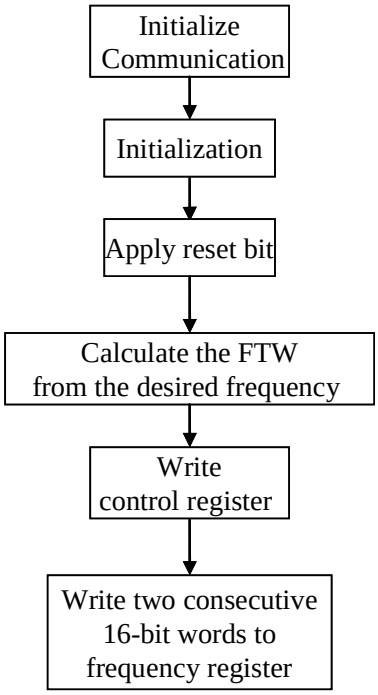

4.2.2 High frequency signal generator

An AD9858 evaluation board was used to generate sinusoidal signals with user-selected frequencies within the range of 1 MHz to 400 MHz. Frequencies of generated sinusoidal signals were determined by a 32-bit frequency tuning word and a 1 GHz system clock. The desired frequency was converted into the frequency tuning word (FTW), which can be written to the FTW register followed by a frequency update. The relationship between the desired frequency

and the frequency tuning word was identical with that for the low frequency signal generator AD9833 (Equation 4.12)

In this study, 499 frequencies were selected in a linear scale from 1.6 MHz to 400 MHz with a 0.8 MHz interval. The waiting period between two frequencies was 100ms. AD9858 had three modes of operation: single tone, frequency sweeping, and full sleep. In this study, the single tone mode was used by programming frequency tuning word at parallel addresses from 0x0A to 0x0D (Table 4.10).

Table 4.10 Register map for AD9858 (Analog Devices, Inc. 2003)

Register Name	Address Ser	Address Par	(MSB) Bit7	Bit6	Bit5	Bit4	Bit3	Bit2	Bit1	(LSB) Bit0	Default value	Pro-file
Control Function Register (CFR)	00x00	0x00 <7:0>	Not Used	2Ghz Divider Disable	SYNCLK Out Disable	Mixer PwrDown	Phase Detect PwrDwn	Power Down	SDIO input Only	LSB First	0x18	N/A
		0x01 <15:8>	Freq. Sweep Enable	Enable Sine Output	Charge Pump Offset Bit	Phase Detector Divider Ratio (N)		Charge Pump Polarity	Phase Detector Divider ratio(M)		0x00	N/A
		0x02 <23:16>	AutoClr Freq. Accum	AutoClr Phase Accum	Load Delta-Freq Timer	Clear Freq Accum	Clear Phase Accum	Open	Fast-Lock Enable	Don't Use FTW For Fast-Lock	0x00	N/A
		0x03 <31:24>	Frequency Detect Charge Pump Current		Final Closed-Loop Charge Pump Current			Wide Closed-Loop Charge Pump Current			0x00	N/A
Delta-Freq Tuning Word	0x01	0x04	Delta Frequency Word <7:0>								-	
		0x05	Delta Frequency Word <15:8>								-	
		0x06	Delta Frequency Word <23:16>								-	
		0x07	Delta Frequency Word <31:24>								-	
DFRRW	0x02	0x08	Delta Frequency Ramp Rate word <7:0>								-	
		0x09	Delta Frequency Ramp Rate word <15:8>								-	
Frequency Tuning Word No.0	0x03	0x0A	Frequency Tuning Word No.0 <7:0>								0x00	0
		0x0B	Frequency Tuning Word No.0 <15:8>								0x00	0
		0x0C	Frequency Tuning Word No.0 <23:16>								0x00	0
		0x0D	Frequency Tuning Word No.0 <31:24>								0x00	0
Phase Offset Word 0	0x04	0x0E	Phase offset Word No.0<7:0>								0x00	0
		0x0F	Not Used	Not Used	Phase offset Word No.0 <13:8>						0x00	0
Frequency Tuning Word No.1	0x05	0x10	Frequency Tuning Word No.1 <7:0>								-	1
		0x11	Frequency Tuning Word No.1 <15:8>								-	1
		0x12	Frequency Tuning Word No.1 <23:16>								-	1
		0x13	Frequency Tuning Word No.1 <31:24>								-	1
Phase Offset Word 1	0x06	0x14	Phase Offset Word No.1 <7:0>								-	1
		0x15	Not Used	Not Used	Phase Offset Word No.1 <13:8>						-	1
Frequency Tuning Word No.2	0x07	0x16	Frequency Tuning Word No.2 <7:0>								-	2
		0x17	Frequency Tuning Word No.2 <15:8>								-	2
		0x18	Frequency Tuning Word No.2 <23:16>								-	2
		0x19	Frequency Tuning Word No.2 <31:24>								-	2
Phase Offset Word 2	0x08	0x1A	Phase Offset Word No.2 <7:0>								-	2
		0x1B	Not Used	Not Used	Phase Offset Word No.2 <13:8>						-	2
Frequency Tuning Word No.3	0x09	0x1C	Frequency Tuning Word No.3 <7:0>								-	3
		0x1D	Frequency Tuning Word No.3 <15:8>								-	3
		0x1E	Frequency Tuning Word No.3 <23:16>								-	3
		0x1F	Frequency Tuning Word No.3 <31:24>								-	3
Phase Offset Word 3	0x0A	0x20	Phase Offset Word No.3 <7:0>								-	3
		0x21	Not Used	Not Used	Phase Offset Word No.3 <13:8>						-	3
Reserved	0x0B	0x22	Reserved, Do Not Write, Leave at 0xFF								0xFF	N/A
		0x23	Reserved, Do Not Write, Leave at 0xFF								0xFF	N/A

A flow chart for the section of the control program that generates 499 frequencies using the AD9858 signal generator is shown in Figure 4.21.

Figure 4.21 Flow chart for the AD9858 signal generator

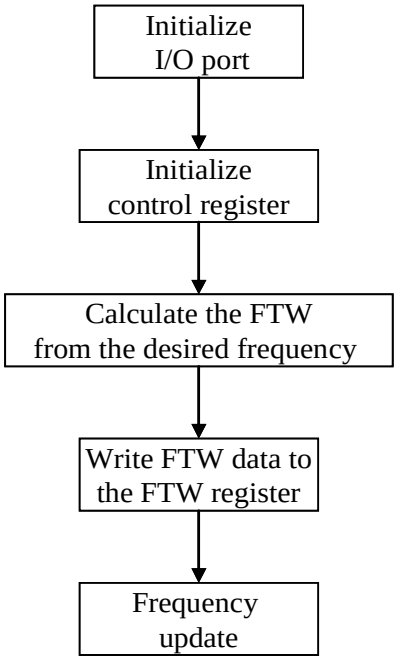

4.2.3 A/D module

The C167CR microcontroller provided an Analog/Digital Converter with 10-bit resolution and an on-chip sample & hold circuit, which can be accessed via Port 5 set to the alternate functions. The analog data from the outputs of the gain and phase detector were sent to the A/D converter in the "auto scan, single conversion mode", which automatically converted a sequence of analog signals beginning at port P5.3 and ending at P5.0. The converted data were recorded when an interrupt request flag was set high at the end of A/D conversion. The result of a conversion was stored in bit field ADRES of the 16-bit result register ADDAT, as shown in Table 4.11. The higher four bits of the register ADDAT (CHNR) are used to identify the analog channels.

Table 4.11 ADC result register of C167CR (Infineon technologies, 2000)

Bit	Name	Function
0-9	ADRES	A/D conversion result The 10-bit digital result of the most recent conversion.
10	-	
11	-	
12-15	CHNR	Channel number (identifies the converted analog channel)

4.2.4 Programmable gain amplifier

To improve the resolution of measured FR data, two programmable gain amplifiers MCP6S21 were used to amplify the outputs of the gain and phase detector. The amplifiers were controlled via standard, SPI compatible serial communication. The communication initialization was similar to that for the low frequency signal generator (Section 4.2.1). The amplifiers were programmed using a 16-bit word, which was sent into the amplifier through the pin (SI) of MCP6S21 (Section 4.1.5). The first byte of the 16-bit word was the instruction byte, which went into the instruction register. The second byte was determined by the indirect address bit A0 in the instruction register (Table 4.12).

Table 4.12 Instruction register of MCP6S21 (Microchip Technology Inc., 2003)

Bit	Name	Function
Bit 7	M2	M2-M0 are the command bits that determine the following functions: 000=NOP (Default); 001= PGA enters Shutdown Mode once a full 16-bit word is sent and /CS is raised; 010= Write to register; 011 and 1xx= NOP
Bit 6	M1	
Bit 5	M0	
Bit 4	-	Unimplemented: read as 0
Bit 3	-	
Bit 2	-	
Bit 1	-	
Bit 0	A0	A0 is the indirect Address Bit: 1=Addresses the Channel Register 0=Addresses the Gain Register (Default)

In this study, bits M2 to M0 were assigned 001, which let the program gain amplifier enter the shutdown mode as soon as a full 16-bit word is sent and the chip select pin (/CS) is set to high. The shutdown mode puts the amplifier to a low power mode. In this mode, the internal registers maintain their values until either a valid command is sent to the device or the device is powered down and backed up again. Bit A0 was set to 0 so that the second byte of the 16-bit word goes to the gain register (Table 4.13).

Table 4.13 Gain register of MCP6S21 (Microchip Technology Inc., 2003)

—	—	—	—	—	G2	G1	G0
bit 7							bit 0

In the gain register, bits G2 to G0 are gain select bit to define the gain whereas bits 3 to 7 were not used. The gain of the amplifier can be set between +1V/V and +32V/V through programming bits G0 - G2 (Table 4.14).

Table 4.14 Gain selected bits of MCP6S21 (Microchip Technology Inc., 2003)

G2	G1	G0	Gain
0	0	0	1
0	0	1	2
0	1	0	4
0	1	1	5
1	0	0	8
1	0	1	10
1	1	0	16
1	1	1	32

4.2.5 Serial EEPROM

A serial EEPROM 25AA1024 was added to the system for data storage. It contains an 8-bit instruction register and a 24-bit address, with seven MSBs being “don’t care” bits. The instruction set is listed in Table 4.15.

Table 4.15 Instruction set (Microchip Technology Inc., 2006)

Instruction Name	Instruction Format	Description
READ	0000 0011	Read data from memory array beginning at selected address
WRITE	0000 0010	Write data to memory array beginning at selected address
WREN	0000 0110	Set the write enable latch (enable write operations)
WRDI	0000 0100	Reset the write enable latch (disable write operations)
DRSR	0000 0101	Read STATUS register
WRSR	0000 0001	Write STATUS register
PE	0100 0010	Page Erase-erase one page in memory array
SE	1101 1000	Sector Erase-erase one sector in memory array
CE	1100 0111	Chip Erase-erase all sectors in memory array
RDID	1010 1011	Release from Deep power-down and read electronic signature
DPD	1011 1001	Deep Power-Down mode

For reading data from the serial EEPROM, the chip select pin needed to be pulled low so that the device is selected. Then the 8-bit READ instruction was sent to the 25AA1024 followed by a 24-bit address. After the correct READ instruction and address were sent, the data stored in the memory at the selected address was shifted out on the SO pin (Figure 4.22).

For writing data into the memory, the write enable latch must be set prior to a write command. Once the write enable latch was set, the chip select pin needed to be set low. The WRITE instruction was sent to the 25AA1024, followed by the 24-bit address, and then the data was written via the SPI serial data input SI (Figure 4.23).

Figure 4.22 Read sequence of 25AA1024 (Microchip Technology Inc., 2006)

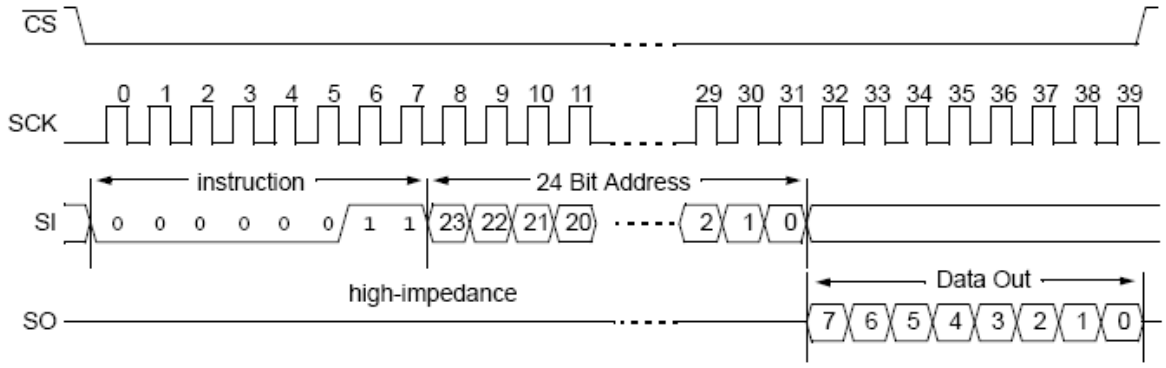

Figure 4.23 Byte write sequence of 25AA1024 (Microchip Technology Inc., 2006)

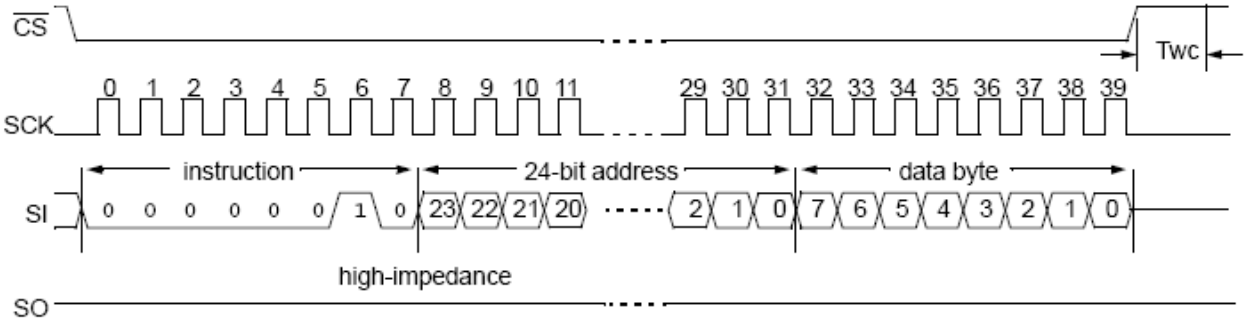

4.2.6 Microcontroller

A C program in machine-readable format was downloaded to the flash memory of kitCON-167 microcontroller using the FlashTools 16W via serial interface. The program was set to run three times for each measurement. The measured FR data were delivered to a PC through RS232 serial interface. The HyperTerminal tool available under the windows operation system was responsible for accepting the data and saving it in text files in the PC. The flow chart for control program written for the kitCON-167 microcontroller is shown in Figure 4.24.

Figure 4.24 Flow chart of the microcontroller program

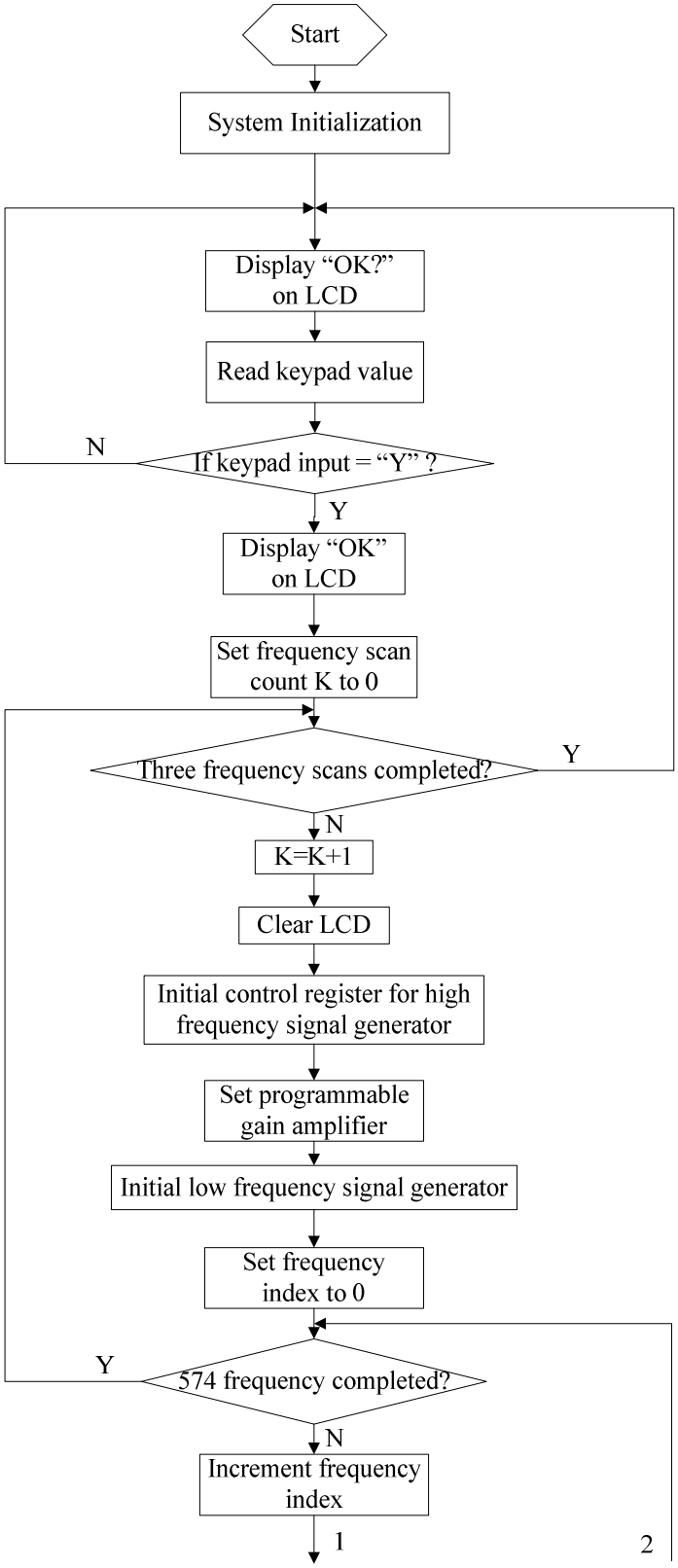

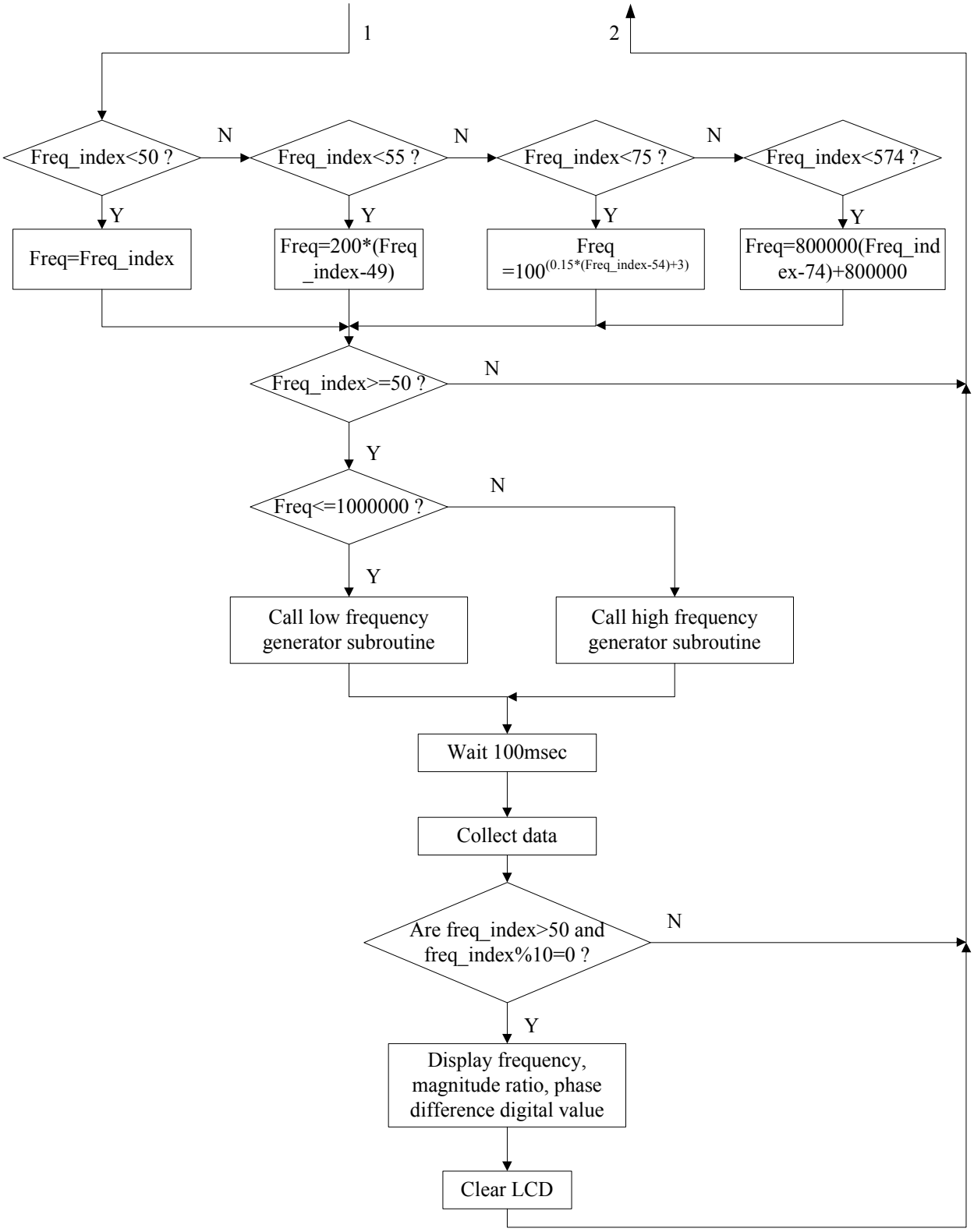
1
2
Freq_index<50 ?
N
Freq_index<55 ?
N
Freq_index<75 ?
N
Freq_index<574 ?
Y
Y
Y
Y
Freq=Freq_index
Freq=200*(Freq_index-49)
Freq =100^(0.15*(Freq_index-54)+3)
Freq=800000(Freq_index-74)+800000
Freq_index>=50 ?
N
Y
Freq<=1000000 ?
N
Y
Call low frequency generator subroutine
Call high frequency generator subroutine
Wait 100msec
Collect data
Are freq_index>50 and freq_index%10=0 ?
N
Y
Display frequency, magnitude ratio, phase difference digital value
Clear LCD

CHAPTER 5 - Impedance Transformation Models

Permittivity is a property of dielectric materials. Permittivity relates to a material's ability to conduct AC currents. When a probe is immersed in a dielectric material, the permittivity and corresponding admittance of the probe becomes a measure of how easily a current can flow through the dielectric material within the probe. Thus, permittivity of the dielectric material can be found by measuring the admittance of a probe immersed in the material and then removing the geometric factor. Impedance is the reciprocal of admittance and, therefore, permittivity of the dielectric material also can be found by measuring the impedance of the probe immersed in the material and then removing the geometric factor.

In this study, impedance of the sensor probe was derived from measured FR data. To study the probe impedance, impedance transformation models for the sensor probe, the coaxial cable that connects the control system with the sensor probe and the signal processing circuit were investigated.

5.1 Transmission line theory

5.1.1 Introduction of transmission line theory

A transmission line is used to guide energy in the form of electromagnetic waves, acoustic waves, or electric power, from the source to the receiver. In many electric circuits, transmission wires connecting various components can be generally neglected, because the voltage at each point along the wire can be considered identical at a given time due to the short

lengths of the wires. However, if the wires are sufficiently long and the frequency is sufficiently high so that voltages along the wire at a given time can no longer be considered identical, the transmission line becomes important (Coleman, 2004). A rule-of-thumb commonly used is that, when the length of a wire is greater than 1/10 of the wavelength, the wire should be treated as a transmission line. If a design ignores the transmission line effect when it should be considered, signal reflection along the wires and cables would result in significant variations in the impedance present at different points on the line. In the transmission line theory, models for coaxial cables and twin parallel wires are the most common models in circuit analysis. In this study, a coaxial cable connecting the control box with the permittivity sensor probe was studied.

5.1.2 Coaxial cable

Coaxial cables (C1166 RG 58/U) of different lengths were used to connect the control box with the sensor probe. The shortest cable used in this study was 33cm. The highest frequency of the signal from the signal generator was 400 MHz. One tenth of its wavelength was 5cm after accounting for a relative propagation velocity of 0.66. Therefore, it was necessary to study the transmission line losses along the cable.

To simplify the analysis, a coaxial cable can be considered as a distribution of discrete capacitances and inductances, as shown in Figure 5.1.

Figure 5.1 Distributed impedance model for a transmission line (Coleman, 2004)

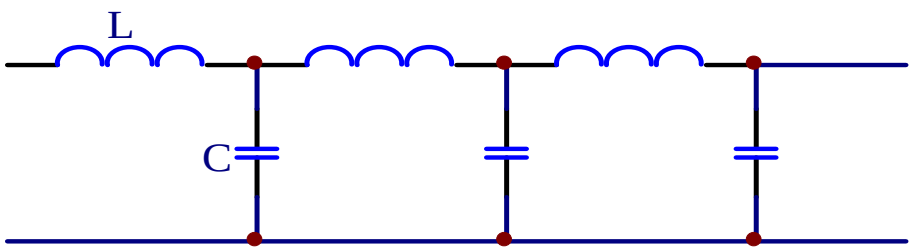

The inductances and capacitances in Figure 5.1 can be determined by Equation 5.1 and 5.2, respectively.

$$L = \frac{\mu}{2\pi} \ln(\frac{b}{a}) \quad (5.1)$$

$$C = \frac{2\pi\varepsilon}{\ln(\frac{b}{a})} \quad (5.2)$$

where L is the inductance per unit length of the cable,

C is the capacitance per unit length of the cable,

ε is the permittivity of the medium between the conductors,

μ is the permeability of the medium between the conductors,

b is the outer diameter of the cable, and

a is the inner diameter of the cable.

The characteristic impedance of the transmission line can be derived from the inductance and capacitance per unit length of the cable.

$$Z_0 = \sqrt{L/C} \quad (5.3)$$

where Z_0 is the characteristic impedance of the transmission line

For a transmission line of length *l* terminated with a load, if a sinusoidal with voltage V^+ is launched into an end of the line, a portion of the power will be absorbed by the load and the remaining power will be reflected back through the line. The voltage of the reflected sinusoidal can be expressed by:

$$V^- = \Gamma V^+ \qquad (5.4)$$

where V^+ is the input voltage,

V^- is the reflected voltage, and

Γ is the reflection coefficient.

In Equation 5.4, all quantities are complex. Thus, both phase changes and amplitude information are included.

The reflection coefficient Γ_L at a general load Z_L can be acquired by:

$$\Gamma_L = \frac{Z_L - Z_0}{Z_L + Z_0} \qquad (5.5)$$

where Γ_L is the reflection coefficient at a general load Z_L, and

Z_L is the impedance of the load.

Power will not be reflected back when $\Gamma_L = 0$. Under this condition, $Z_L = Z_0$, and the load is said to be matched to the line. However, in general, $Z_L \neq Z_0$ and a portion of the signal is reflected. Moreover, due to phase variation along the line, which is caused by time delays in signal propagation, the ratio of V^- to V^+ changes in phase. Thus, the reflection coefficient

looking into the transmission line Γ_{in} is different from that looking into the load Γ_L. The relationship between Γ_{in} and Γ_L is

$$\Gamma_{in} = \Gamma_L \exp(-2j\beta l) \qquad (5.6)$$

where β is the propagation constant, and

l is the length of the transmission line.

From Equation 5.6, it can be seen that the magnitude of the reflected wave remains the same, while the phase changes. Since Γ_{in} is different from Γ_L, the impedance looking into the transmission line Z_{in} is also different from the impedance of the load Z_L (Figure 5.2).

Figure 5.2 Transmission line of length *l* terminated with a load

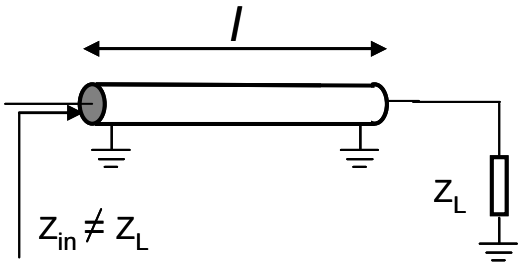

According to transmission line theory, the relationship between Z_L and Z_{in} can be expressed as:

$$Z_{in} = \frac{Z_L + jZ_0 \tan \beta l}{Z_0 + jZ_L \tan \beta l} Z_0 \qquad (5.7)$$

From Equation 5.7, Z_L can also be derived from Z_{in} using the following equation:

$$Z_L = \frac{Z_{in} - jZ_0 \tan \beta l}{Z_0 - jZ_{in} \tan \beta l} Z_0 \qquad (5.8)$$

Equation 5.8 is critical to the measurement system since the electronics measuring impedance is not at the probe. Rather, it is a distance *l* away.

In real transmission lines, the wavelength λ of the signal transmitted through the transmission line is different from λ_0, which is the wavelength of electromagnetic waves in free space. λ is influenced by the propagation velocity, and is related to β (Coleman, 2004). In this study, the velocity of propagation for RG 58/U cable is 0.66. Therefore the real part of β can be acquired by

$$\beta = \frac{2\pi}{\lambda} = \frac{2\pi f}{0.66 \times c} \qquad (5.9)$$

where *f* is the frequency of the signal transmitted through the transmission line, and

c is velocity of light (3×10^8 m/s).

The imaginary part of β can be obtained from the fact that signal attenuation per unit length of the transmission line is $8.686 \left| imag\{\beta\} \right|$ (dB/m) (Coleman, 2004). According to data sheet of RG 58/U coaxial cable, the signal attenuation is related to frequencies (Table 5.1).

Table 5.1 Signal attenuation in coaxial cable C1166 RG 58/U

Frequency (MHz)	1	10	50	100	200	500	1000
Attenuation (dB/100')	0.40	1.20	2.90	4.20	6.00	10.17	16.50
Attenuation (dB/m)	0.01312	0.03937	0.09514	0.1378	0.1969	0.33371	0.5413

Several regression models, including a linear model, a polynomial model, and a power model, were developed based on the data shown in Table 5.1 to predict signal attenuations in the cable at various frequencies. The result showed that the power model had the highest R^2 value of 0.9975 (Figure 5.3). Therefore, the power model was used to calculate the attenuation.

Figure 5.3 Models for attenuation per unit length for the coaxial cable C1166 RG 58/U

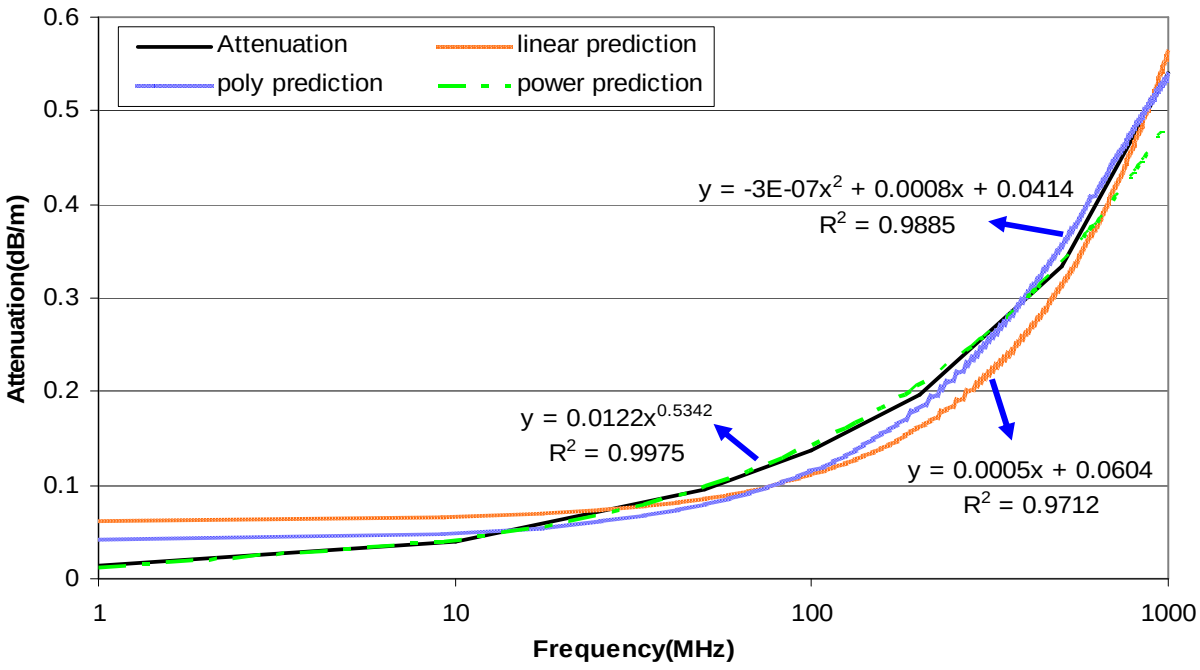

5.2 Sensor probe model

The sensor probe consisted of six aluminum plates placed in parallel, with identical spacing between adjacent plates. Two sensor probes with different size are shown in Figure 5.4.

The larger probe (Figure 5.4 (a)) was 7.5cm×3.5cm in size, with 4mm spacing. The smaller probe (Figure 5.4 (b)) was 5cm ×3.5cm in size, with 4mm spacing. In this thesis, these probes will be referred to as the "7.5cm" and "5cm" probes, respectively.

Figure 5.4 Sensor probes

(a) The 7.5cm probe

(b) The 5cm probe

On each probe, alternating plates were electrically connected to form a capacitor that looks similar to the old-fashioned air capacitor. Because each pair of adjacent plates forms a simple two-plate capacitor, the six plates on the probe form five capacitors in a parallel connection. Thus, the total capacitance of the probe can be estimated as:

$$C_L = 5 \cdot \varepsilon \cdot \frac{A}{d} = 5 \cdot \varepsilon' \varepsilon_0 \cdot \frac{A}{d} \qquad (5.10)$$

where C is the capacitance (F),

A is the area of each plate (m^2),

ε' is the dielectric constant of the material,

ε_0 is the permittivity of free space ($8.854*10^{-12}$ F/m), and

d is the spacing between adjacent plates (m).

When the probe is immersed in a dielectric medium, a part of the imaginary component of the permittivity of the medium (Equations 3.2 and 3.3) between adjacent plates also forms a parallel resistor. Due to the alternating electric connections among the plates, the total resistance of the probe can be viewed as a parallel connection of five identical resistors. Thus, the total resistance of the probe can be estimated as:

$$R_L = \frac{1}{5} \cdot \frac{d \cdot \rho}{A} \tag{5.11}$$

where A is the area of each plate (m^2), and

ρ is the resistivity of the material.

With both capacitive and resistive effects considered, the probe can be viewed as a parallel connection of C_L and R_L. Thus, the total impedance of the probe can be expressed as:

$$Z_L = Z_R // Z_C = \frac{R_L \cdot \frac{1}{j\omega C_L}}{R_L + \frac{1}{j\omega C_L}} = \frac{R_L}{1 + j\omega C_L R_L} \tag{5.12}$$

where ω is the angular frequency of the external electric field.

5.3 Circuit model

The signal processing circuit in the new control box was different from that in the old control box. Thus, the circuit models for FR measurement were investigated for the new and old control boxes, respectively.

5.3.1 Circuit model for the new control box

The circuit schematic for FR measurement using the new control box is shown in Figure 5.5. The circuit consisted of three parts: part A is for analog-to-digital conversion, part B is for the transformation between the input and output signals of the gain and phase detector, and part C is for impedance transformation between the input signals of the gain and phase detector, V_3 and V_4 , and Z_{in}.

The parallel connection of R_3 (3kΩ) and C_2 (2pF) in part B is the input impedance of the gain and phase detector. In part C, C_1 is a ceramic capacitor of 22uF; both R_{ref} and R_2 are thin film chip resistors of 50 Ω.

Figure 5.5 Circuit schematic for FR measurement using the new control box

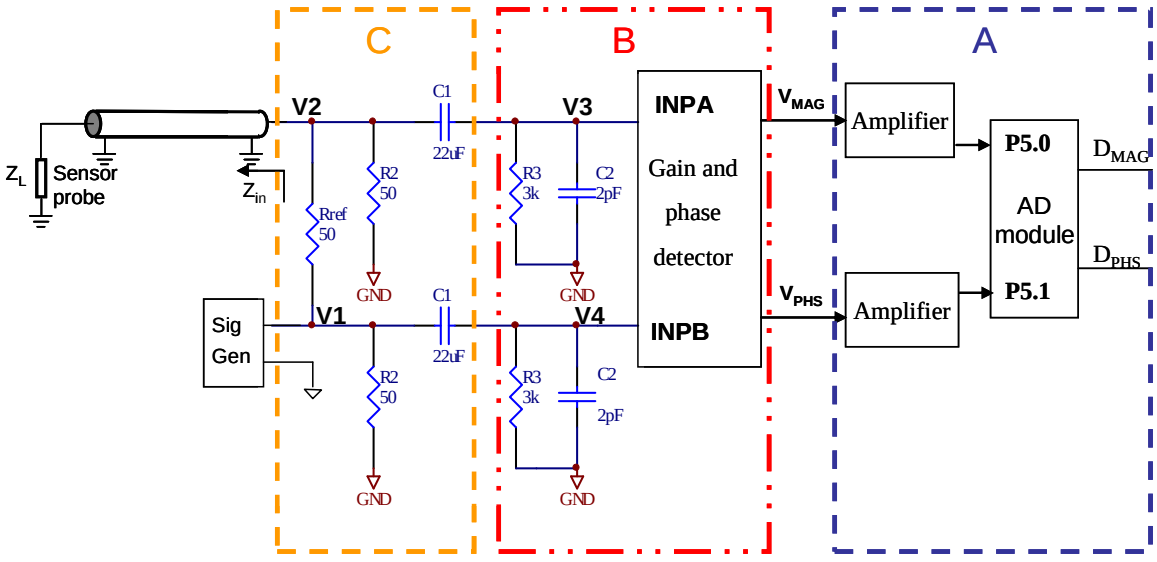

For part A, the two outputs V_{MAG} and V_{PHS} of the gain and phase detector can be derived from the measured FR data D_{MAG} and D_{PHS}, respectively. Assuming the gain of each amplifier is M and N, respectively, V_{MAG} and V_{PHS} can be calculated as:

$$V_{MAG} = (D_{MAG} \times 5000/1024)/M \quad (5.13)$$

$$V_{PHS} = (D_{PHS} \times 5000/1024)/N \quad (5.14)$$

For part B, the relationship between the input signals, V_3 and V_4, and the output signals, V_{MAG} and V_{PHS}, of the gain and phase detector can be acquired based on Equation 4.6 and 4.7 (Section 4.1.4):

$$20\log\left|V_3/V_4\right| = V_{MAG}/30 - 30 \quad (5.15)$$

$$\Phi(V_3) - \Phi(V_4) = V_{PHS}/10 - 180^\circ \quad (5.16)$$

Therefore, V_3/V_4 can be derived from the following equation:

$$V_3/V_4 = \left|V_3/V_4\right|\cos(\Phi(V_3) - \Phi(V_4)) + j\left|V_3/V_4\right|\sin(\Phi(V_3) - \Phi(V_4)) \quad (5.17)$$

For part C, the goal of modeling was to express Z_{in} as a function V_3/V_4. To achieve this goal, several impedances in the transmission paths need to be defined.

$$Z_{R_3C_2} = \frac{R_3 \cdot \frac{1}{j\omega C_2}}{R_3 + \frac{1}{j\omega C_2}} = \frac{R_3}{j\omega R_3 C_2 + 1} \quad (5.18)$$

where $Z_{R_3C_2}$ is the total parallel impedance of R_3 and C_2.

$$Z_{C_1} = \frac{1}{j\omega C_1} \quad (5.19)$$

where Z_{C_1} is the impedance of C_1.

The relationship between V_2 and V_3, V_1 and V_4 can be expressed as follows:

$$\frac{V_3}{Z_{R_3C_2}} = \frac{V_2}{Z_{R_3C_2} + Z_{C_1}} \quad (5.20)$$

$$\frac{V_4}{Z_{R_3C_2}} = \frac{V_1}{Z_{R_3C_2} + Z_{C_1}} \quad (5.21)$$

where V_1 is the signal from the signal generator, and

V_2 is the signal measured at the Z_{in} end of the cable that connects the control box and the sensor probe. It can also be viewed as output of a voltage divider that consisted of resistor R_1 and impedance Z_{in}

The following equation can be derived by combining Equations 5.20 and 5.21.

$$\frac{V_3}{V_4} = \frac{V_2}{V_1} \tag{5.22}$$

Applying the Kirchhoff's current law to the Z_{in} end of the cable, the relationship between V_1 and V_2 can be expressed by:

$$\frac{V_1 - V_2}{R_{ref}} = \frac{V_2}{Z_{in}} + \frac{V_2}{R_2} + \frac{V_2}{Z_{R_3C_2} + Z_{C_1}} \tag{5.23}$$

Therefore, Z_{in} can be expressed as:

$$Z_{in} = \frac{R_{ref}}{V_1 / V_2 - R_{ref} / R_2 - R_{ref} / (Z_{R_3C_2} + Z_{C_1})^{-1}} \tag{5.24}$$

By substituting equation 5.22 into 5.24, Z_{in} can be estimated from the two input signals, V_3 and V_4, of the gain and phase detector.

$$Z_{in} = \frac{R_{ref}}{V_4 / V_3 - R_{ref} / R_2 - R_{ref} / (Z_{R_3C_2} + Z_{C_1})^{-1}} \tag{5.25}$$

Combining models for parts A, B, and C, Z_{in} can be derived from measured digital FR data. The probe impedance Z_L can be obtained from Equation 5.8.

5.3.2 Circuit model for the old control box

The circuit schematic for FR measurement using the old control box is shown in Figure 5.6. The circuit also consisted of three parts. The function of each part is the same as that of the new control box, as described in Section 5.3.1. R_{ref} in part C is a metal film resistor of 249Ω.

Figure 5.6 Circuit schematic for FR measurement using the old control box

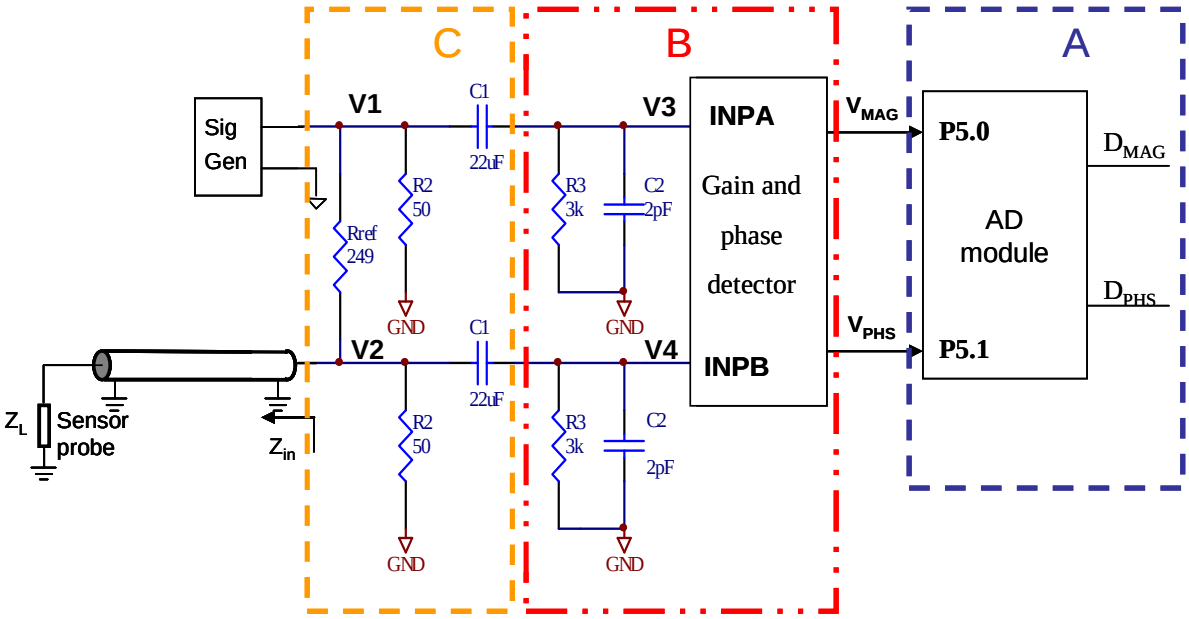

For part A, the outputs of the gain and phase detector, V_{MAG} and V_{PHS}, can be derived from the measured FR data D_{MAG} and D_{PHS}, respectively.

$$V_{MAG} = D_{MAG} \times 5000/1024 \qquad (5.26)$$

$$V_{PHS} = D_{PHS} \times 5000/1024 \qquad (5.27)$$

For part B, the relationship between the input signals, V_3 and V_4, and the output signals, V_{MAG} and V_{PHS}, of the gain and phase detector are identical to that of the new control box (Equations 5.15-5.17).

For part C, the relationship between V_1 and V_3, V_2 and V_4 can be expressed as follows:

$$\frac{V_3}{Z_{R_3C_2}} = \frac{V_1}{Z_{R_3C_2} + Z_{C_1}} \tag{5.28}$$

$$\frac{V_4}{Z_{R_3C_2}} = \frac{V_2}{Z_{R_3C_2} + Z_{C_1}} \tag{5.29}$$

The following equation can be derived by combining Equations 5.28 and 5.29.

$$\frac{V_3}{V_4} = \frac{V_1}{V_2} \tag{5.30}$$

Therefore, by substituting equation 5.30 into 5.24, Z_{in} can be estimated from the two input signals, V_3 and V_4, of the gain and phase detector:

$$Z_{in} = \frac{R_{ref}}{V_3/V_4 - R_{ref}/R_2 - R_{ref}/(Z_{R_3C_2} + Z_{C_1}) - 1} \tag{5.31}$$

Combining models for parts A, B, and C, Z_{in} can be derived from measured digital FR data. The probe impedance Z_L can be obtained from Equation 5.8.

CHAPTER 6 - Experiment

The laboratory experiment conducted in this study included: tests of the impedance transformation models using sensor probes with different sizes, coaxial cables of the same length terminated with different loads, and coaxial cables of different lengths terminated with the same load.

6.1 Sensor probes with different sizes

FR data were acquired using different sensor probes constructed with the same material and structure, but different sizes. A test was designed to examine if the sensor probe model, which was described in Section 5.2, can be used to remove the effect of probe size on the measurement.

In this test, a deionized water sample was measured by the 7.5cm and 5cm sensor probes, respectively. The FR data were measured using the old control box. FR data measured by the 7.5cm sensor probe were used to calculate the load impedance $Z_{L\_7.5cm}$ using the impedance transformation models (Equations 5.31 and 5.8).

Based on the sensor probe model (Equations 5.10, 5.11, and 5.12), the relationship between the impedance of the 7.5cm sensor probe ($Z_{L\_7.5cm}$) and that of the 5cm sensor probe (Z_{L_5cm}) can be expressed in the following equation:

$$Z_{L\_5cm} = 1.5 \bullet Z_{L\_7.5cm} \qquad (6.1)$$

The calculated Z_{L_5cm} was substituted into Equation 5.7 to calculate Z_{in} so that relationship between the input signals of the gain and phase detector can be predicted using the analysis for part C in the circuit model (Section 5.3.2). The FR data by the 5cm sensor probe can be then predicted using the analysis for part A and B. The measured and predicted FR data for the 5cm sensor probe were compared to examine the validity of the impedance model for the probes. Similarly, the measured and predicted FR data for the 7.5cm sensor probe were also compared.

6.2 Coaxial cable of the same length with different loads

This test was designed to examine if the impedance transformation models was capable of predicting the impedances of several "standard" loads.

6.2.1 Standard loads

The "standard" loads tested were open circuit, short circuit and a 50Ω resistor. One end of the coaxial cable was connected to the load, whereas the other end was connected to the control box through a BNC connector. For each load, FR data were measured by both the old and new control boxes. The length of the cables was 33cm.

Figure 6.1 Coaxial cable with open, short and 50Ω loads

The measured FR data were converted to Z_L using the impedance transformation models. The measured Z_L was then compared with the known impedance of the loads. The real part of the known Z_L should be, theoretically, very large for the open circuit, 0Ω for the short circuit, and 50Ω for the 50Ω resistor. The imaginary part of the known Z_L should be, theoretically, very large for the open circuit, 0Ω for both the short and 50Ω loads.

6.2.2 Parallel capacitor-resistor load

In order to further verify the load impedance models, a 50Ω resistor connected in parallel with a capacitor was used as the terminating load of the coaxial cable. Because the impedance of a capacitor Z_c varies with the frequency (Equation 6.2), different capacitors were selected to match the impedance of the 50Ω resistor within different frequency ranges.

$$Z_c = \frac{1}{j\omega C} = \frac{1}{j2\pi fC} \qquad (6.2)$$

where ω is the angular frequency of the signal,

f is the frequency of the signal, and

C is the capacitance.

The capacitors used for the frequency ranges of below 1 kHz, between 1 kHz and 1 MHz, and above 1 MHz were 10uF, 0.33uF and 68pF, respectively.

The actual impedance of the load ($Z_{L\text{-actual}}$) can be calculated by:

$$Z_{L\text{-actual}} = \frac{50 \times Z_c}{50 + Z_c} \qquad (6.3)$$

The FR data measured by the old control box were converted to the load impedance Z_L using the models. Z_L derived from the FR data was then compared with the actual load.

6.3 Coaxial cables of different lengths with the same load

This test was designed to investigate the possibility of removing the effect of cable lengths on permittivity measurement. Coaxial cables with lengths of 37cm and 141cm, which will be referred to as the “short” cable and the “long” cable in this thesis, respectively, were used for the test (Figure 6.2).

Figure 6.2 Coaxial cables

FR data of a 50Ω load were measured by the old control box using the two cables. A similar test was also conducted using the 7.5cm sensor probe to measure the frequency responses of air. FR data measured by the old control box with the short and long cables, respectively, were used to calculate the load impedance Z_L using impedance transformation models. Different cable lengths were substituted into Equation 5.8 for the calculation. The calculated Z_L with the short cable was compared to that with the long cable.

CHAPTER 7 - Results and Discussions

Results of the impedance transformation model tests were reported in this chapter. During the tests, the gain and phase detector was found to give unexpected readings. Several additional tests were conducted to evaluate the gain and phase detector.

7.1 Sensor probes with different sizes

The same deionized water sample was measured by the old control box with the 7.5cm and 5cm sensor probes, respectively. Comparisons of measured gain and phase responses by the 7.5cm and 5cm sensor probes are shown in Figures 7.1 and 7.2. The probes gave similar trends in both gain and phase within the measurement frequency range. However, shifting in frequency of gain response patterns can be observed within the frequency range from 10 MHz to 65 MHz. Similar shifting can be observed on phase responses.

Figure 7.1 Comparison of gains measured by the 7.5cm and 5cm probes

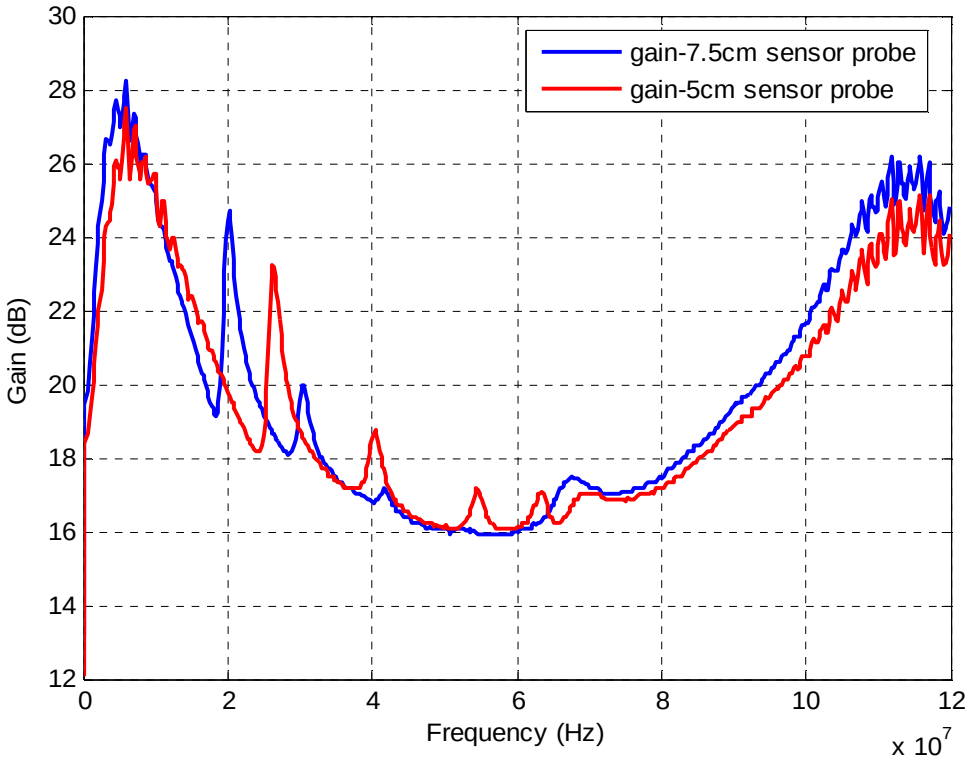

Figure 7.2 Comparison of phases measured by the 7.5cm and 5cm probes

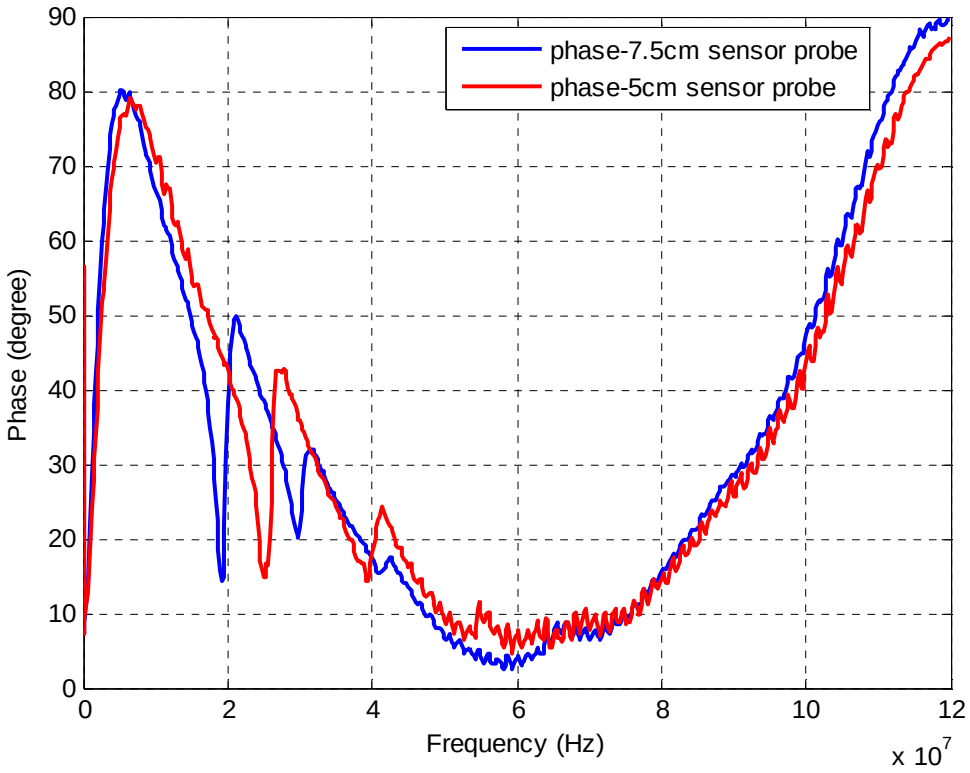

The measured gain and phase by the 7.5cm sensor probe was used to calculate the impedance of the 7.5cm sensor probe. The impedance of the 5cm sensor probe can be then derived by Equation 6.1. From the derived probe impedance, the gain and phase responses of the 5cm sensor were predicted using the impedance transformation model. Comparisons between the predicted and measured FR data for the 5cm probe are shown in Figures 7.3 and 7.4.

Figure 7.3 Comparison between the predicted and measured gain for the 5cm probe

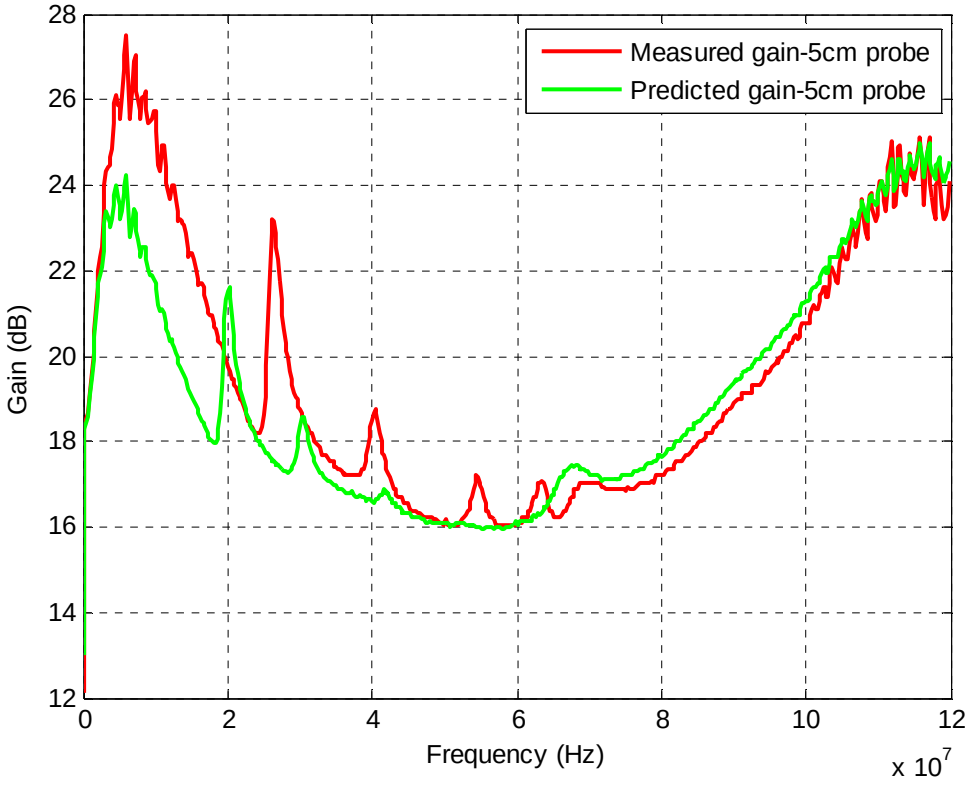

Figure 7.4 Comparison between the predicted and measured phase for the 5cm probe

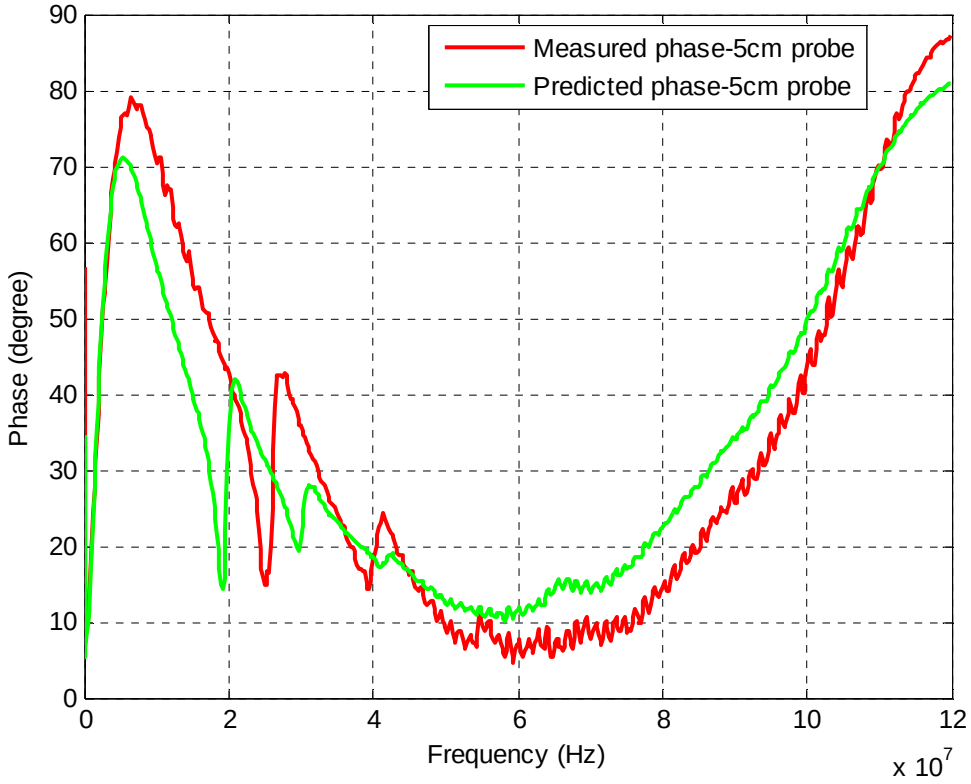

From Figures 7.3 and 7.4, the measured and predicted gain and phase responses were different. Shifting in frequency of gain response patterns can be observed. Similar shifting can be observed on phase responses as well.

The measured gain and phase by the 5cm sensor probe was used to calculate the impedance of the 5cm sensor probe. The impedance of the 7.5cm sensor probe can be then derived by Equation 6.1. From the derived probe impedance, the gain and phase responses of the 7.5cm sensor were predicted using the impedance transformation model. Comparisons between the predicted and measured FR data for the 7.5cm probe are shown in Figures 7.5 and 7.6.

Figure 7.5 Comparison between the predicted and measured gain for the 7.5cm probe

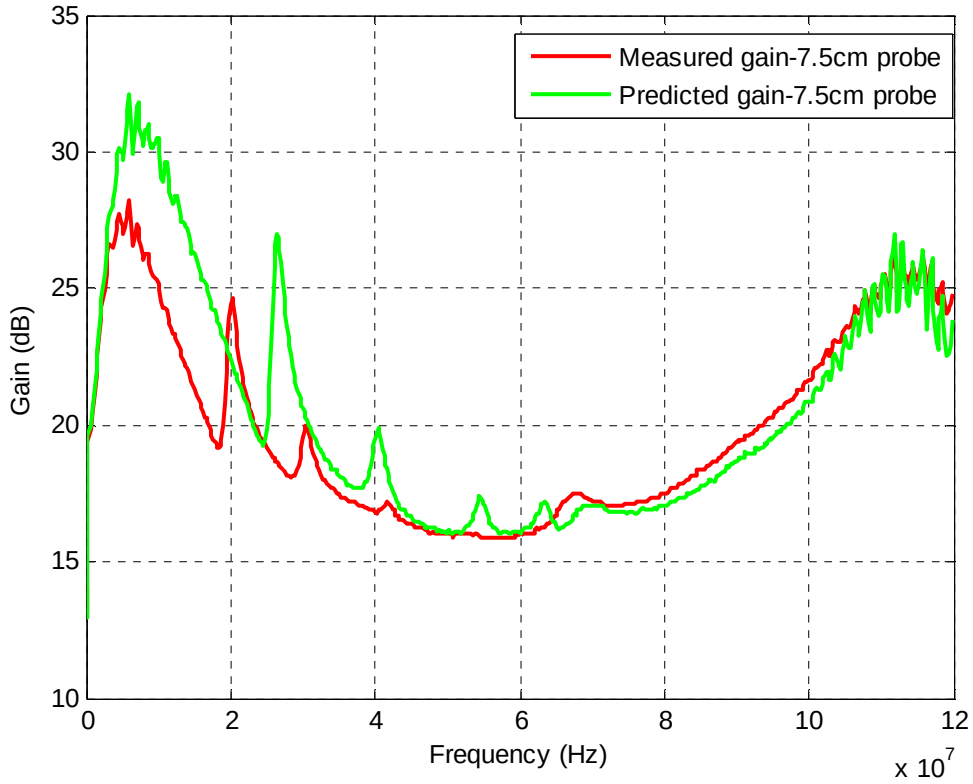

Figure 7.6 Comparison between the predicted and measured phase for the 7.5cm probe

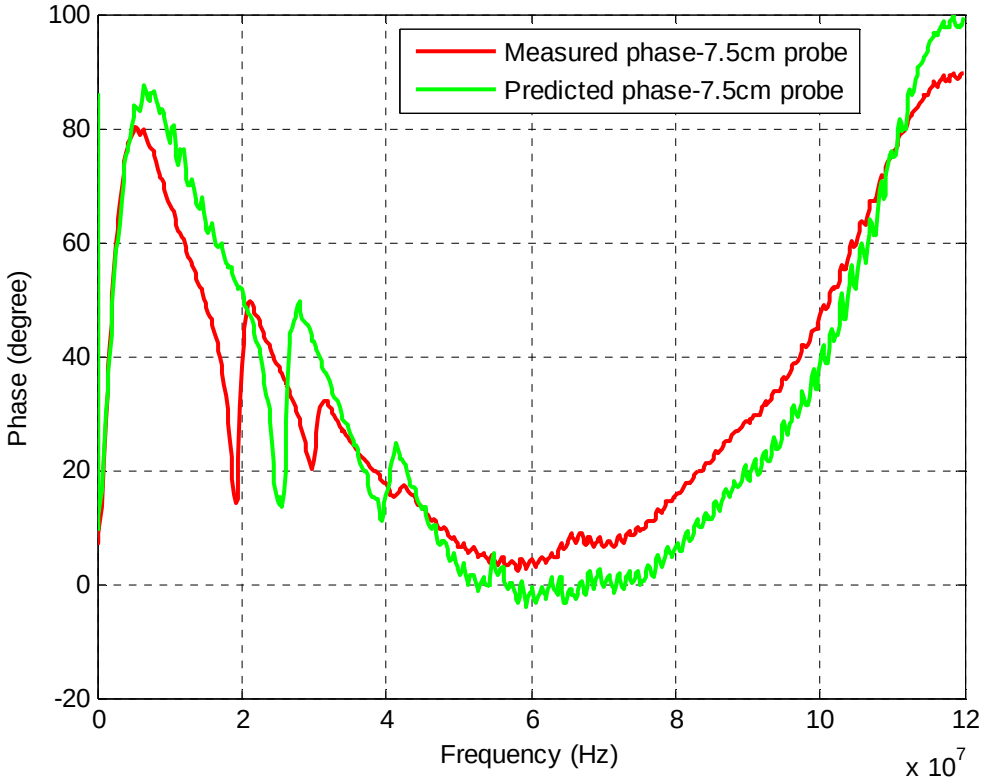

The result indicted that the simple sensor probe parallel R-C model for the actual probe does not describe the probe impedance accurately. Additional inductance caused by the bolts and wires in the container (Figure 5.4) should probably be considered in the model.

7.2 Coaxial cable of the same length with different loads

Several simple loads were connected with a 33cm coaxial cable during the tests. Results of these tests were discussed in this section.

7.2.1 Standard loads

Gain and phase responses measured by the old control box for open, short and 50Ω loads plotted against linear and logarithm frequency axes are shown in Figures 7.7 and 7.8, respectively.

Figure 7.7 Gain responses measured by the old control box for open, short and 50Ω loads on (a) linear and (b) log scales

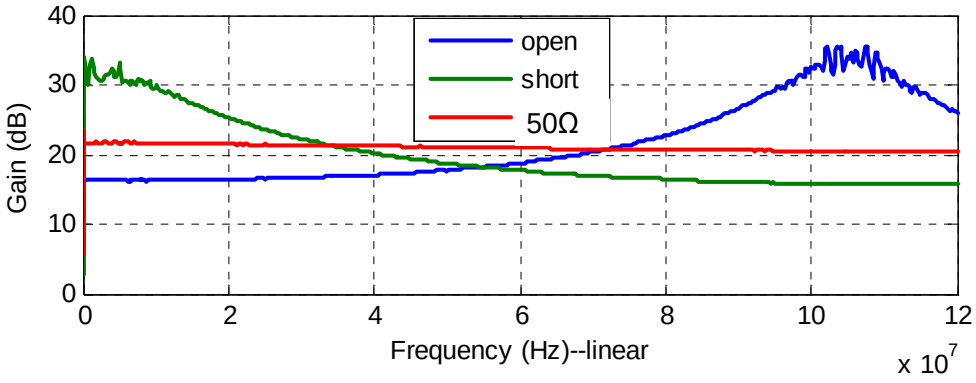

(a)

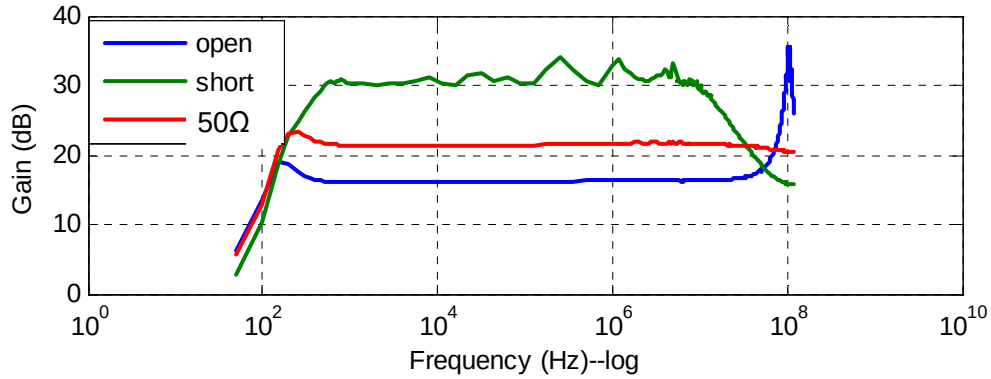

(b)

Figure 7.8 Phase responses measured by the old control box for open, short and 50Ω loads on (a) linear and (b) log scales

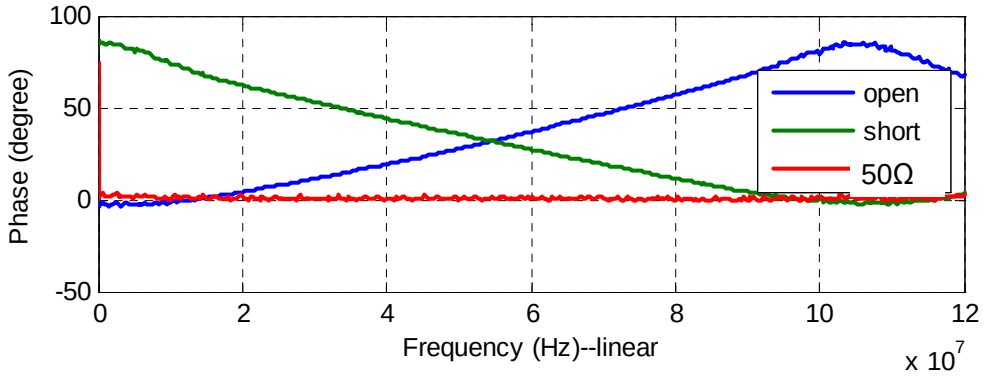

(a)

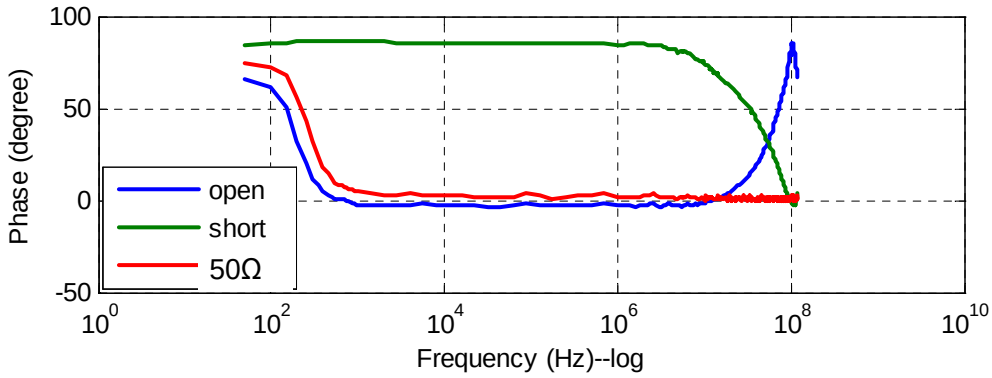

(b)

The measured gain and phase responses were converted to the real and imaginary parts of the impedance of the load using the impedance transformation models.

The result for the open circuit load is shown in Figure 7.9. Both the real and imaginary parts of the measured Z_L were relatively large, except for the low frequency regions (below 1 kHz), where the measured Z_L were close to 0. A possible cause for this discrepancy was that the system was not stable during the beginning seconds when the low frequency data were collected. This assumption was supported by the measured FR data.

Figure 7.9 Real and imaginary parts of Z_L for the open circuit load measured by the old control box

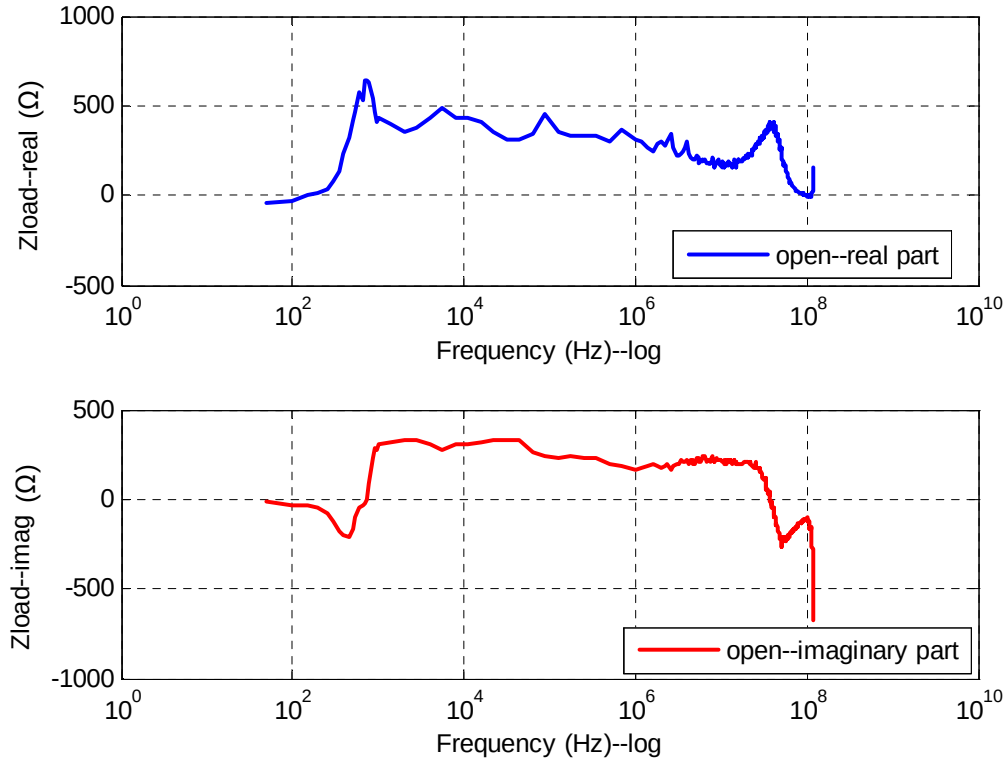

Results for the short circuit and 50Ω resistor loads are shown in Figures 7.10 and 7.11, respectively. For the short circuit load, both the real and imaginary parts of the measured Z_L were close to 0Ω at frequencies below 50 MHz. For the 50Ω resistor load, the real part was close to 50Ω and the imaginary part was close to 0Ω at the frequencies higher than 1 kHz. For frequencies below 1 kHz, measured imaginary part of Z_L deviated from the actual values probably due to signal instability as discussed previously.

Figure 7.10 Real and imaginary parts of Z_L for the short circuit load measured by the old control box

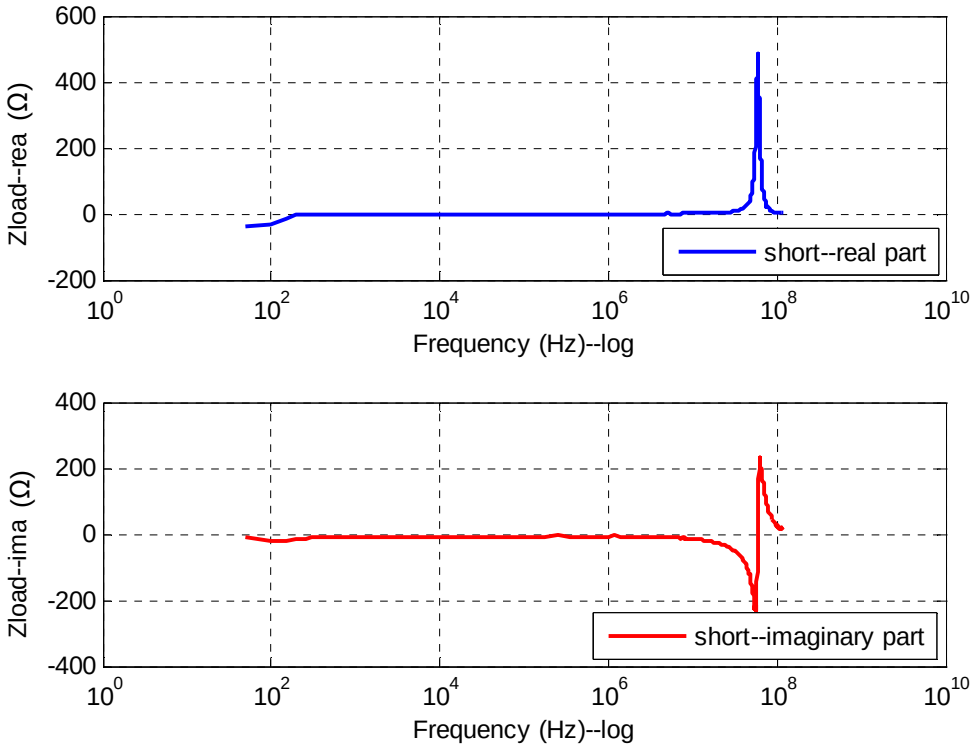

Figure 7.11 Real and imaginary parts of Z_L for the 50Ω resistor load measured by the old control box

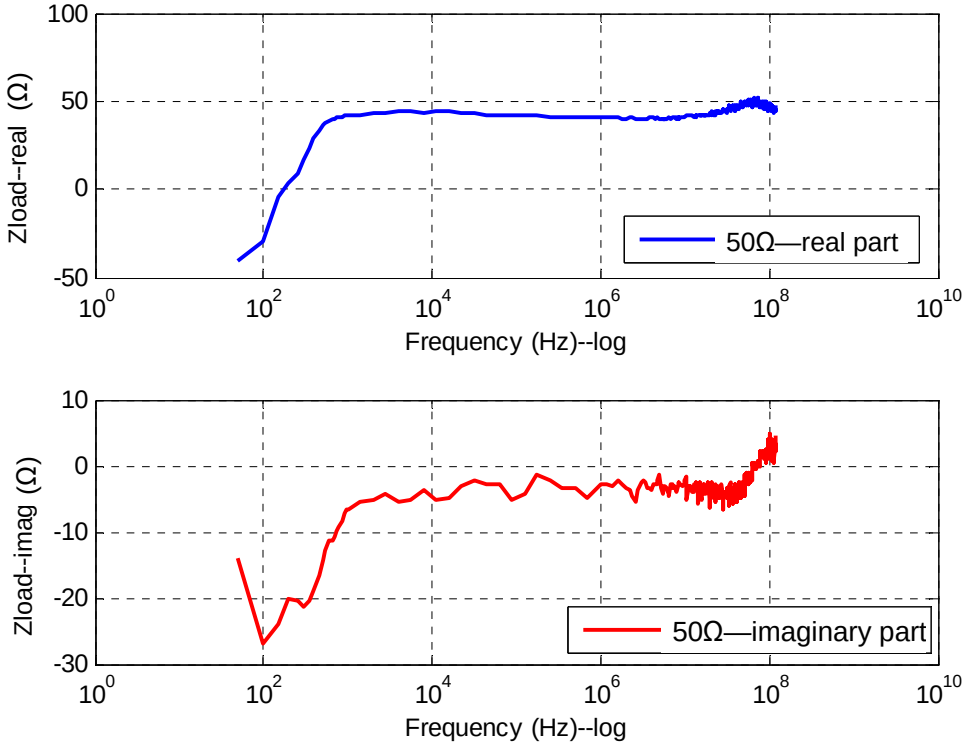

Gain and phase responses measured by the new control box for open, short and 50Ω loads plotted against linear and logarithm frequency axes are shown in Figures 7.12 and 7.13, respectively. The measured gain and phase responses were obviously different among the open, short and 50Ω resistor loads.

Figure 7.12 Gain responses measured by the new control box for open, short and 50Ω loads on (a) linear and (b) log scales

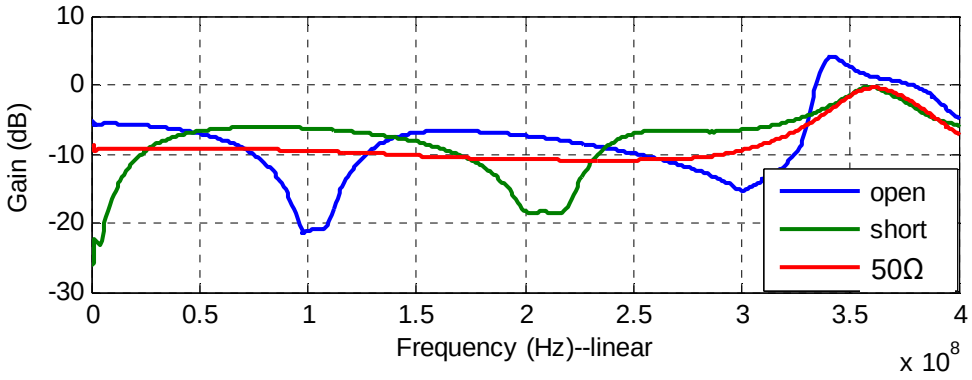

(a)

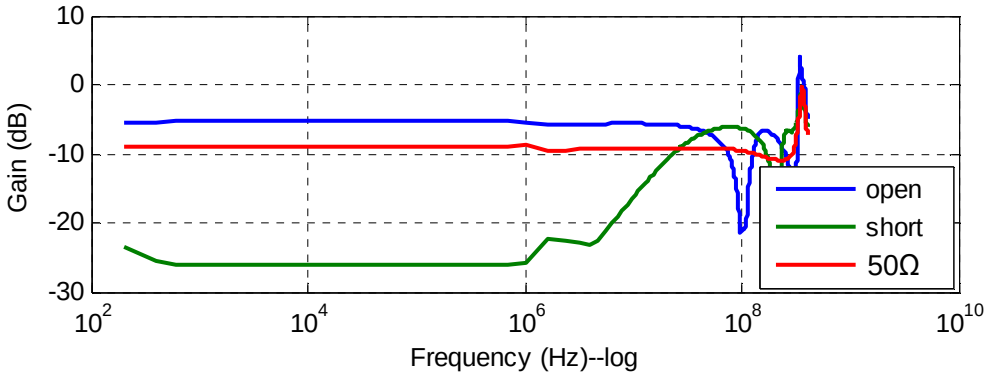

(b)

Figure 7.13 Phase responses measured by the new control box for open, short and 50Ω loads on (a) linear and (b) log scales

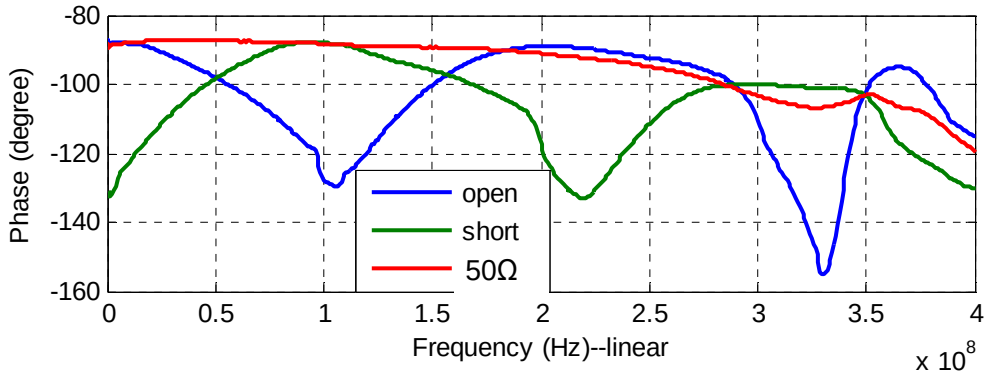

(a)

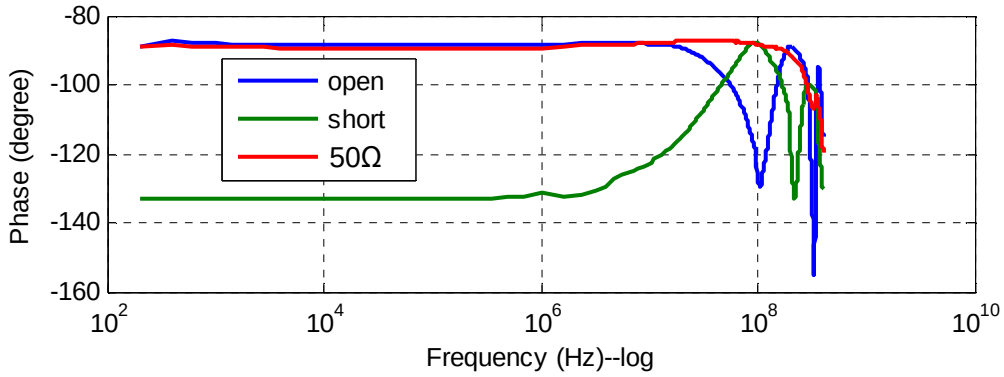

(b)

The measured gain and phase were converted to the real and imaginary parts of the impedance of the load using the impedance transformation models.

Z_L of 50Ω resistor as calculated from the FR data is shown in Figure 7.14. Both the real and imaginary parts were quite different from the actual load. Z_L of open and short circuits as calculated from the FR data are shown in Figures 7.15 and 7.16, respectively. Both the real and imaginary parts were quite different from the actual load. A possible reason for these

discrepancies was that wiring of the new control box was more complicated than the old box so that additional factors may need to be taken into account.

Figure 7.14 Real and imaginary parts of Z_L for the 50Ω resistor load measured by the new control box

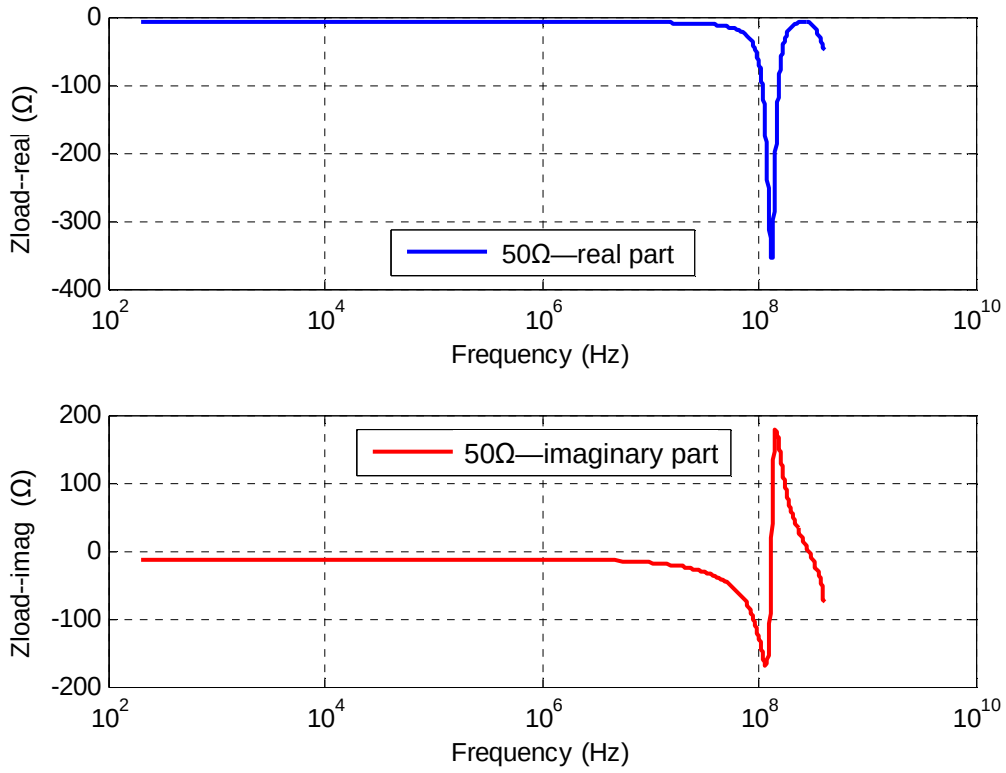

Figure 7.15 Real and imaginary parts of Z_L for the open load measured by the new control box

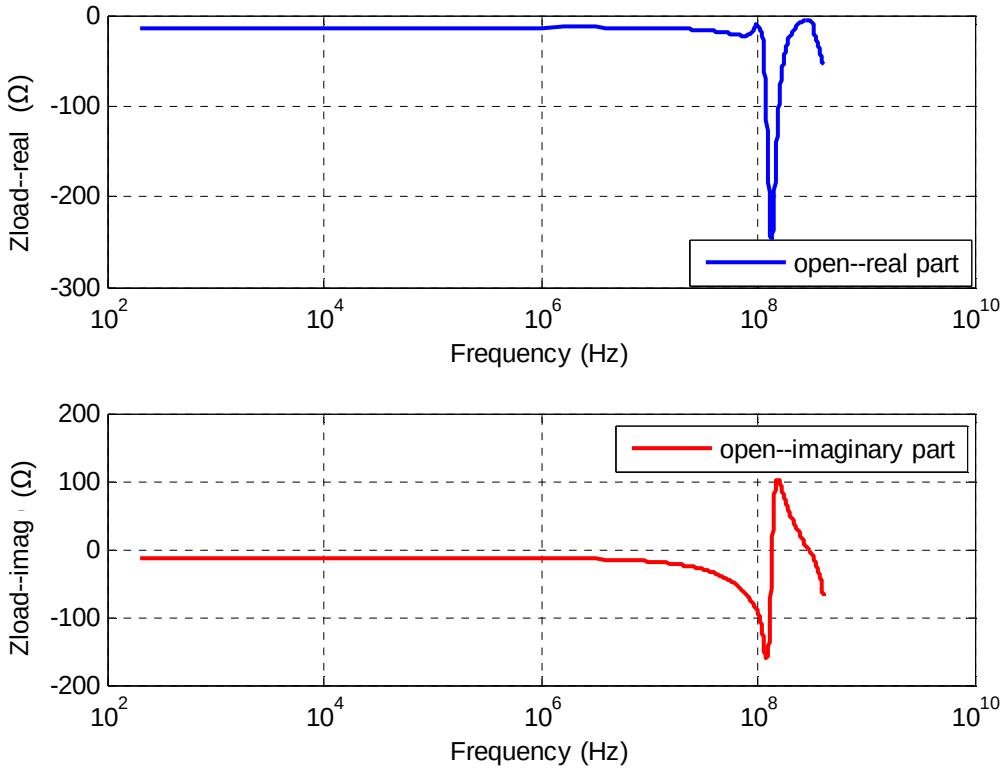

Figure 7.16 Real and imaginary parts of Z_L for the short load measured by the new control box

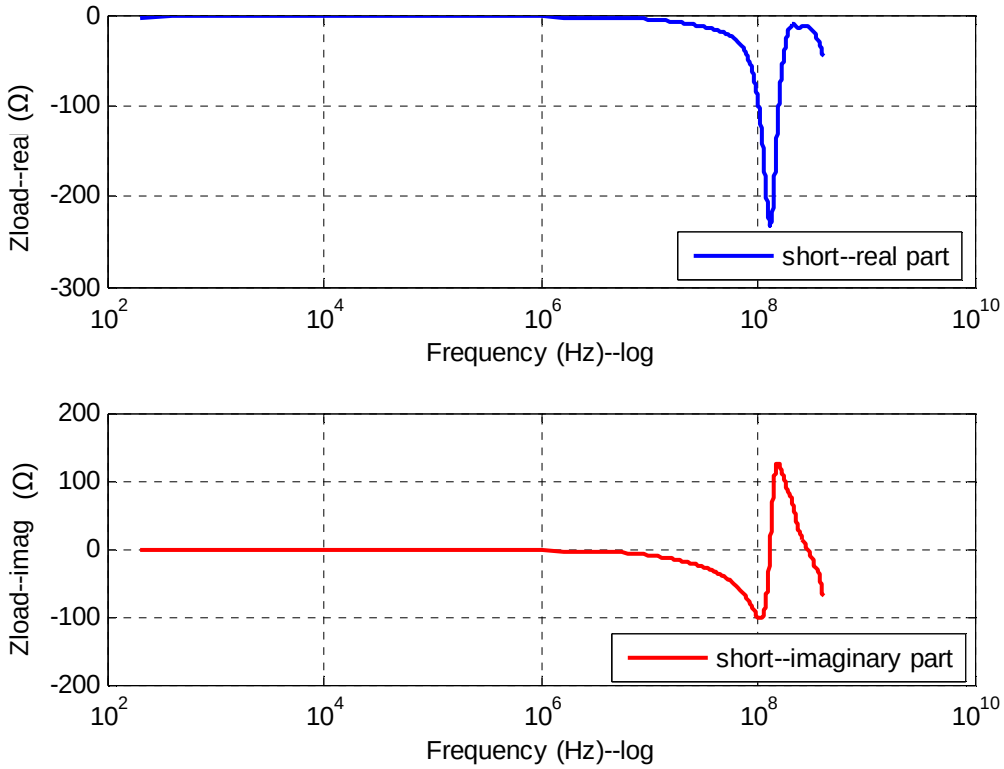

In summary, relatively good results were obtained for the open, short and 50Ω resistor loads measured by the old control box. The impedance transformation models developed for the old control box were capable of predicting the impedances of these special loads. However, the results obtained for the new control box were not correct.

7.2.2 Parallel capacitor-resistor load

This section reports the results of frequency response tests with parallel R-C loads. Only the old control box was tested for these loads.

The real and imaginary parts of the load impedance as measured by the old control box are compared with the actual loads in Figures 7.17 and 7.18, respectively. Three different loads were used within different frequency ranges. Below 1 kHz, the load was a parallel connection of a 50Ω resistor and a 10uF capacitor. While the same resistor was used for the higher frequency regions, the capacitor used for 1 kHz – 1 MHz and above 1 MHz were 0.33uF and 68pF, respectively.

The results showed that the real part of the load impedance measured by the old control box was close to the actual value within the frequency range of 350 Hz – 50 MHz. For frequencies below 350 Hz, the measured values were quite different from the actual loads. As described in Section 7.2.1, difference between measured and actual impedances at the low frequencies was probably due to the instability of the control box during the first few seconds of measurement. Giving a “warmup” time at the beginning of measurement may help alleviate this problem. The result showed that the measured imaginary part of load impedances was close to the actual load at most frequencies, except for frequencies above 50 MHz.

Figure 7.17 Comparison of real part of the load impedance measured by the old control box with that calculated for the actual loads

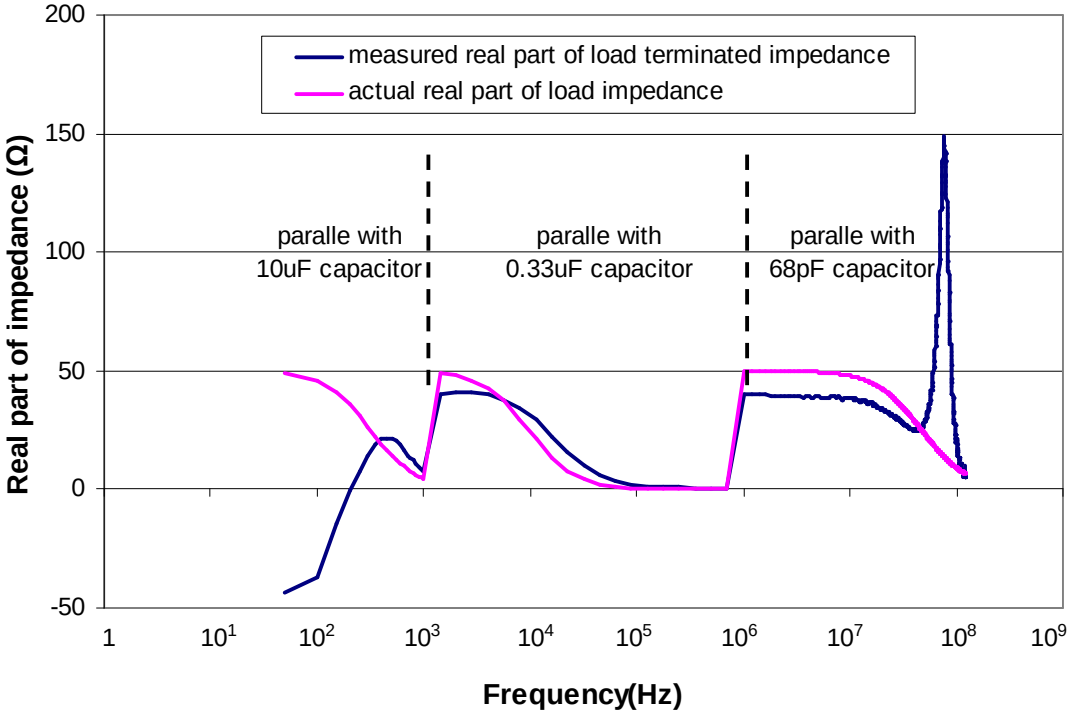

Figure 7.18 Comparison of imaginary part of the load impedance measured by the old control box with that calculated for the actual loads

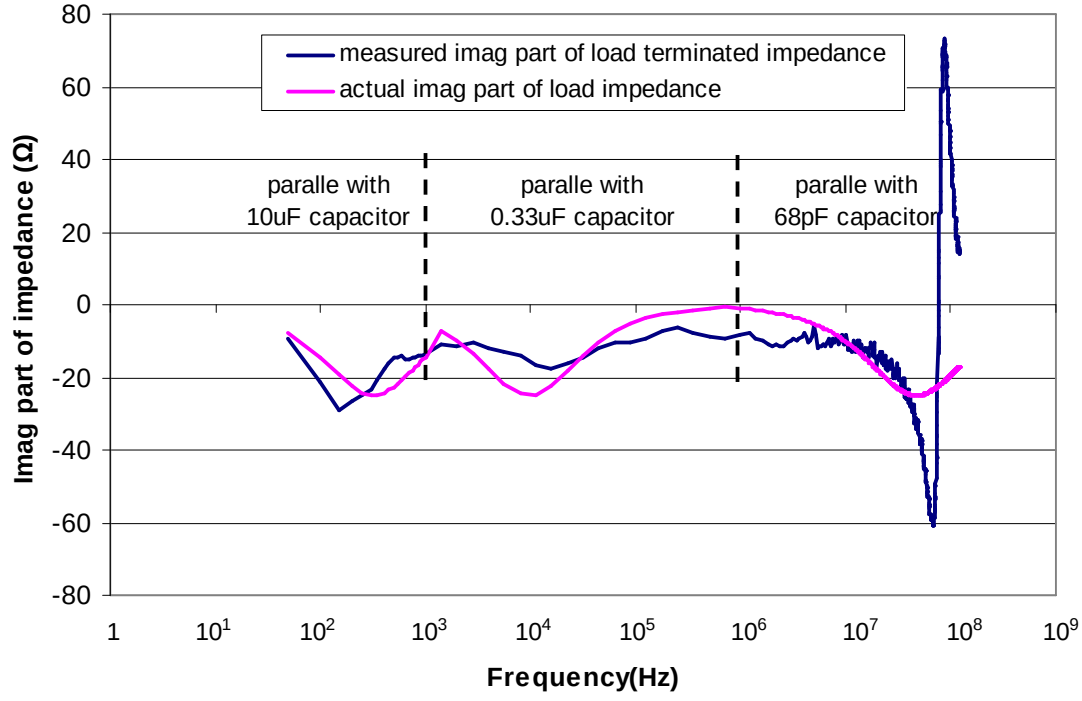

In summary, the impedance transformation models were able to predict the impedance of parallel R-C loads at frequencies below 50 MHz. However, the models needed to be further improved to reduce the predicted error.

7.3 Coaxial cables of different lengths with the same load

Gain and phase responses measured by the old control box with the short (37cm) and long (141cm) cables, both terminated with a 50Ω resistor, are shown against linear and logarithm frequency axes in Figures 7.19 and 7.20, respectively. The results showed that both gain and phase responses measured with the short and the long cables were very similar within the measurement frequency range, indicating that the measurement was not affected by the cable length. This is probably due to the fact that the characteristic impedance of both cables was 50Ω, which matched the load impedance.

Figure 7.19 Gain responses measured using the short (37cm) and long (141cm) cables, both terminated with a 50Ω resistor, on (a) linear and (b) log scales

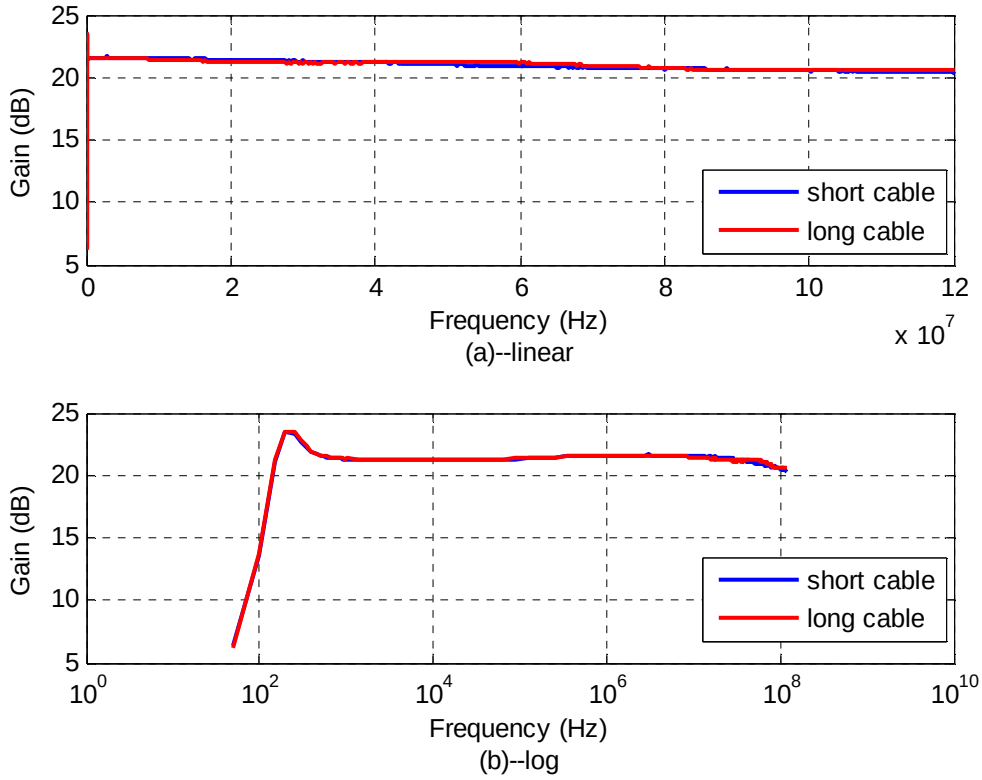

Figure 7.20 Phase responses measured using the short (37cm) and long (141cm) cables, both terminated with a 50Ω resistor, on (a) linear and (b) log scales

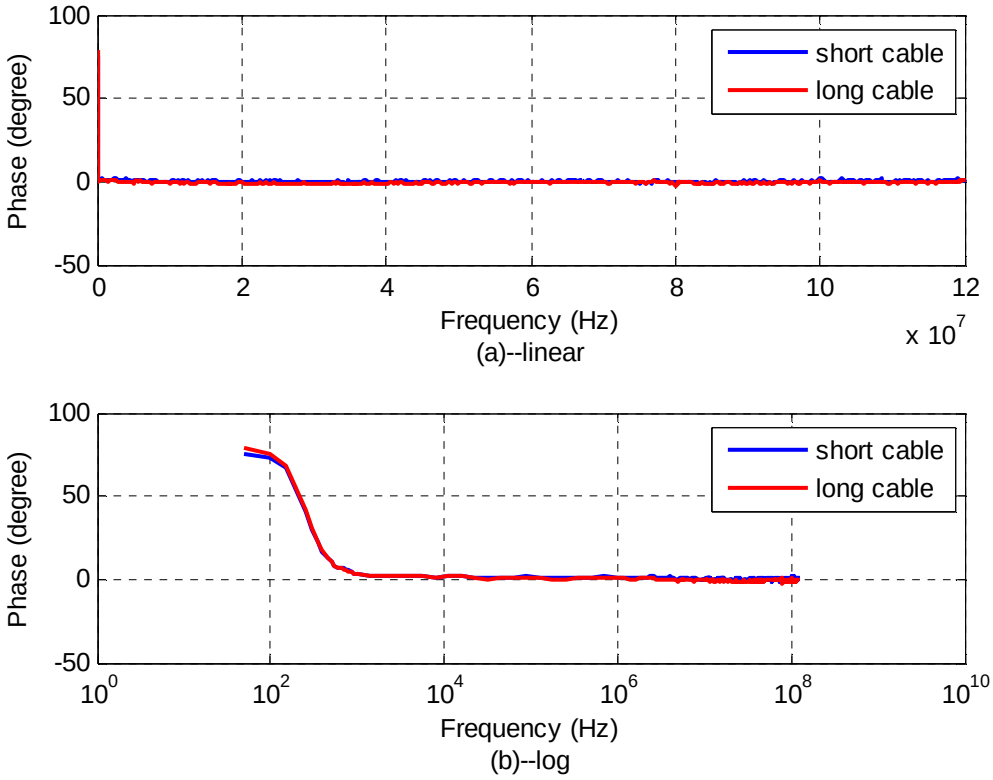

The real parts of the load impedance calculated from the FR data for the short and long cables are shown in Figure 7.21. The values are very close to 50Ω throughout the frequency range.

Figure 7.21 The real part of measured 50Ω load using the short (37cm) and long (141cm) cables on (a) linear and (b) log scales

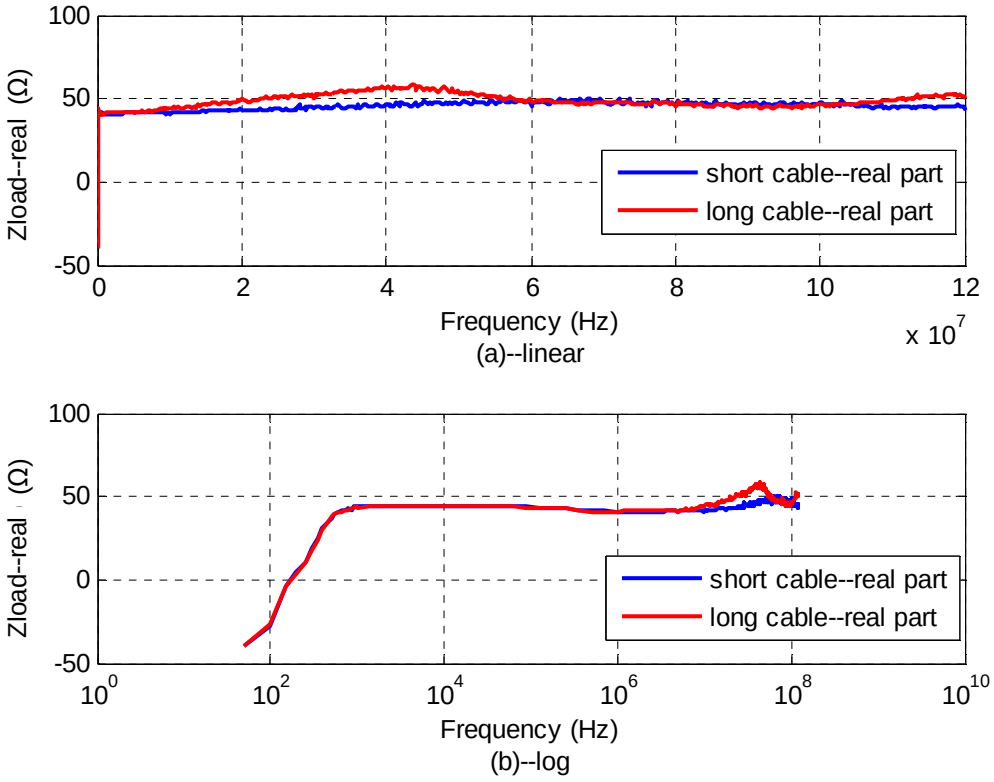

The imaginary parts of the load impedance calculated from the FR data measured using the short and long cables are shown in Figure 7.22. Below 20 MHz, the imaginary parts measured using the two cables were very similar. Above 20 MHz, the imaginary part of the load impedance measured using the short cable was slightly different from that using the long cable. However, the differences were less than 10Ω.

Figure 7.22 The imaginary part of measured 50Ω load using the short (37cm) and long (141cm) cables on (a) linear and (b) log scales

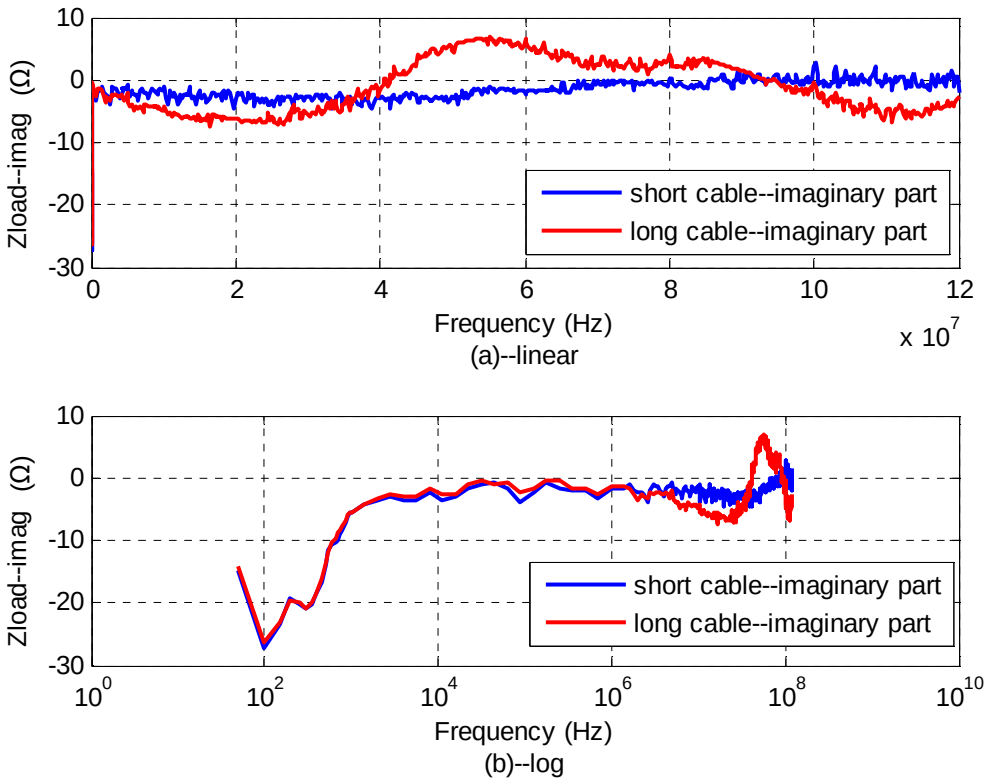

The short and long cables terminated with the 7.5cm sensor probe were also tested. Measured gain and phase responses are shown against linear and logarithm frequency axes in Figures 7.23 and 7.24, respectively. The gain and phase responses measured using the short cable was different from that using the long cable. The gain and phase responses measured with the long cable displayed more peaks. For example, three peaks showed up at 23 MHz, 62 MHz and 106 MHz in the gain response for the long cable, while only one peak showed up at 40 MHz for the short cable (Figure 7.23 (a)). It is obvious that the cable length influenced the measurements.

Figure 7.23 Gain responses measured using the short (37cm) and long (141cm) cables, both terminated with the 7.5cm sensor probe, on (a) linear and (b) log scales

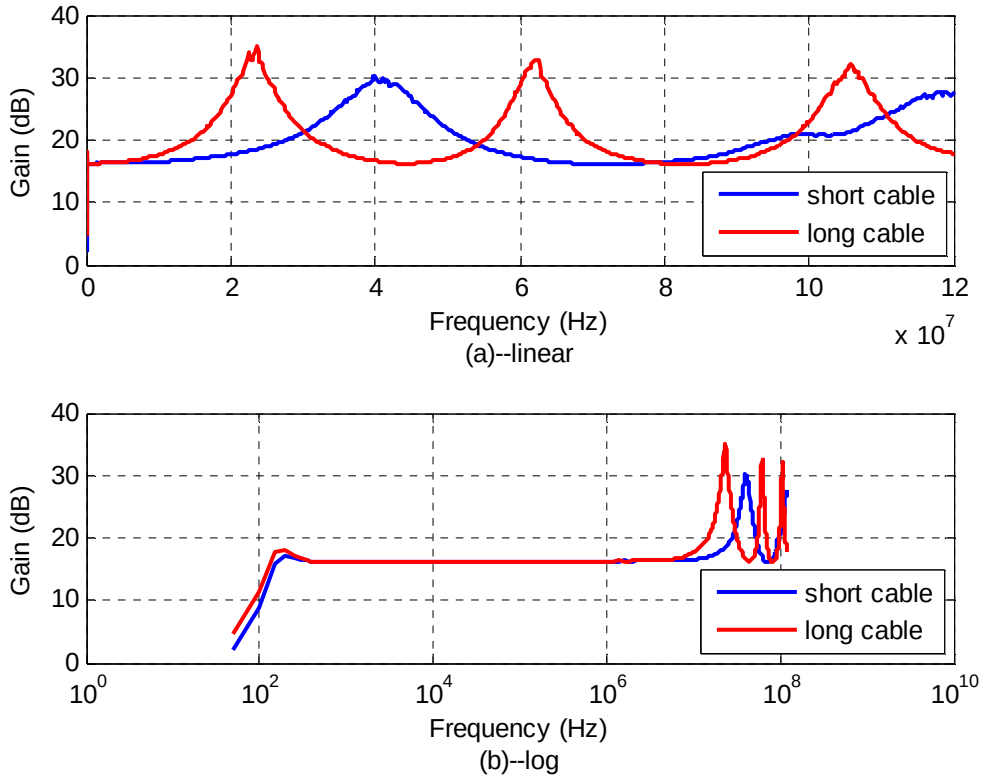

Figure 7.24 Phase responses measured using the short (37cm) and long (141cm) cables, both terminated with the 7.5cm sensor probe, on (a) linear and (b) log scales

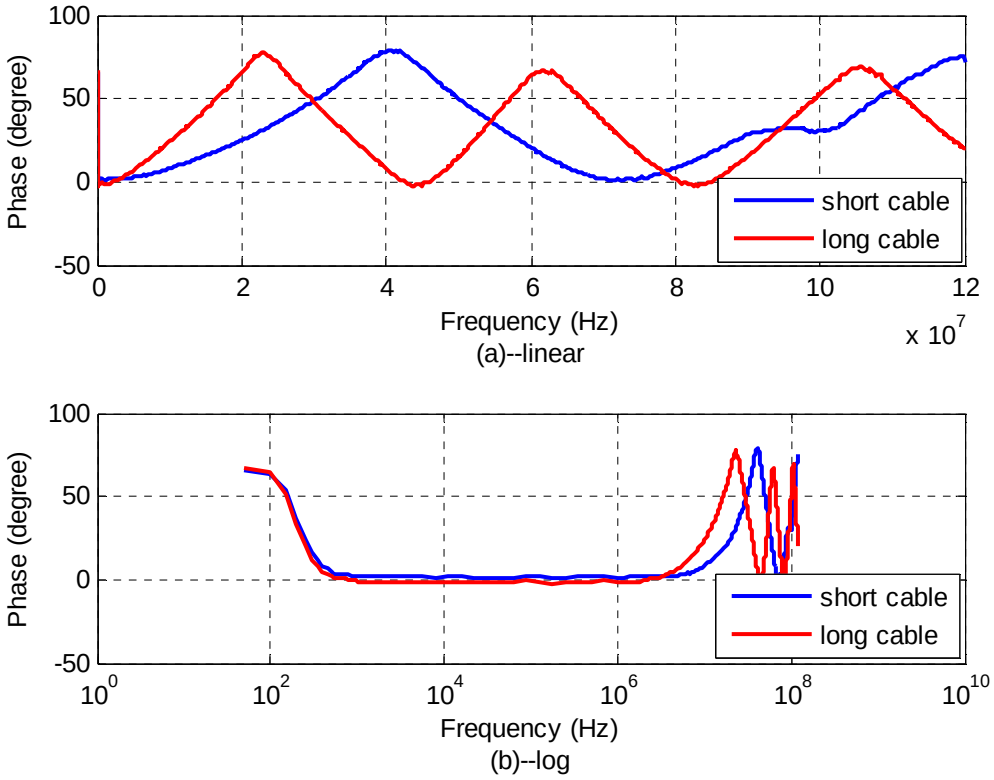

The real parts of the load impedance calculated from the FR data for the short and long cables are shown in Figure 7.25. Below 20MHz, no obvious difference was observed. At frequencies higher than 20MHz, peaks were observed at different frequencies for the short and long cables.

Figure 7.25 The real part of load impedance of the 7.5cm sensor probe measured using the short (37cm) and long (141cm) cables, on (a) linear and (b) log scales

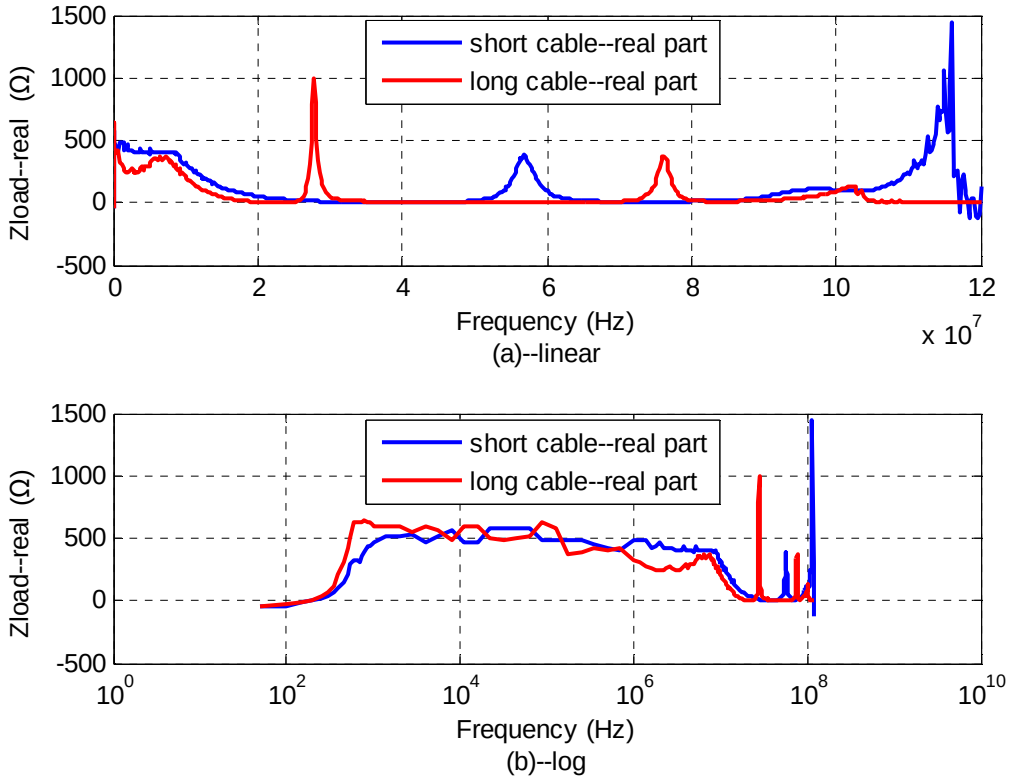

The imaginary parts of the load impedance calculated from the FR data for the short and long cables are shown in Figure 7.26. Differences can be observed within the entire test frequency range.

Figure 7.26 The imaginary part of load impedance of the 7.5cm sensor probe measured using the short (37cm) and long (141cm) cables, on (a) linear and (b) log scales

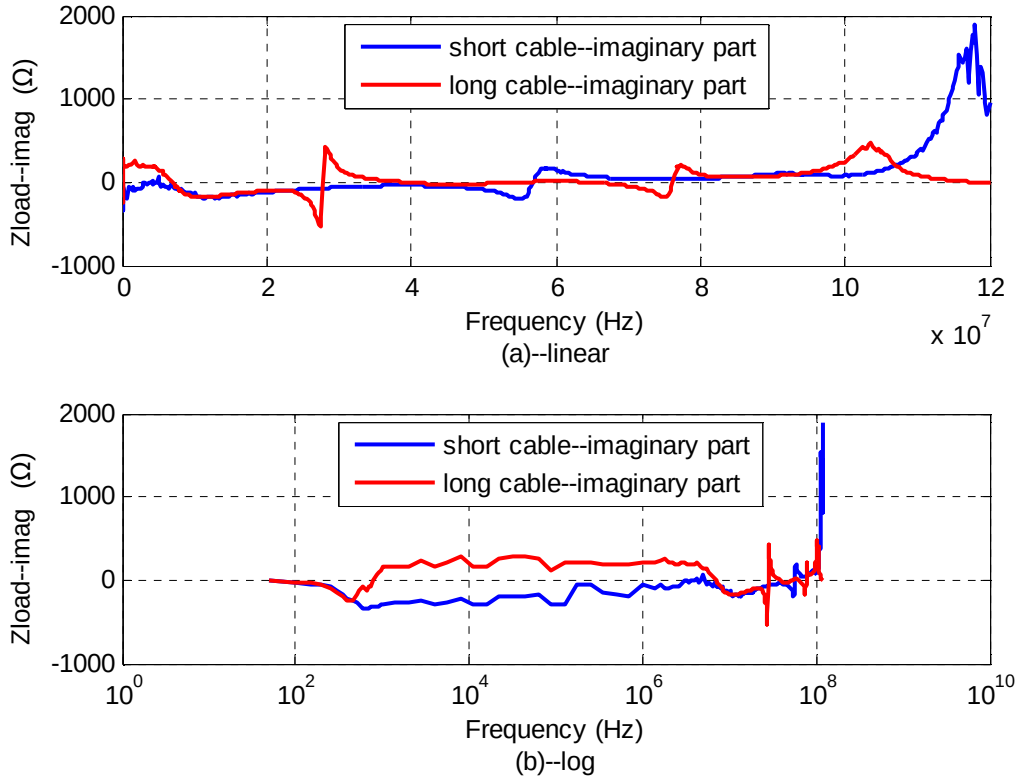

In summary, the impedance transformation models were capable of describing the effect of cable length on the measurement of the real part of load impedance below 20 MHz. This model was not effective for the real parts when frequencies were above 20 MHz. It was not effective in describing the imaginary part of the load impedance within the entire frequency range.

7.4 Problem with the gain and phase detector

During the experiment, the measured phase angles all fell in the 0°~90° range. A general trend was to bounce between 0° and 90° as frequency increased. This trend did not agree with the model. To investigate this discrepancy, a series of tests were conducted on gain and phase detector. Results of these tests are discussed in this section.

7.4.1 Test on a gain and phase detector evaluation board

An evaluation board for the 8302 gain and phase detector (Analog Devices, Inc.) was used in the test. A signal generator (Agilent 33220A) was used to generate sine wave signal, which was sent to channel B (INPB) of the gain and phase detector. An RC circuit formed a low-pass filter with a corner frequency of 1 MHz. This filter generated a delayed sine wave, which was sent to channel A (INPA) of the gain and phase detector (Figure 7.27). Thus, the phase delay generated by the RC circuit was measured by the gain and phase detector. Twelve frequencies, including 500 Hz, 1, 10,100 and 500 kHz, and 1, 2, 5, 8, 10, 15, and 20 MHz, were selected for the test. Test at each frequency was repeated twice.

Figure 7.27 An RC circuit generated phase delays

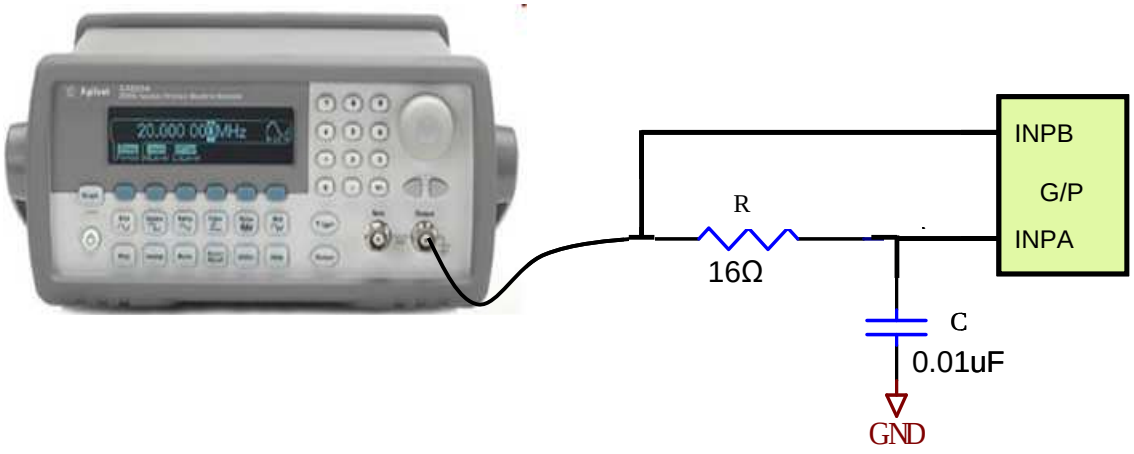

The phase output from the gain and phase detector $V_{PHS,}$ was read with a digital multimeter (HP 34401A). The phase delay (in degree) can be calculated from measured V_{PHS} using Equation 7.1.

$$\text{Phase delay } (^\circ) = 180^\circ - V_{PHS}/10 \qquad (7.1)$$

The two input signals sent to channels INPA and INPB of the gain and phase detector were also monitored by an oscilloscope (Agilent 54621A) set at the XY horizontal mode. The XY horizontal mode gave a volts-versus-time display to a volts-versus-volts display (the Lissajous graph) for the two input signals (Figure 7.28). The phase delay between the two signals can be calculated using the following equation:

$$\sin\theta = \frac{A}{B} \quad \text{or} \quad \sin\theta = \frac{C}{D} \qquad (7.2)$$

Figure 7.28 Lissajous graph between two signals (Agilent 54621A, User's Guide, 2000)

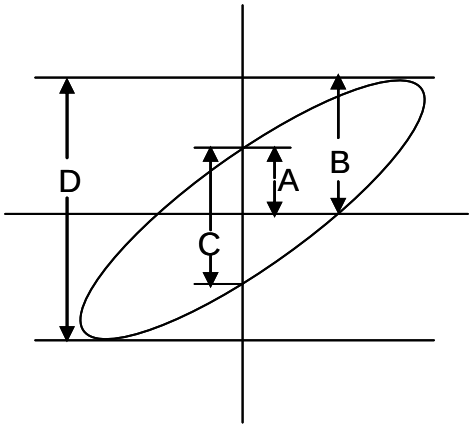

The phase delay observed from the oscilloscope using the Lissajous method was compared with that measured by the gain and phase detector. The results are shown in Figures 7.29 and 7.30 on logarithmic and linear frequency axes, respectively.

Figure 7.29 Phase delay observed from the oscilloscope and measured by the gain and phase detector on a logarithmic frequency axis

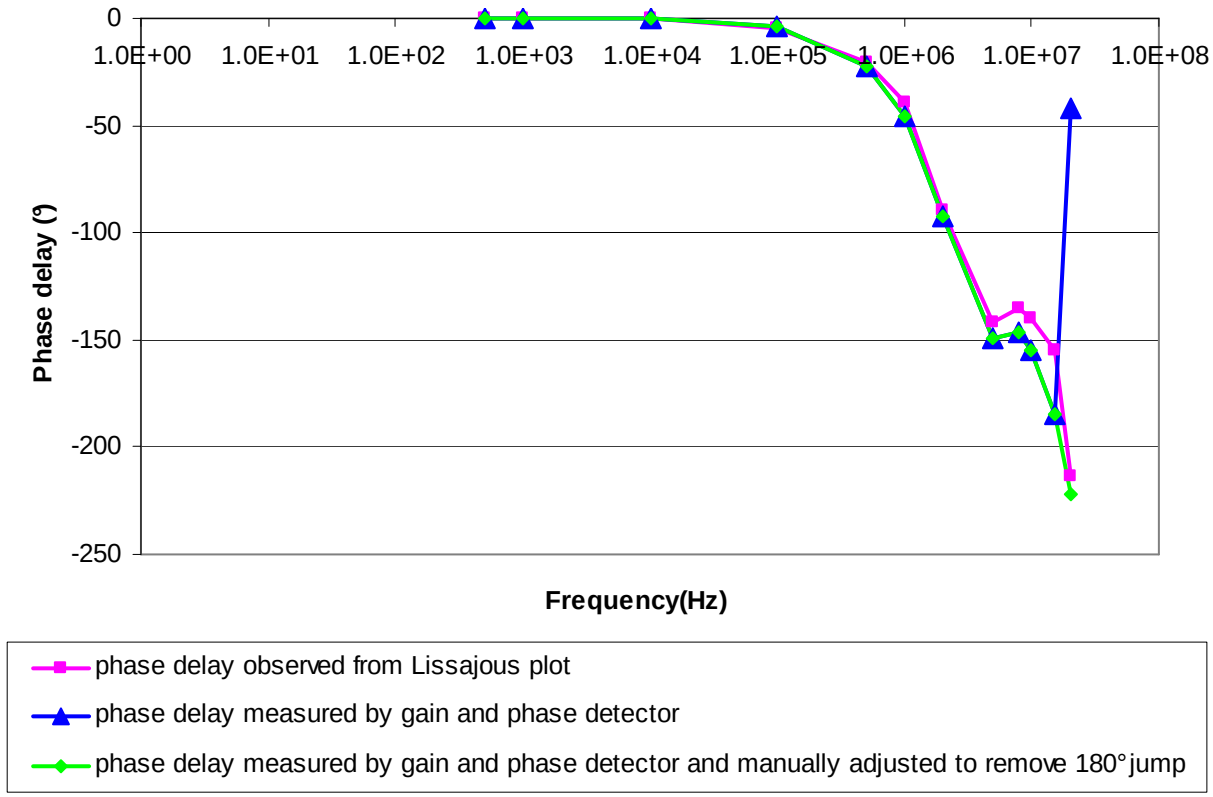

Figure 7.30 Phase delay observed from the oscilloscope and measured by the gain and phase detector on a linear frequency axis

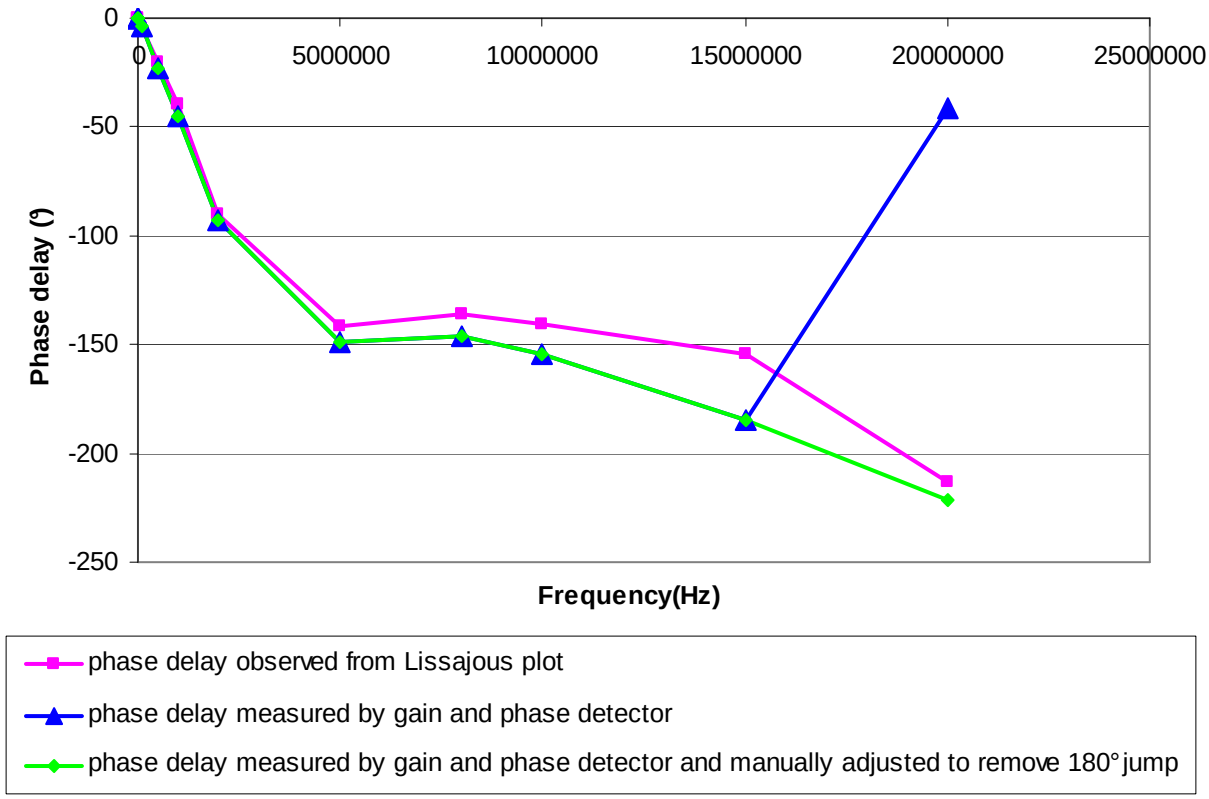

The results showed that the phase delay observed from Lissajous method had the same trend with that measured by the gain and phase detector as the frequencies increased, although larger discrepancies took place at the frequencies higher than 5 MHz. The errors may have resulted from inaccuracy in data reading on Lissajous plot. At 20 MHz, the phase delay angle observed from Lissajous plot was -213°. However, the gain and phase detector gave -41° at this frequency. This was because that the range of the phase reading from the gain and phase detector was from -180° to 0° (or 0°~180°). Due to the periodicity of the arctangent function, -41° was adjusted to -221° to remove the 180° jump and to maintain the continuity of measured phase delay.

7.4.2 Test on the old control box at single frequencies

In this part of the experiment, signals on the channels A (INPA) and B (INPB) of the gain and phase detector in the old control box were monitored and recorded by an oscilloscope (Agilent 54621A). The 7.5cm probe was connected to the old control box through the short (37cm) coaxial cable. The probe was placed in air. The system ran at frequencies between 20 MHz and 110 MHz with 10 MHz interval. From Figure 7.24 (Section 7.3), the phase responses measured with the long cable displayed several peaks and valleys at various frequencies. In order to study this trend, frequencies selected were those close to the turning points of the phase response measured with the long cable.

Signals on the INPB and INPA inputs at 50, 60, 70 and 80 MHz recorded by the oscilloscope are shown in Figure 7.31. The results showed that the phase delay between INPA and INPB continuously increased with frequency with no peaks and valleys observed. Obviously, this result was different from the phase response data measured using the old control box.

Figure 7.31 Signals on the INPA and INPB inputs of the gain and phase detector recorded by an oscilloscope at (a) 50MHz, (b) 60 MHz, (c) 70 MHz, and (d) 80 MHz

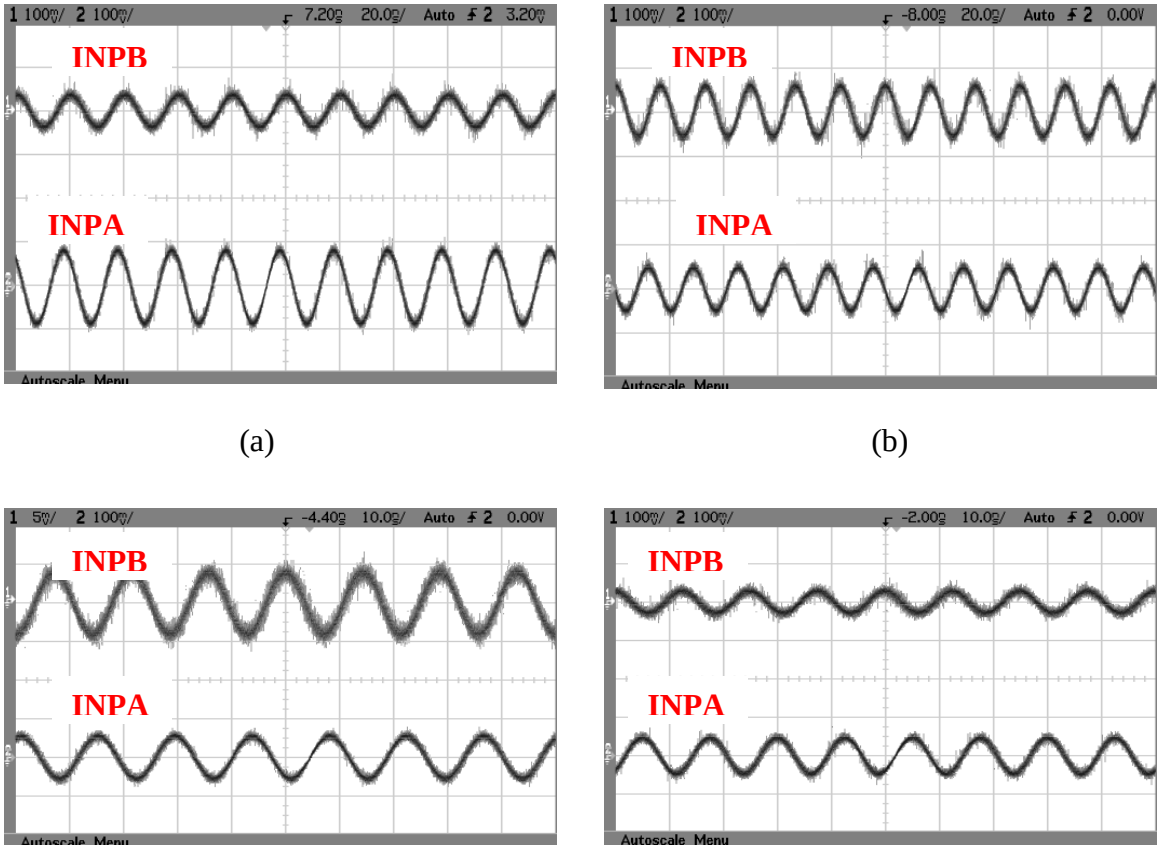

7.4.3 Tests in single-frequency and frequency-sweep modes

The objective of this test was to further compare FR data observed on an oscilloscope (Agilent infiniium MSO8104A, 1GHz) with that measured by the gain and phase detector, and to detect if the FR data measured at single frequencies were consistent with those measured in a frequency-sweep mode.

7.4.3.1 Comparison of measurements by the control box and oscilloscope at the single frequency mode

For the single frequency test, signal at each selected frequency was run for 3.5min so that the oscilloscope (Agilent infiniium MSO8104A, 1GHz) had sufficient time to record the signals at INPA and INPB. Frequencies selected were those at or around the turning points of the phase response measured with the long cable, including 40, 44.8, 50, 55, 62, 70, 75, 82.6, 87, 90, 95, 100, 104.8, and 110MHz (Figure 7.24). The measurement at each frequency was repeated 10 times. Both the short and long cables were used in this test.

Results of these tests are shown in Figures 7.32 – 7.35. For the short cable, the measured gain response had a similar trend with that observed on the oscilloscope. However, the gain measured by the control box was in general higher than that observed on the oscilloscope by about 10dB (Figure 7.32). Similar trend can be found for the data obtained via the long cable at frequency higher than 70 MHz (Figure 7.33). The phase responses measured by the control box and the oscilloscope were almost identical below 60 MHz and started to deviate from each other when the phase angle reached 90° (Figure 7.34 and 7.35). An effort to correct the phase angle based on the periodicity of the arctangent function also failed to yield a reasonable result.

Figure 7.32 Comparison of gain measured by the old control box with that observed on the oscilloscope. The short cable was used in the test.

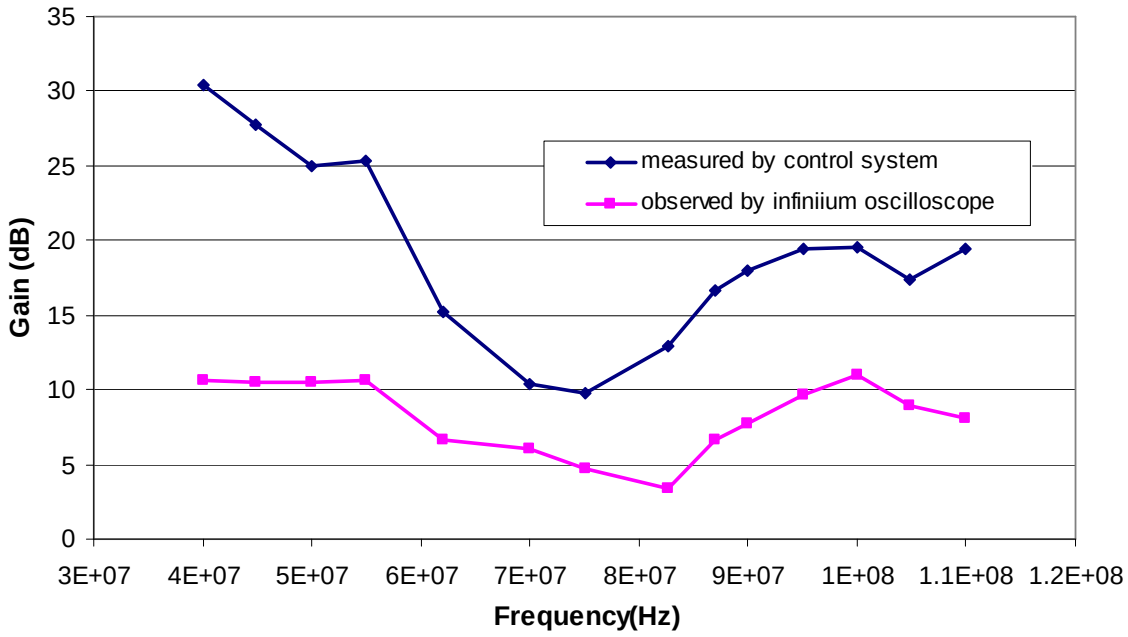

Figure 7.33 Comparison of gain measured by the old control box with that observed on the oscilloscope. The long cable was used in the test.

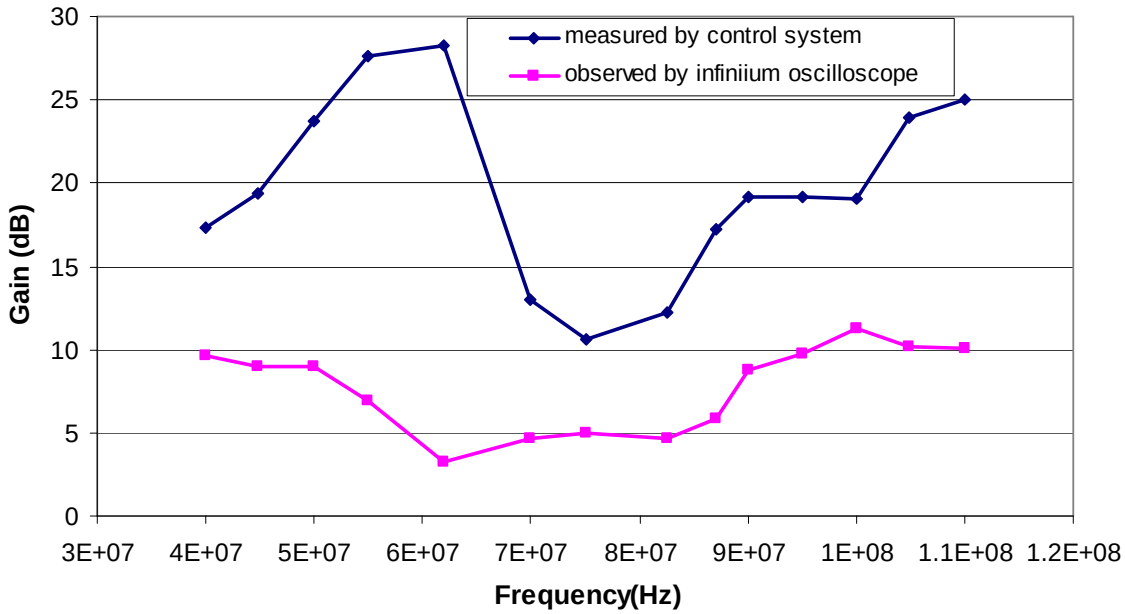

Figure 7.34 Comparison of phase measured by the old control box with that observed on the oscilloscope. The short cable was used in the test.

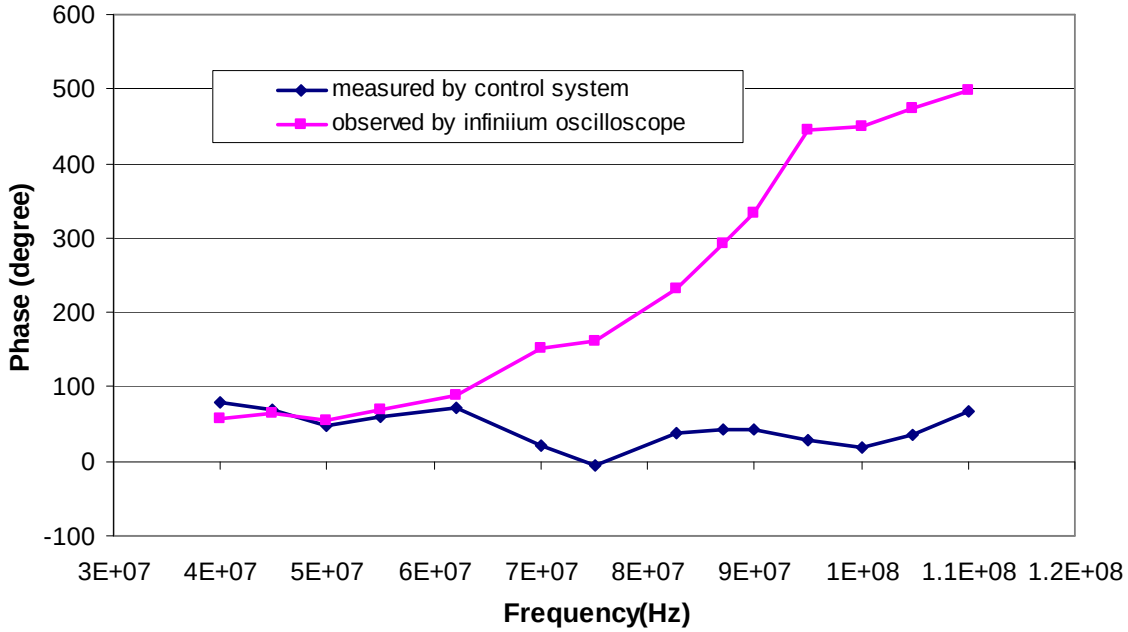

Figure 7.35 Comparison of phase measured by the old control box with that observed on the oscilloscope. The long cable was used in the test.

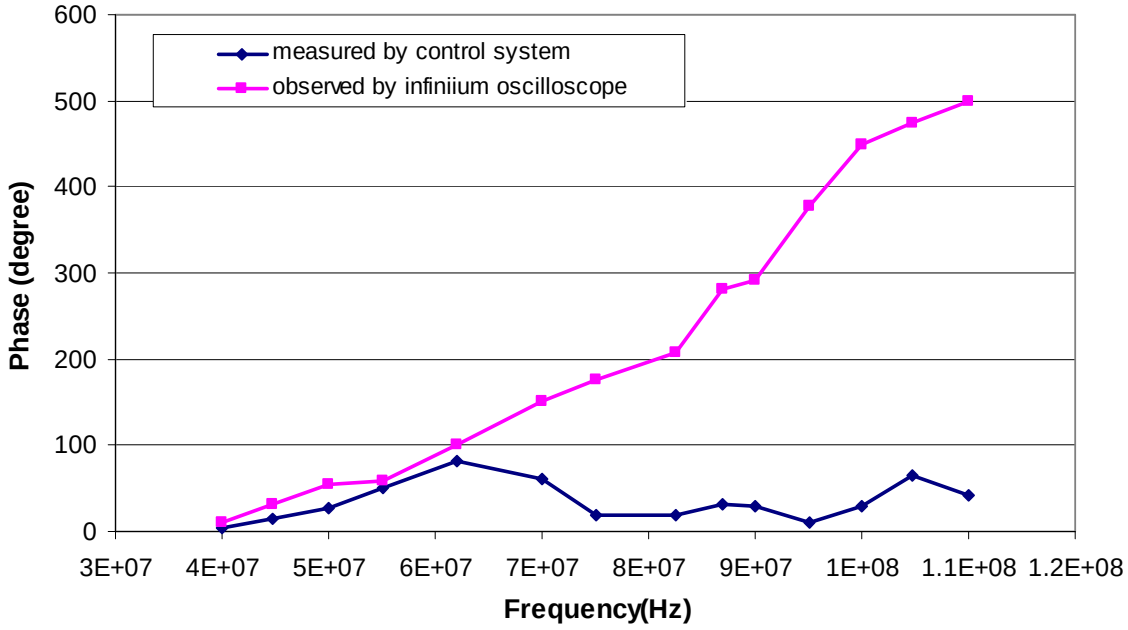

7.4.3.2 Comparison between single-frequency and frequency-sweep modes

Comparisons of gain and phase measured at single frequencies with that measured in a frequency-sweep mode for the short and long cables are shown in Figures 7.36 – 7.39.

For the short cable, the gain responses measured at single frequencies were different from that measured in the frequency-sweep mode. The frequency-sweep mode gave smoother gain responses than the single frequency mode (Figure 7.36). A relatively similar trend can be found for the data obtained via the long cable (Figure 7.37). The phase responses measured at single frequencies were quite different from that measured in the frequency-sweep mode for the short cable (Figure 7.38). However, for the long cable, a similar trend can be observed for the phase responses within the frequency range from 44.8 MHz to 75 MHz and 95 MHz to 110 MHz (Figure 7.39).

Figure 7.36 Comparison of gain measured at the single frequency and the frequency sweep modes. The short cable was used in the test.

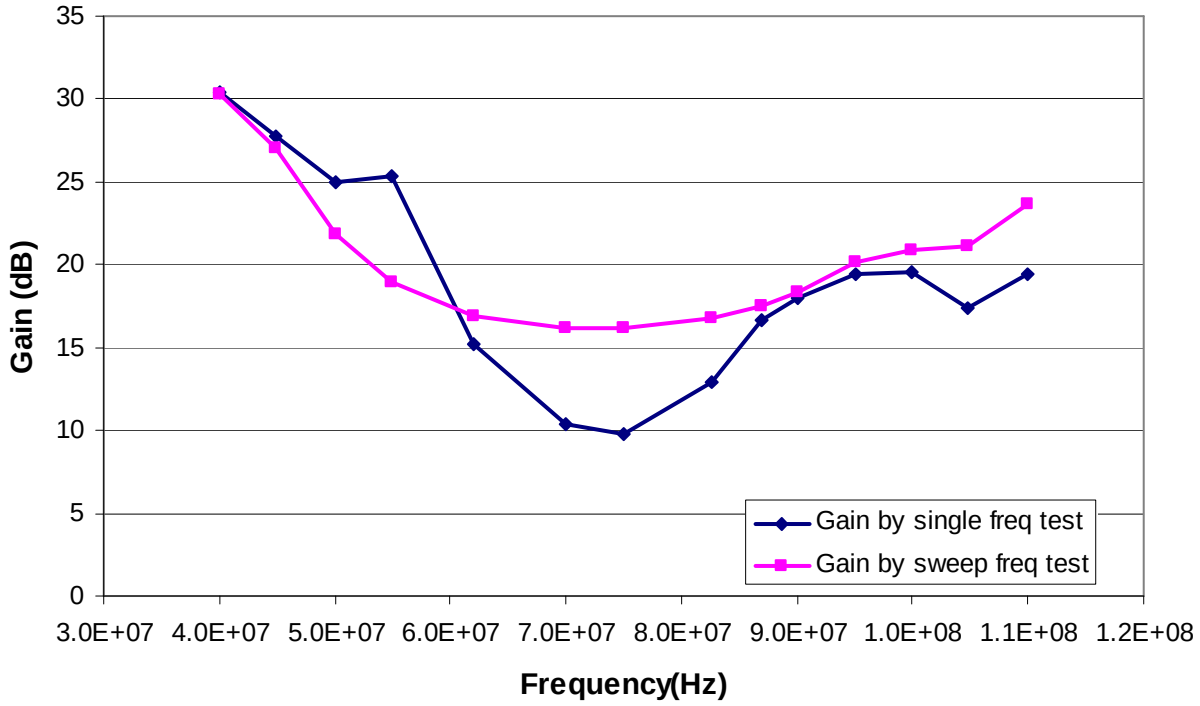

Figure 7.37 Comparison of gain measured at the single frequency and the frequency sweep modes. The long cable was used in the test.

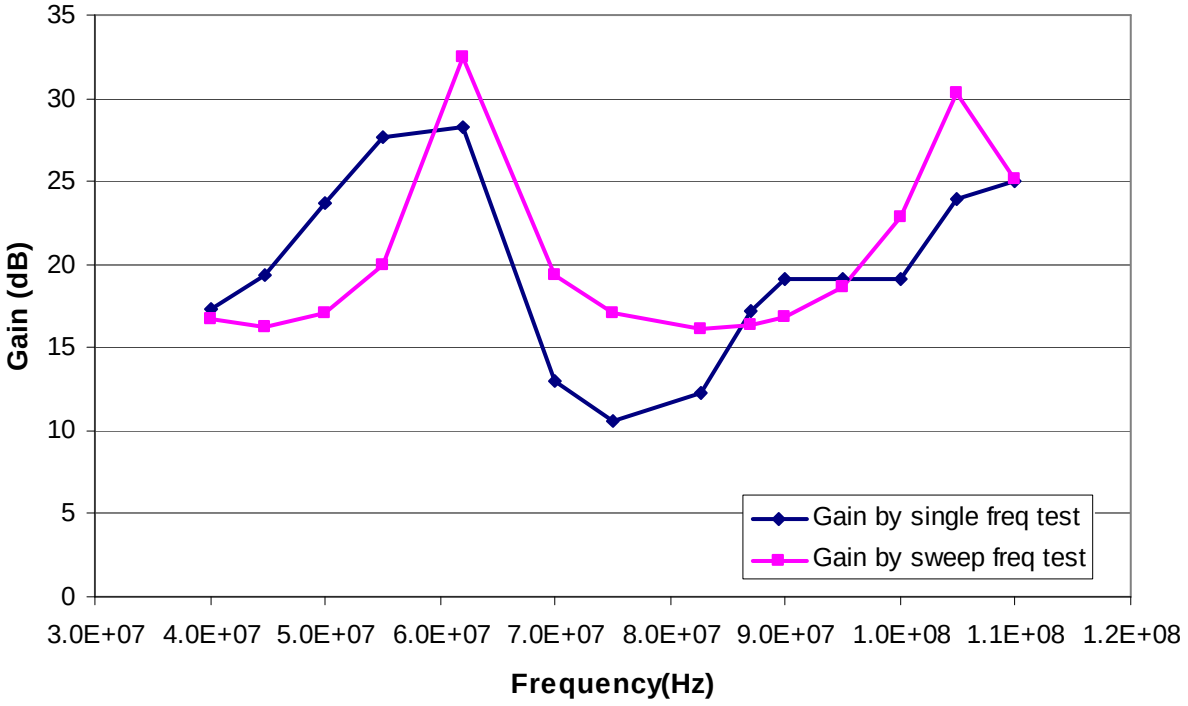

Figure 7.38 Comparison of phase measured at the single frequency and the frequency sweep modes. The short cable was used in the test.

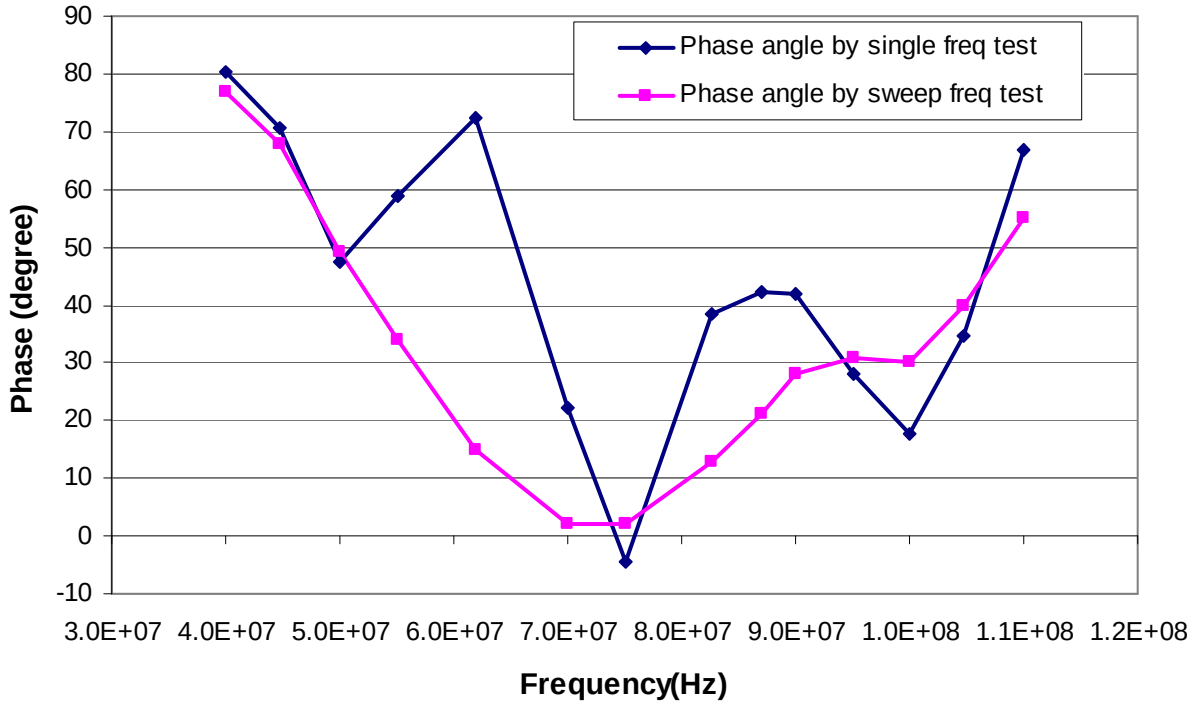

Figure 7.39 Comparison of phase measured at the single frequency and the frequency sweep modes. The long cable was used in the test.

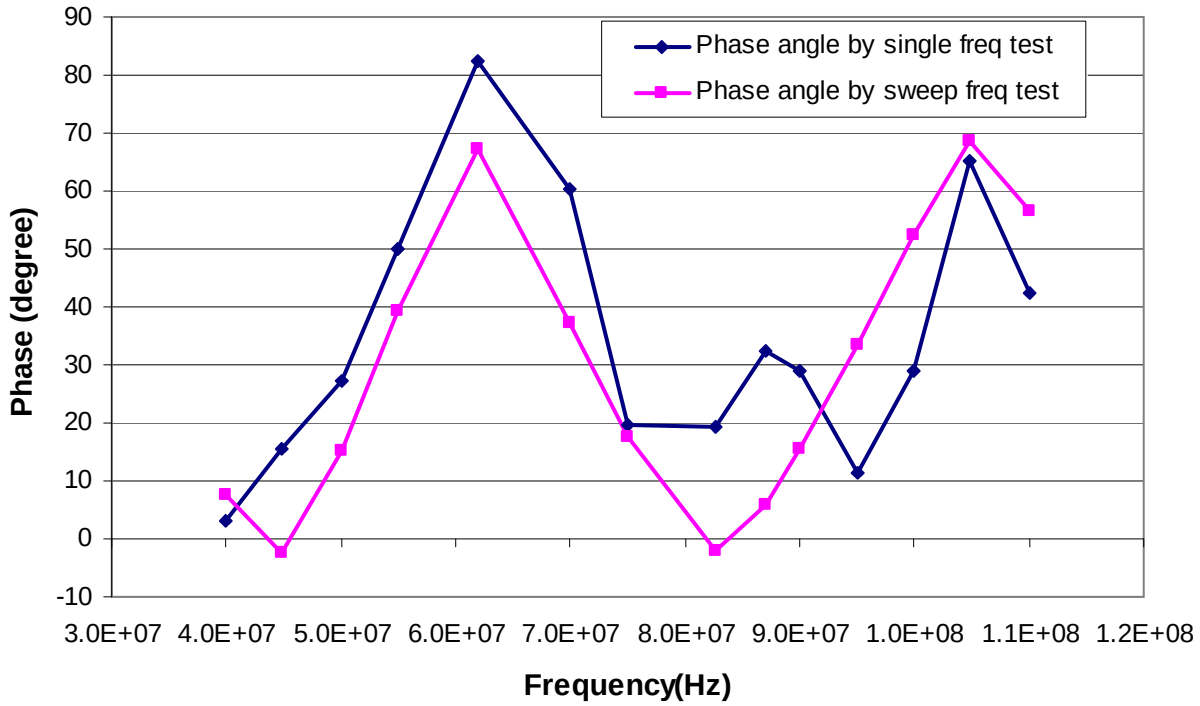

In summary, the issues with the gain and phase detector were not solved through this experiment. One of the possible reasons for the discrepancy in gain and phase measurement is that the signal from the sensor probe (INPB input) was noisy. The discrepancy between signals measured at the single frequency and frequency-sweep modes may indicate that, for frequency sweeping, a longer waiting time is needed between frequency changes. More tests are needed to solve these issues.

CHAPTER 8 - Conclusions

Conclusions drawn from each stage of this study are summarized as follows:

8.1 Control system

A real-time control system for a frequency response (FR)-based permittivity sensor was developed. A C program was developed in the TASKING Embedded Development Environment to control the system. The new control system embodied improvements over a previously designed system in the following aspects:

- The system used a printed circuit board.
- The measurement frequency range was extended from 120 MHz to 400 MHz.
- The resolution of measured FR data was improved by using programmable gain amplifiers.
- A data storage module was added to the system.
- A temperature measurement module was added to the system.
- An LCD display and a keypad were added to the system to display the frequency response data with corresponding frequencies and to allow users to enter commands.

8.2 Impedance transformation models tests

Impedance transformation models for the control system with (1) sensor probes of different sizes, (2) coaxial cables of the same length terminated with different loads, and (3) coaxial cables of different lengths terminated with the same load were developed and tested.

Several additional tests for the gain and phase detector were also conducted to evaluate its performance.

- Tests on 7.5cm and 5cm probes indicated that a simple parallel R-C model did not describe the probe impedance accurately.
- Tests on the old control box and a coaxial cable terminated with three “standard” loads - an open circuit, a short circuit, and a 50Ω resistor - indicated that the impedance transformation models were capable of predicting the impedances of these loads. However, the results obtained for the new control box were not satisfactory. Test results also showed that the impedance of parallel R-C loads at frequencies below 50 MHz can be predicted by the impedance transformation models. However, the models needed to be further improved to reduce the prediction error.
- Tests on coaxial cables with different lengths indicated that the impedance transformation model were capable of describing the effect of cable length on the measurement of the real part of load impedance only at frequencies below 20 MHz. The model was not effective in describing the imaginary part of the load impedance within the entire frequency range tested.
- Issues with the gain and phase detector need additional study.

CHAPTER 9 - Recommended Future Research

The following technical issues need to be further investigated:

1. Signals from the thermocouple were not stable within the frequency range tested. A greater signal drop can be observed at frequencies between 20 and 110MHz. Causes for signal drop need to be further investigated.

2. Software for saving FR data to the newly added flash memory needs to be completed.

3. Tests on sensor probes of different sizes have indicated that the impedance model for sensor probe was not accurate. An improved model that incorporates impedances of the connecting wires and bolts needs to be studied. Moreover, a new, simple sensor probe with only two parallel plates is recommended. This probe can be used to test “standard” dielectric liquids with known permittivities and compare permittivities derived from the FR data with the known values.

4. Issues with the gain and phase detector need additional study. The following procedure is recommended to identify the factors that limited the measured phase difference to 0-90º. 1) Repeat the test described in Section 7.4.1 with the signal generator (Figure 7.27) replaced with an AD9854 evaluation board. Results of this test can be used to explain whether the issue is related to the AD9854 evaluation board. 2) If phase differences of above 90º can still be

measured, replace the RC circuit in Figure 7.27 with R_{ref} (Figures 4.1, 4.3, 5.5, and 5.6) and a sensor probe with a coaxial cable, and then observe the measured phase difference range.

5. Discrepancies in gain and phase responses measured at the single-frequency and the frequency-sweep modes need to be further studied through tests. A longer waiting time may be added during frequency switching.

References

Abdulnour, J., C. Akyel and K. Wu. 1995. A generic approach for permittivity measurement of dielectric materials using a discontinuity in a rectangular waveguide or a microstrip line. *IEEE Transactions on Microwave Theory and Techniques* 43(5): 1060-1066.

Agilent Technologies. 2000. Agilent 54621A oscilloscope user's guide.

Analog Devices, Inc. 1999. AD623 data sheet. Available online at http://www.analog.com.

Analog Devices, Inc. 2002. AD8302 data sheet. Available online at http://www.analog.com.

Analog Devices, Inc. 2003a. AD9858 data sheet. Available online at http://www.analog.com.

Analog Devices, Inc. 2003b. AD9833 data sheet. Available online at http://www.analog.com.

Analog Devices, Inc. 2003c. AD8186 data sheet. Available online at http://www.analog.com.

Afsar, M.N., J.R. Birch, R.N. Clarke and G.W. Chantry. 1986. The measurement of the properties of materials. *Proceedings of the IEEE 74(1)*: 183-199.

Baker-Jarvis, J., E.J. Vanzura and W.A. Kissick. 1990. Improved technique for determining complex permittivity with the transmission/reflection method. *IEEE Transactions on Microwave Theory and Techniques* 38(8): 1096-1103.

Bois, K.J., L.F. Handjojo, A.D. Benally, K. Mubarak and R. Zoughi. 1999. Dielectric plug-loaded two-port transmission line measurement technique for dielectric property characterization

of granular and liquid materials. *IEEE Transactions on Instrumentation and Measurement* 48(6): 1141-1148.

Bussey, H.E. 1967. Measurement of RF properties of materials a survey. *Proceedings of the IEEE* 55(6): 1046-1053.

Catala-Civera, J.M., A.J. Canos, F.L. Penaranda-Foix and de los Reyes Davo, E. 2003. Accurate determination of the complex permittivity of materials with transmission reflection measurements in partially filled rectangular waveguides. *IEEE Transactions on Microwave Theory and Techniques* 51(1 Part 1): 16-24.

Chen, L., C.K. Ong, C.P. Neo, V.V. Varadan and V.K. Varadan. 2004. Microwave electronics: measurement and material characterization. Wiley Hoboken, NJ.

Coleman, C., 2004. An Introduction to Radio Frequency Engineering. The press syndicate of the University of Cambridge.

Crystek Crystals Corporation. 2005. CVCSO-914-1000 crystal oscillator data sheet. Available online at http:www.crystek.com.

Dean, T.J., J.P. Bell and A.J.B. Baty. 1987. Soil moisture measurement by an improved capacitance technique. I: Sensor design and performance. *Journal of hydrology (Amsterdam)* 93(1-2): 67-78.

Dionigi, M., A. Ocera, E. Fratticcioli and R. Sorrentino. 2004. A new resonant probe for dielectric permittivity measurement. *Microwave Conference*, 2004. 34th European 2: 673-676.

Dudorov, S.N., D.V. Lioubtchenko, J.A. Mallat and A.V. Raisanen. 2005. Millimeter-wave permittivity measurement of deposited dielectric films using the spherical open resonator. *IEEE Microwave and Wireless Components Letters [see also IEEE Microwave and Guided Wave Letters]* 15(9): 564-566.

Fan, G., 2002. Simultaneous sensing of soil conductive and capacitive properties. A Master's thesis, Department of Biological and Agricultural Engineering, Kansas State University.

Fratticcioli, E., M. Dionigi and R. Sorrentino. 2004. A simple and low-cost measurement system for the complex permittivity characterization of materials. IEEE Transactions on Instrumentation and Measurement 53(4): 1071-1077.

Ghodgaonkar, D.K., V.V. Varadan and V.K. Varadan. 1990. Free-space measurement of complex permittivity and complex permeability of magnetic materials at microwave frequencies. *IEEE Transactions on Instrumentation and Measurement* 39(2): 387-394.

Infineon technologies. 2001. C167CR data sheet. Available online at http://www.infineon.com.

Lee, K.H., 2005. A dielectric permittivity sensor for simultaneous measurement of multiple soil properties. A Ph.D. Dissertation, Department of Biological and Agricultural Engineering, Kansas State University.

Lee, K.H., N. Zhang, W.B. Kuhn, and G.J. Kluitenberg. 2007a. A frequency-response permittivity sensor for simultaneous measurement of multiple soil properties: Part I. The frequency-response method. *Transactions of the ASABE*, 50(6): 2315-2326.

Lee, K.H. and N. Zhang. 2007b. A frequency-response permittivity sensor for simultaneous measurement of multiple soil properties: Part II. Calibration-model tests. *Transactions of the ASABE*, 50(6): 2327-2336.

Matytsin, S.M., K.N. Rozanov and N.A. Simonov. 1996. Permittivity measurement using slotted coaxial resonator. *IEEE Instrumentation and Measurement Technology Conference*, 1996. IMTC-96. Conference Proceedings. 'Quality Measurements: The Indispensable Bridge between Theory and Reality' 2:(987-990).

Meitzler, A.H. and G.S. Saloka. 1992. Two alternative, dielectric-effect, flexible-fuel sensors. *SAE transactions* 101(3): 1455-1466.

Microchip Technology Inc.. 2003. MCP6S21 data sheet. Available online at http://www.microchip.com.

Microchip Technology Inc.. 2006. 25AA1024 data sheet. Available online at http://www.microchip.com.

Micro/sys. Inc. 2001. LC0240 & KEYPAD16 user's manual.

National Semiconductor, 2008. LM185-2.5 data sheet. Available online at http://www.national.com.

Nelson, S.O. 1999. Dielectric Properties Measurement Techniques and Applications. *Transactions of the ASAE-American Society of Agricultural Engineers* 42 (2):523-530.

Nelson, S.O. 1991. Dielectric properties of agricultural products: measurements and applications. *IEEE transactions on electrical insulation* 26(5): 845-869.

Nelson, S.O. 2003. Frequency-and temperature-dependent permittivities of fresh fruits and vegetables from 0.01 to 1.8 GHz. *Transactions of the ASAE-American Society of Agricultural Engineers* 46(2): 567-576.

Nelson, S.O., W.R. Forbus Jr and K.C. Lawrence. 1995. Assessment of microwave permittivity for sensing peach maturity. *Transactions of the ASAE-American Society of Agricultural Engineers* 38(2): 579-585.

Nozaki, R. and T.K. Bose. 1990. Broadband complex permittivity measurements by time-domain spectroscopy. *IEEE Transactions on Instrumentation and Measurement* 39(6): 945-951.

Nyfors, E. 2000. Industrial Microwave Sensors—A Review. *Subsurface Sensing Technologies and Applications* 1(1): 23-43.

Ocera, A., M. Dionigi, E. Fratticcioli and R. Sorrentino. 2006. A novel technique for complex permittivity measurement based on a planar four-port device. *IEEE Transactions on Microwave Theory and Techniques* 54(6): 2568.

Payero, J.O., D.D. Tarkalson and S. Irmak. 2006. Use of time domain reflectometry for continuous monitoring of nitrate-nitrogen in soil and water. *Applied Engineering in Agriculture* 22(5): 689-700.

PHYTEC America, LLC. 1999. kitCON-167 Hardware-Manual. Available online at http://www.phytec.com

Raveendranath, U., J. Jacob and K.T. Mathew. 1996. Complex permittivity measurement of liquids with coaxial cavity resonators using a perturbation technique. *Electronics Letters* 32(11): 988-990.

Robinson, D.A., C.M.K. Gardner and J.D. Cooper. 1999. Measurement of relative permittivity in sandy soils using TDR, capacitance and theta probes: comparison, including the effects of bulk soil electrical conductivity. *J HYDROL* 223(3): 198-211.

Robinson, D.A., S.B. Jones, J.M. Wraith, D.Or and S.P. Friedman. 2003. A Review of Advances in Dielectric and Electrical Conductivity Measurement in Soils Using Time Domain Reflectometry. *Vadose Zone Journal* 2(4): 444-475.

Sheen, N.I. and I.M. Woodhead. 1999. An open-ended coaxial probe for broad-band permittivity measurement of agricultural products. *Journal of Agricultural Engineering Research* 74(2): 193-202.

Sri Ranjan, R. and C.J. Domytrak. 1997. Effective volume measured by TDR miniprobes. *Transactions of the ASAE-American Society of Agricultural Engineers* 40(4): 1059-1066.

STMicroelectronics. 1999. TS925 data sheet. Available online at http://www.st.com.

Stoakes, D.S. and K.D. Brock. 1973. Oil Permittivity sensor. United States Patent.

Stuchly, S.S., M.A. Rzepecka and M.F. Iskander. 1974. Permittivity measurements at microwave frequencies using lumped elements. *IEEE Transactions on Instrumentation and Measurement* 23(1): 56-62.

Tanaka, F., K. Morita, P. Mallikarjunan, Y.C. Hung and G.O.I. Ezeike. 2002. Analysis of dielectric properties of rice vinegar and sake. *Transactions of the ASAE-American Society of Agricultural Engineers* 45(3): 733-740.

Topp, G.C. and J.L. Davis. 1985. Measurement of Soil Water Content using Time-domain Reflectrometry (TDR): A Field Evaluation. *Soil Science Society of America Journal* 49(1): 19.

Topp, G.C., S. Zegelin and I. White. 2000. Impacts of the Real and Imaginary Components of Relative Permittivity on Time Domain Reflectometry Measurements in Soils. *Soil Science Society of America Journal* 64(4): 1244-1252.

Trabelsi, S. and S.O. Nelson. 2003. Free-space measurement of dielectric properties of cereal grain and oilseed at microwave frequencies. *Measurement Science and Technology* 14(5): 589-600.

Venkatesh, M.S. and G.S.V. Raghavan. 2005. An overview of dielectric properties measuring techniques. *vol* 47:7.15-7.30.

Wang, N. 2002. Design of a real-time, embedded weed-detection and spray-control system. A Ph.D. Dissertation, Department of Biological and Agricultural Engineering, Kansas State University.

Yu, K.B., S.G. Ogourtsov, V.G. Belenky, A.B. Maslenikov and A.S. Omar. 2000. Accurate microwave resonant method for complex permittivity measurements of liquids [biological]. *IEEE Transactions on Microwave Theory and Techniques* 48(11): 2159-2164.

Zhang, N., G. Fan, K.H. Lee, G. Kluitenburg, and T. Loughin. 2004. Simultaneous measurement of soil water content and salinity using a frequency-response method. *Soil Science Society of America Journal*, 68:1515-1525.

Zhang, N., G. Kluitenburg, and P. Barnes. 2006. A real-time permittivity sensor for simultaneous measurement of multiple water-quality parameters. *Proceedings of Water and the Future of Kansas Conference*, March, 2006, Topeka, KS.

Zhang, N., K. Lee, X. Xi, and N. Tang. 2007. A frequency-response permittivity sensor for simultaneous measurement of multiple properties of solid, liquid, and gaseous dielectric materials. *Proceedings of the Biological Sensorics Conference*; June 15-17, 2007, Minneapolis, MN.

Appendix A - Circuit schematic of the Control System

Figure A.1 Circuit schematic of the control board in the new control box

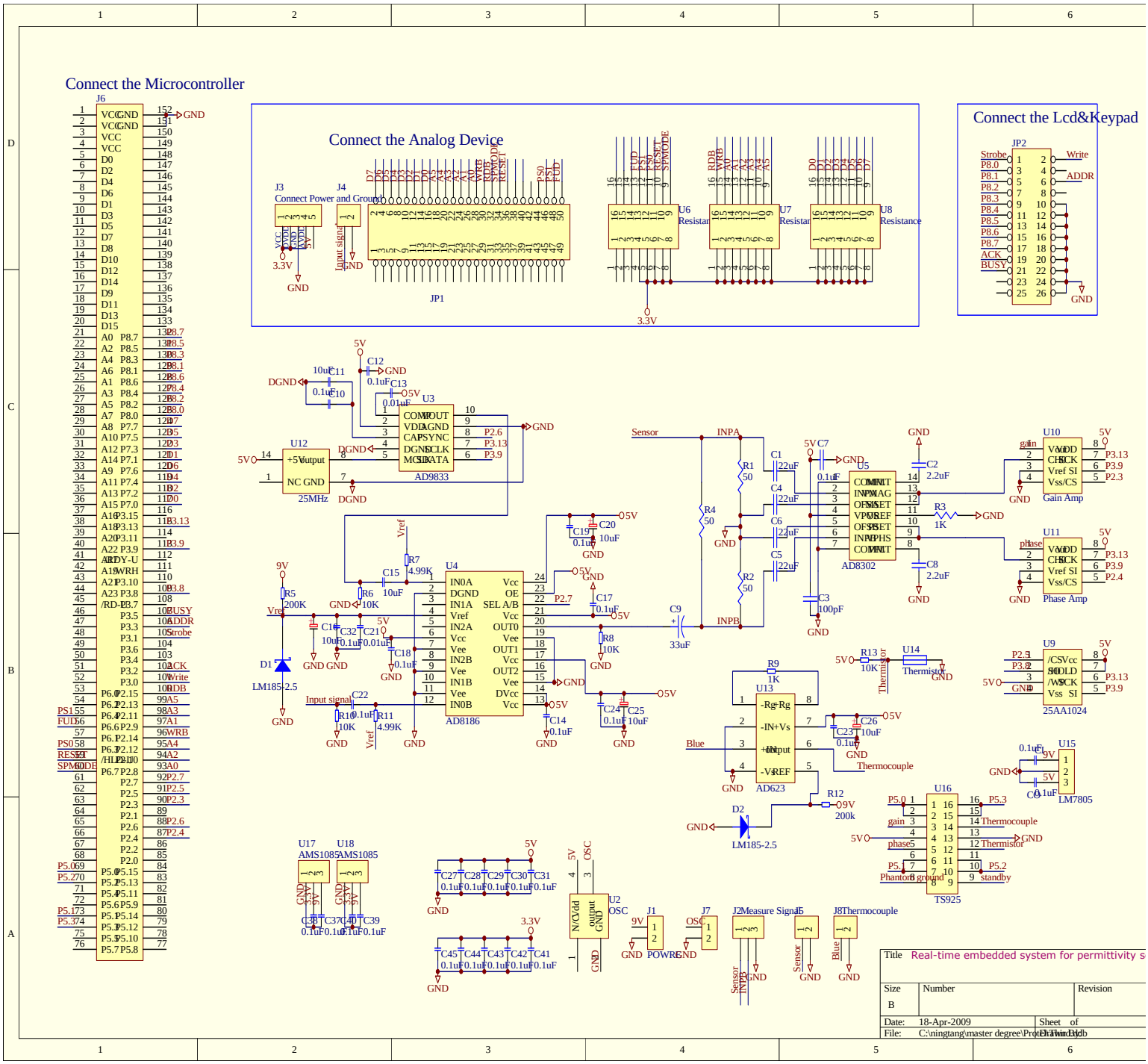

Appendix B - Circuit layout of the Control System

Figure B.1 Circuit layout of the control board in the new control box

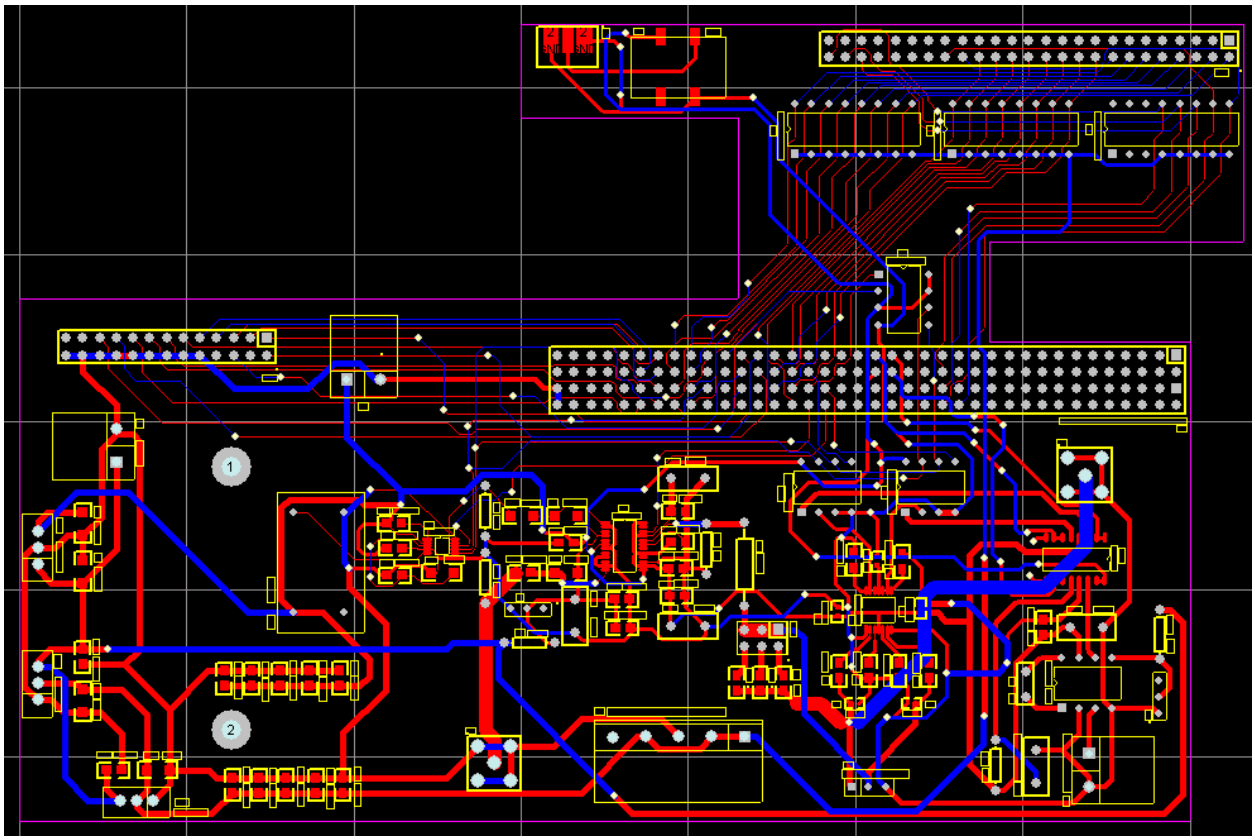

Appendix C - Microcontroller Program

```
#include <stdio.h>
#include <stdlib.h>
#include <math.h>
#include <reg167.h>
#include "serio.h"
#include "LCDKEY167.h" //for lcd&keypad
#include "amplifier.h"

unsigned int data0=0;  //digital data for gain
unsigned int data1=0;  //digital data for phase
unsigned int data2=0;  //digital data for thermistor
unsigned int data3=0;  //digital data for thermocouple

unsigned int gain=0;    // gain and phase are global variable
unsigned int phase=0;   // gain and phase are global variable
unsigned int T=0;
double Temp=0.0;

unsigned char Instruction=0x40;
unsigned char Gain=0x02;  //Gain is set "4 times"
unsigned char Phase=0x01;  //Phase is set "2 times"

unsigned int control=0x2800;  // command for low frequency register
unsigned int control_reset=0x0100;  // command for low frequency register

unsigned int LSB=0;    // for low freuqncy register
unsigned int MSB=0;    // for low freuqncy register
unsigned int LSB_send=0;  //for low freuqncy register
unsigned int MSB_send=0;  //for low freuqncy register

void P6_init(void);   //I/O port of kitCON for control bus of signal generator
void P7_init(void);   //I/O port of kitCON for data bus of signal generator
void P2_init(void);   //I/O port of kitCON for address bus of signal generator

//For low frequency generator
void InitDDSCommunication(void);
void InitDDS(void);
void frequency_low(double d_freq, double r_freq);
int *ftw_to_deci_low(double d_freq, double r_freq);
void WriteDDSLow(unsigned int SPI);
void ToggleChipSelect_LowFreq(void);
void WriteLowFreq (unsigned int word);
```

```
//For high frequency generator
void null_cal(void);
void timer_init(void);
void delay_time(unsigned int value);
void io_up(void);
void control_register_init(void);
void frequency(double d_freq, double r_freq);
int *ftw_to_deci(double d_freq, double r_freq);

//For data collection
void collect_data(void);
void collect_data_T(void);
void adc_control(void);


void main(void)
{
  unsigned char k;              //index for the times of collecting data
  unsigned char j,m,n;          //index for the times of collecting data
  double freq_desir=0;                  //target frequency
  unsigned int freq_index;      //index for target frequency
  int freq;
  int freq1;
  unsigned char key;

  //initializing I/O ports of kitCON
  P6_init();
  P7_init();
  P2_init();

  //initializing serial communication
  //included in "serio.c"
  init_serio();

  //initializing LDCKBD1
  P3_init();
  init_LCDKBD1();
  clear_LCD();

  printf("1111\n");
  collect_data_T();

  while(1)
  {
        clear_LCD();
        printchar_LCD("OK?");   //display "ok?" in LCD
        delay_time(500);

        key=read_YESNO();       //wait for the keypad

        if (key=='y')
```

```
      {
       printchar_LCD("OK!");
       delay_time(500);

for(k=0;k<3;k++)
 {
   clear_LCD();
   control_register_init();  //initializing control register of high freq generator board


   //intializing programmable amplifier and setting gain
   for(j=0;j<4;j++)
   {
    InitAmplifierCommunication();
    WriteGainAmplifier(Instruction, Gain);
    WritePhaseAmplifier(Instruction, Phase);
   }

   SSCCON &= 0x7FFF;
   InitDDSCommunication();
   InitDDS();


  for(freq_index=0;freq_index<574;freq_index++)
   {
        if(freq_index<50)
              freq_desir=freq_index;
         else if(freq_index<55)
              freq_desir=(double)200*(freq_index-49);
                                                    //linear scale in the freq. range of 200Hz to 1kHz
         else if(freq_index<75)
              freq_desir=pow(10,(double)(0.15*(freq_index-54)+3));
                                                    //log scale in the freq. range of 1.41kHz to 1MHz
         else if(freq_index<574)
               freq_desir=(double)800000*(freq_index-74)+(double)800000;
                                                   //linear scale in the freq. range of 1.6MHz to 400MHz

                  key=read_YESNO();
                  if(key=='n')
                  break;

                  if(freq_index>=50)
                  {
                    if(freq_desir<=1000000.0)
                     {
                       InitDDSCommunication();
                       InitDDS();
                       frequency_low(freq_desir, 25000000.0);  //changing freq. of the signal generator
                       delay_time(100);
                     }
```

```
                    else if(freq_desir>1000000.0)
                     {
                        frequency_low(0, 25000000.0);
                              frequency(freq_desir, 1000000000.0);
                               delay_time(100);
                              P2_7=0;
                       }

                           freq = (int)(freq_desir/100000.);
                           printf("%d,%d, ",freq_index,freq);
                           collect_data();

                          key=read_YESNO();
                          if(key=='n')
                          break;

                          freq1 = (int)(freq_desir/100000.);
                           if (freq_index>50 && freq_index%10==0)
                            {
                                    printchar_LCD("frequency:");
                                    printint_LCD(freq1);
                                    printchar_LCD("*100KHz");
                                    for(m=0;m<3;m++)
                                    {
                                          write_control_LCD(0xc0);
                                    }
                                    delay_time(10);
                                    printchar_LCD("gain:");
                                    printint_LCD(gain);
                                    for(n=0;n<3;n++)
                                   {
                                          write_control_LCD(0x14);
                                    }
                                    delay_time(10);
                                    printchar_LCD("phase:");
                                    printint_LCD(phase);
                                    delay_time(500);
                                    clear_LCD();
                             }

                 }
                    if(key=='n')
                     break;
                    frequency(0.0, 1000000000.0);
                    printf("5555\n");
                }
              }
              printf("9999\n");
          }
        }
      }
```

```
/*******************************************************
* Wire connection between AD9858 and kitCON167         *
*                                                      *
*     (AD9858)        (kitCON167)                      *
*       D7        --   P7.7                 **********
*       D6        --   P7.6                 *
*       D5        --   P7.5                 *
*       D4        --   P7.4                 *
*       D3        --   P7.3                 *
*       D2        --   P7.2                 *
*       D1         --  P7.1                 *
*       D0        --   P7.0                 *
*                                           *
*       A5        --   P2.13                *
*       A4        --   P2.12                *
*       A3        --   P2.11                *
*       A2        --   P2.10                *
*       A1         --  P2.9                 *
*       A0        --   P2.8                 *
*                                           *
*       (WRB)'    --   P2.14                *
*       (RDB)'    --   P2.15                *
*       SPMODE    --  P6.7                 *
*       FUD       --   P6.6                 *
*       RESET     --  P6.5                 *
*       PS0       --   P6.3                 *
*       PS1        --  P6.4                 *
*******************************************************/


/*************************************************************
*  Function:        P6_init (P6.3, P6.4, P6.5, P6.6 and P6.7)  *
*  P6.3=PS0, P6.4=PS1, P6.5=RESET, P6.6=FUD, P6.7=SPMODE    *
*  Return value:     none                                     *
*  Description:      initialize port 6                        *
*************************************************************/
void P6_init(void)
{
  ODP6=0xF8;
  P6=0x80;   //SPMODE=high, Parallel programming mode, PS0=low,PS1=low
  DP6=0xF8;
}


/*******************************************************
*  Function:        P7_init                             *
*  P7.0 - P7.7: data bus                                *
*  Return value:     none                               *
*  Description:      initialize port 7                  *
```

```
*************************************************/
void P7_init(void)
{
  ODP7=0xFF;
  P7=0x00;
  DP7=0xFF;
}


/*************************************************************************************
*  Function:        P2_init                                                          *
*  P2.8 - P2.16: address bus                                                         *
*  P2.14:(WRB)', P2.15:(RDB)'                                                        *
*  P2.3-P2.7: chip select, P2.6-AD9833, P2.7-AD8186, 1 for chA, 0 for chB, P2.3- Gain, P2.4- Phase,  *
*   P2.5-25AA1024                                                                    *
*  Return value:     none                                                            *
*  Description:      initialize port 2                                               *
*  P2.14((WRB)') and P2.15((RDB)') are high.                                         *
*************************************************************************************/
void P2_init(void)
{
  ODP2=0xFF00;  // push-pull is 0, open drain is 1
  P2=0xC0F8;
  DP2=0xFFFF;  // direction 1 is output
}



/*************************************************************************************
*  Function:        DDS communication initialization (AD9833)                        *
*  Return value:     none                                                            *
*  Description:      SSC                                                             *
*************************************************************************************/

void InitDDSCommunication(void)//only used for AD9833
{
   P2_6 = 1;    // set port data register
   DP2_6  = 1;   // output direction

   // SSC baudrate generator/reload register

         SSCBR = 0x0347;         //set-up the baud rate generator to 11904.7

         // ---------- SSC Control Register ----------
         ///  Master Mode
         ///  transfer data width is 16 bit
         ///  transfer/receive MSB first
         ///  latch receive data on leading clock edge, shift on trailing edge
         ///  idle clock line is high, leading clock edge is low-to-high transition
         ///  ignore receive error
         ///  ignore phase error
```

```
        //SSCCON = 0x4037; //try SSCCON = 0x4017;
         SSCCON = 0x407F;

         P3_9 = 1;          // set high since it is ended with serial data
         P3_13 = 1;

         DP3_9   = 1;     // output
         DP3_13  = 1;   // SCLK output

         SSCCON |= 0x8000;
}


/*****************************************************************************************
*  Function:         DDS initialization (AD9833)                                          *
*  Return value:     none                                                                 *
*  Description:      reset                                                                *
*****************************************************************************************/

void InitDDS(void)
{
 ToggleChipSelect_LowFreq();
 WriteLowFreq(control_reset);
 P2_6=1;
}

/*****************************************************************************************
*  Function:         frequency                                          *
*  Input:           desired freq(Hz), reference freq(Hz) *
*  Return value:     none                                              *
*  Description:      display the sinusoidal signal with the desired frequency *
*  *ftw_to_deci function is used                                       *
*****************************************************************************************/
void frequency_low(double d_freq, double r_freq)
{
  int *ftw_freq;

  ftw_freq=ftw_to_deci_low(d_freq, r_freq);  // convert desired frequency to FTW

  LSB = ftw_freq[0];
  MSB = ftw_freq[1];

  LSB_send = (LSB & 0xBFFF)+0x8000;
  MSB_send = 0x8000+MSB;

  WriteDDSLow(control);
  delay_time(5);
  WriteDDSLow(LSB_send);
  WriteDDSLow(MSB_send);
```

```
}
/*****************************************************************************
*  Function:         DDS initialization (AD9833)                               *
*  Return value:     none                                                      *
*  Description:      reset                                                     *
*****************************************************************************/

void WriteDDSLow(unsigned int SPI)
{
   ToggleChipSelect_LowFreq();
   WriteLowFreq(SPI);
    P2_6 = 1;
}

void WriteLowFreq (unsigned int word)
{
   SSCTIR = 0; //clear transmit interrupt flag
   SSCTB = word;
   while(!SSCTIR);  //wait for transmission buffer to be empty
   while(SSCBSY);       //wait for transmission to be completed
}

void ToggleChipSelect_LowFreq(void)
{
   int i;
   P2_6 = 1;                // disable chip select
   for(i=1;i<30;i++) P2_6  = 1;// wait here at leat 500 nsec
   P2_6 = 0;                // enable chip select
}


/*****************************************************************************
*  Function:         *ftw_to_deci                                *
*  Input:            desired freq(Hz), reference freq(Hz)    *
*  Return value:     4 decimal values(4 arraies) converted from ftw     *
*  Description:      change ftw to decimal values for registers 0A-0D   *
*****************************************************************************/
int *ftw_to_deci_low(double d_freq, double r_freq)
{
  int i=0, j=0;
  int rem[7]={0};
  int a_rem[9]={0};
  int b_rem[2]={0};
  int *de_rem;
  double intpart=0.;
  double c_intpart=0.;
  double c_frac=0.;
  double new_int[7]={0.};
  double c_ftw=0.;
  double ftw=0.;
  double n=28.;
```

```
  de_rem=b_rem;

  for(i=0;i<2;i++)
  de_rem[i]=0;

  ftw=(d_freq*(double)pow(2,n))/(r_freq);
  c_frac=modf(ftw,&c_intpart);  // return the fraction, leave the intpart into &c_intpart

  c_ftw=c_intpart;          // intpart
  new_int[0]=c_ftw;  // put intpart in the new_int[0]

  for(i=0,j=6;i<7;i++,j--)
  {
     rem[i]=(int)fmod(new_int[i],16.); // the remainder
     a_rem[j]=rem[i]; //a_rem[6] is the lowest bit
     new_int[i+1]=new_int[i]/16.;
     modf(new_int[i+1],&intpart);
     new_int[i+1]=intpart;
  }


  a_rem[7]=(a_rem[3]&0x3)+0x4;
  a_rem[8]=a_rem[3]>>2;

  de_rem[0]=(int)(4096*a_rem[7]+256*a_rem[4]+16*a_rem[5]+a_rem[6]);   // for LSB
  de_rem[1]=(int)(1024*a_rem[0]+64*a_rem[1]+4*a_rem[2]+a_rem[8]);  //for MSB
  return (de_rem);
 }

/************************************************************
*  Function:        null_cal                        *
*  Return value:     none                            *
*  Description:      null calculation to delay some time  *
************************************************************/
void null_cal(void)
{
  double i=0;
  i=(0.123456*0.123456)+(0.123456*0.0123456);
}

/************************************************************
*  Function:        adc_control                     *
*  Input ports for analog signals: P5.0, P5.1, P5.2 and P5.3       *
*  Return value:     none                           *
*  Description:      Analog to Digital Convert         *
************************************************************/
void adc_control(void)
{
  extern unsigned int data0;
  extern unsigned int data1;
```

```
  extern unsigned int data2;
  extern unsigned int data3;

  ADCON=0XF023; //ADC conversion time control(ADCTC)=11
            // -> Conversion clock(t_BC)=fcpu/8
            //ADC sample time control(ADSTC)=11
            // -> Sample clock(tsc)=t_BC*64
            //ADC wait for read control(ADWR)=0
            //ADC start bit(ADST)=0
            //ADC mode selection(ADM)=10
            // -> Auto scan single conversion
         //ADC Analog channel input selection(ADCH)=0011, sampling sequence of Channels 3,2,1 and 0.

  ADCIC=0;         //initializing ADC interruupt control
  ADST=1;          //ADC starts
  while(ADCIR==0);
  data3=ADDAT;            //read an ADC result for thermocouple(P5.3)
  ADCIR=0;
  while(ADCIR==0);
  data2=ADDAT;            //read an ADC result for thermistor(P5.2)
  ADCIR=0;
  while(ADCIR==0);
  data1=ADDAT;            //read an ADC result for phase(P5.1)
  ADCIR=0;
  while(ADCIR==0);
  data0=ADDAT;            //read an ADC result for gain(P5.0)

}

 /*******************************************************
*  Function:        timer_init                  *
*  Return value:    none                        *
*  Description:     initialize timer 3            *
*  Timer 3 is used for the delay                  *
*  This function was modified from Dr. Nelison's     *
*******************************************************/
void timer_init(void)
{
  T3CON=0x0087; //T3UDE=0,T3UD=1 -> count down
            //Timer 3 run bit(T3R)=0
            //Timer 3 mode control(T3M)=000 -> Timer Mode
            //Timer 3 Input Selection(T3I)=111 -> 19.531kHz
  T3=0;       //Timer 3 register
  T3IC=0;     //Interrupt Request Flag(T3IR)=0
            //Interrupt Enable Bit(T3IE)=0
            //Interrupt Priority Level(ILVL)=0000
            //Group Level(GLVL)=00
}
```

```
/*****************************************************************************
*  Function:        delay_time                                                *
*  Input:           time to be delayed with the unit of msec                  *
*  Return value:    none                                                      *
*  Description:     delay time with the unit of msec (about 3000msec max.)    *
*  Timer 3 is used for the delay                                              *
*  This function was modified from Dr. Nelison's                              *
*****************************************************************************/
void delay_time(unsigned int value)
{
  timer_init();
  if(value < 1) value=1;
  if(value > 3355) value=3355;
  T3=value*19;
  T3R=1;
  while(T3IR==0);
  T3R=0;
}

/*****************************************************************************
*  Function:        io_up                                                     *
*  Return value:    none                                                      *
*  Description:     active I/O update clock and low                           *
*  null_cal function is used.                                                 *
*****************************************************************************/
void io_up(void)  // for AD9858, it's the similar pin with FUD
{
  P6=0XC0;     // P6.6(FUD update) active (high), P6.7(SPMODE) high
  null_cal();
  null_cal();
  null_cal();
  P6=0X80;      // P6.6(FUD update) low, P6.7(SPMODE) high
}

/*****************************************************************************
*  Function:        control_register_init                                     *
*  Return value:    none                                                      *

*  Description:     initialize MRESET and control registers                   *
*  io_up function is used.                                                    *
*****************************************************************************/
void control_register_init(void)
{
  P6=0XA0;    // Profile 0, P6.5(RESET) active (high), P6.6(I/O update) low, P6.7(SPMODE) high
  null_cal();     // null calculation to delay short time for writing
  P6 = 0x80;    // Profile 0, P6.5(RESET) low, P6.6(I/O update) low, P6.7(SPMODE) high


  P2=0XC0F8;    // address 00 and P2.6((WRB)') high, P2.7((RDB)') high
  P7=0x58;          // 2GHz Divider disabled, mixer and phase detect power down active
```

```
  P2=0X80F8;     // P2.7((RDB)') high, P2.6(WRB)' active (low) to move the data to I/O buffer
  null_cal();      // null calculation to delay short time for writing
  P2=0XC0F8;     // P2.6(WRB)' high to stop writing, P2.7((RDB)') high
  io_up();

  P2=0XC1F8;     // address 01 and P2.6((WRB)') high, P2.7((RDB)') high
  P7=0x40;     // Freq.sweep disabled, sine output enabled
  P2=0X81F8;     // P2.7(RDB)' high, P2.6(WRB)' active (low) to move the data to I/O buffer
  null_cal();      // null calculation to delay short time for writing
  P2=0XC1F8;     // P2.6(WRB)' high to stop writing, P2.7((RDB)') high
  io_up();
}

/*****************************************************************************
*  Function:        frequency                                                 *
*  Input:           desired freq(Hz), reference freq(Hz) *
*  Return value:    none                                                      *
*  Description:     display the sinusoidal signal with the desired frequency *
*  *ftw_to_deci function is used                                             *
*****************************************************************************/
void frequency(double d_freq, double r_freq)
{
  int *ftw_freq;

  ftw_freq=ftw_to_deci(d_freq, r_freq);  // convert desired frequency to FTW

  P2 = 0xCA78;// address 0A (ftw 1[7:0]), P2.6((WRB)') high, P2.7((RDB)') high
  P7=ftw_freq[3];     // data for ftw 1[7:0]
  P2 = 0X8A78;            // P2.7((RDB)') high, P2.6(WRB)' active (low) to move the data to I/O buffer
  null_cal();      // null calculation to delay short time for writing
  P2 = 0XCA78;            // P2.6(WRB)' high to stop writing, P2.7((RDB)') high
  io_up();

  P2 = 0xCB78;// address 0B (ftw 1[15:8]) and P2.6((WRB)') high
  P7=ftw_freq[2];     // data for ftw 1[15:8]
  P2=0X8B78;      // P2.7((RDB)') high,P2.6(WRB)' active (low) to move the data to I/O buffer
  null_cal();      // null calculation to delay short time for writing
  P2=0XCB78;     // P2.6(WRB)' high to stop writing, P2.7((RDB)') high
  io_up();

  P2 = 0xCC78;// address 0C (ftw 1[23:16]) and P2.6((WRB)') high
  P7=ftw_freq[1];     // data for ftw 1[23:16]
  P2=0X8C78;           // P2.7((RDB)') high,P2.6(WRB)' active (low) to move the data to I/O buffer
  null_cal();      // null calculation to delay short time for writing
  P2=0XCC78;     // P2.6(WRB)' high to stop writing, P2.7((RDB)') high
  io_up();

  P2 = 0xCD78;            // address 0D (ftw 1[31:24]) and P2.6((WRB)') high
  P7=ftw_freq[0];     // data for ftw 1[31:24]
  P2=0X8D78;           // P2.7((RDB)') high,P2.6(WRB)' active (low) to move the data to I/O buffer
  null_cal();      // null calculation to delay short time for writing
```

```
  P2=0XCD78;     // P2.6(WRB)' high to stop writing, P2.7((RDB)') high
  io_up();
}

/*************************************************************************
*  Function:         *ftw_to_deci                                        *
*  Input:           desired freq(Hz), reference freq(Hz)    *
*  Return value:     4 decimal values(4 arraies) converted from ftw     *
*  Description:      change ftw to decimal values for registers 0A-0D   *
*************************************************************************/
int *ftw_to_deci(double d_freq, double r_freq)
{
  int i=0, j=0;
  int rem[8]={0};
  int a_rem[8]={0};
  int b_rem[4]={0};
  int *de_rem;
  double intpart=0.;
  double c_intpart=0.;
  double c_frac=0.;
  double new_int[9]={0.};
  double c_ftw=0.;
  double ftw=0.;
  double n=32.;

  de_rem=b_rem;

  for(i=0;i<4;i++)
  de_rem[i]=0;

  ftw=(d_freq*(double)pow(2,n))/(r_freq);
  c_frac=modf(ftw,&c_intpart);

  c_ftw=c_intpart;
  new_int[0]=c_ftw;

  for(i=0,j=7;i<8;i++,j--)
  {
     rem[i]=(int)fmod(new_int[i],16.);
     a_rem[j]=rem[i];
     new_int[i+1]=new_int[i]/16.;
     modf(new_int[i+1],&intpart);
     new_int[i+1]=intpart;
  }

  de_rem[0]=(int)(16*a_rem[0]+a_rem[1]);
  de_rem[1]=(int)(16*a_rem[2]+a_rem[3]);
  de_rem[2]=(int)(16*a_rem[4]+a_rem[5]);
  de_rem[3]=(int)(16*a_rem[6]+a_rem[7]);

  return (de_rem);
```

```
}


/*****************************************************************************
*  Function:        collect_data                                    *
*  Input:           none                                    *
*  Return value:    none                                    *
*  Description:     collecting data of gain,phase,current           *
*****************************************************************************/
void collect_data(void)
{
  unsigned char rt;

  unsigned int tgain[3]={0};
  unsigned int tphase[3]={0};
  unsigned int tthermistor[3]={0};
  unsigned int tthermocouple[3]={0};

  double thermistor=0;
  double thermocouple=0;
  unsigned int thermistor_1=0;
  unsigned int thermocouple_1=0;
  double V_thermistor=0;
  double R_thermistor=0;
  double T_thermistor=0;
  long double T_thermocouple=0;
  double V_thermocouple=0;
  double V_thermocouple_1=0;
  int T_thermocouple_P=0;
  int T_thermistor_P=0;

  double A=1.92E-3;
  double B=9.86315E-5;
  double C=6.6032E-7;
  double D=0;
  double F=0;

  for(rt=0;rt<3;rt++)
  {
    adc_control();       //A/D conversion
    tgain[rt]=data0;          //digitized value for gain
    tphase[rt]=(data1-4096);      //digitized value for phase
    tthermistor[rt]=(data2-8192);
    tthermocouple[rt]=(data3-12288);
  }

  gain=(int)((tgain[0]+tgain[1]+tgain[2])/3);
                                          //calculating the average value of three digital values for gain
  phase=(int)((tphase[0]+tphase[1]+tphase[2])/3);
                                         //calculating the average value of three digital values for phase
  thermistor=(float)((tthermistor[0]+tthermistor[1]+tthermistor[2])/3);
```

```
                                        //calculating the average value of three digital values for thermistor
  thermocouple=(float)((tthermocouple[0]+tthermocouple[1]+tthermocouple[2])/3);
                                      //calculating the average value of three digital values for thermocouple
  thermistor_1=(int)thermistor;
  thermocouple_1=(int)thermocouple;

  V_thermistor=thermistor*5.075/1024;
  R_thermistor=10000*V_thermistor/(5-V_thermistor);
  F=log(R_thermistor);
  T_thermistor=1/(A+B*F+C*pow(F,3))-274.4;

  V_thermocouple_1=thermocouple*5.075/1024;
  V_thermocouple=(thermocouple*5.075/1024-2.5087+Temp-0.007)/101;
  D=V_thermocouple;
  T_thermocouple=0.100860910+25727.94369*D-767345.8295*pow(D,2)+78025595.81*pow(D,3)-
9.247486589E9*pow(D,4)+6.97688E11*pow(D,5)-2.66192E13*pow(D,6)+3.94078E14*pow(D,7);

  T=(int)((T_thermistor+T_thermocouple)*10);

  printf(" %d, %d, %d, %d, %d \n",gain,phase,thermistor_1,thermocouple_1,T);
                                                    //downloading data for gain, phase, and current
}

/*****************************************************************************
*  Function:        collect_data                                              *
*  Input:           none                                                      *
*  Return value:    none                                                      *
*  Description:     collecting data of gain,phase,themistor, thermocouple     *
*****************************************************************************/
void collect_data_T(void)
{
  unsigned char rt;

  unsigned int tthermocouple[3]={0};

  double thermocouple=0;
  double V_thermistor=0;
  double V_thermocouple=0;

  for(rt=0;rt<3;rt++)
  {
    adc_control();       //A/D conversion
    tthermocouple[rt]=(data3-12288);
  }

  thermocouple=(float)((tthermocouple[0]+tthermocouple[1]+tthermocouple[2])/3);
                                      //calculating the average value of three digital values for thermocouple
  V_thermocouple=thermocouple*5.075/1024;
  Temp=(double) (2.509-V_thermocouple);
}
```